NOTE TO USERS

New Techniques for the Investigation of Deformation Mechanisms in Flow of Fine-Grained Ice I_h

Shannon M. McDaniel

A dissertation submitted in partial fulfillment of
the requirements for the degree of

Doctor of Philosophy

University of Washington

2005

Program Authorized to Offer Degree: Earth and Space Sciences

UMI Number: 3198819

INFORMATION TO USERS

The quality of this reproduction is dependent upon the quality of the copy submitted. Broken or indistinct print, colored or poor quality illustrations and photographs, print bleed-through, substandard margins, and improper alignment can adversely affect reproduction.

In the unlikely event that the author did not send a complete manuscript and there are missing pages, these will be noted. Also, if unauthorized copyright material had to be removed, a note will indicate the deletion.
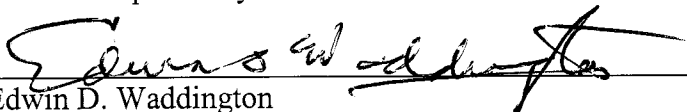
UMI®

University of Washington
Graduate School

This is to certify that I have examined this copy of a doctoral dissertation by

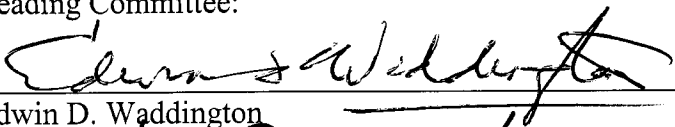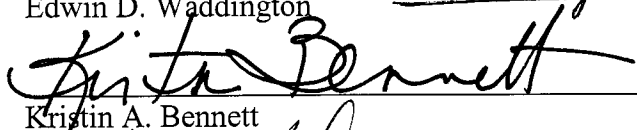Shannon M. McDaniel

and have found that it is complete and satisfactory in all respects,
and that any and all revisions required by the final
examining committee have been made.

Chair of Supervisory Committee:

_____

Edwin D. Waddington

Reading Committee:

_____

Edwin D. Waddington

_____

Kristin A. Bennett

_____

William B. Durham

_____

Charles F. Raymond

Date:_____2005____October 24____

In presenting this dissertation in partial fulfillment of the requirements for the doctoral degree at the University of Washington, I agree that the Library shall make its copies freely available for inspection. I further agree that extensive copying of the dissertation is allowable only for scholarly purposes, consistent with "fair use" as prescribed in the U.S. Copyright Law. Requests for copying or reproduction of this dissertation may be referred to Proquest Information and Learning, 300 North Zeeb Road, Ann Arbor, MI 48106-1346, to whom the author has granted "the right to reproduce and sell (a) copies of the manuscript in microform and/or (b) printed copies of the manuscript made from microform."

Signature

Date   20 Oct 2005

University of Washington

Abstract

New Techniques for the Investigation of Deformation Mechanisms in Flow of Fine-Grained Ice I_h

Shannon M. McDaniel

Chair of the Supervisory Committee:
Professor Edwin D. Waddington
Department of Earth and Space Sciences

This dissertation focuses on experimental work using new techniques to advance the field of glaciology. I examined the development of texture in bulk, fine-grained (2-10 μm) laboratory ice samples, the evolution of grain growth under static conditions, and the measurement of texture (lattice-preferred orientation) of ice grains. I used three techniques to investigate texture and grain size: (1) low-temperature neutron diffraction to measure texture, (2) low-temperature scanning electron microscopy (LTSEM), and (3) simultaneous deformation and neutron diffraction of ice using a new apparatus.

The first technique was used to measure the quantitative textures in the bulk-deformed samples. The second technique, LTSEM, was used to quantify the degree of grain growth in each sample. The third technique combines the advances in neutron science spectrometry with deformation capabilities for ice. I built a deformation apparatus with low-temperature capability and no confining pressure requirement. I performed the first experiment of its kind of deformation and *in situ* texture analysis and documented expected texture results.

The growth rates of fine-grained ice during static annealing do not follow the same growth law as ice found in icesheets. However, the activation energies are

comparable. I suggest that the differences in the measured and expected growth rates can be attributed to differences in the pre-exponential factor (K_o) of equation 2.3. Samples annealed for short durations were still affected by a transient grain-size adjustment period. Extrapolations from the laboratory scale to natural settings, such as in an icesheet, should be made with caution.

The contribution of grain-size sensitive (GSS) creep to deformation and texture development of ice I_h remains unclear. Grain-morphology results show that dislocation creep, GSS creep and/or recrystallization are active in the deformation of these samples. Texture results show that ice samples deformed under conditions of low stress, where GSS creep is expected to dominate, develop a non-random texture. Ice that is deformed under conditions where dislocation creep should dominate develops a similar non-random texture. Further work is needed with both texture measurements and LTSEM to more clearly define the role of GSS creep in the deformation of ice I_h.

TABLE OF CONTENTS

LIST OF FIGURES

LIST OF TABLES

ACKNOWLEDGEMENTS

acknowledge the Lujan Center with special thanks to Mark Taylor for help with design and construction and to Darrick Williams for exceptional assistance with the experiment.

Most of all, I want to thank my family for their unflagging support throughout my academic life thus far. To my mother and father, Ingeborg and John McDaniel, for not only letting me dissect that cat from anatomy class on the dining room table, but sitting there and asking me questions about it during the process. That sheer fascination with the world around us was imparted to me from you, and I can only hope that I pass that remarkable quality on to my children. To my husband, Tay, for all the nights and weekends spent alone or on baby duty and for cheering me on when I needed it most. To my mother-in-law and father-in-law Charla and Lyle Naish, for reading parts of this dissertation enthusiastically, and for always being proud of me. And to my entire family on both sides for their love and support.

We do not grow absolutely, chronologically. We grow sometimes in one dimension, and not in another, unevenly. We grow partially. We are relative. We are mature in one realm, childish in another. -*Anaïs Nin*

When you come to the end of all the light you know, and it's time to step into the darkness of the unknown, faith is knowing that one of two things shall happen: Either you will be given something solid to stand on or you will be taught to fly. -*Edward Teller*

DEDICATION

This dissertation is dedicated to my beloved daughter, Anaïs Luna Naish, my boundless source of inspiration. May you always seek your wildest dreams and accomplish your biggest goals.

Chapter 1

INTRODUCTION

1.1 Background

Ice is a remarkable material that has 14 currently known solid phases, including 3 amorphous phases (Figure 1). In this dissertation, I study the most common phase of ice found on the Earth's surface, hexagonal ice or ice I_h. The other phases of ice occur under various pressure and temperature conditions that may exist on planets in the outer solar system, but are rare on Earth [*Petrenko and Whitworth*, 1999]. Over 80% of our planet's freshwater exists as polar ice caps [*Ferrigno, et al.*, 2002]. As the human population grows and water becomes an invaluable resource for global sustainability, ice caps may provide the answers to future water sources for the planet.

The extent of ice cap and ice sheet coverage over the Earth has varied throughout Earth's history. Many terrestrial landforms exist as a result of ice sheet advances and retreats. The extent of ice on the surface of the Earth varies as a function of surface temperature, and has a direct influence on the climate feedback cycle [*Alley*, 2000]. Experimental and theoretical investigations of how ice-sheets develop and change form a critical component in understanding climate variation. Using experimental research to constrain and enhance ice-sheet modeling has been a valuable method for furthering knowledge of ice rheology [*Hubbard*, 1999].

This dissertation describes three laboratory and experimental techniques in ice-deformation research. It is divided into three sections. I used the techniques of low-temperature scanning electron microscopy (LTSEM) and neutron diffraction. I examined the evolution of grain growth under static conditions, the development of crystal-orientation (fabric), otherwise known as texture throughout this work, in bulk, fine-grained (2-10 μm) laboratory-synthesized, deuterated (D_2O) ice samples, and the measurement of texture of polycrystalline ice aggregates. I used neutron diffraction to measure the quantitative textures in the bulk-deformed samples, and LTSEM to quantify the degree of grain growth in each statically annealed sample. I also built an *in situ* deformation apparatus to use with neutron diffraction. This apparatus allows for real-time deformation concurrent with neutron diffraction. To date, this is the only *in situ* deformation apparatus for use with neutron diffraction with the capability to collect data at low-temperatures (and no confining-pressure requirements) of its kind in the world.

1.1.1 Deformation of Ice I_h

The standard deformation mechanisms of ice I_h have been well characterized for ice larger than 250 μm [*Ashby and Duval*, 1985; *Duval, et al.*, 1983; *Goodman, et al.*, 1981]. In this dissertation I refer to ice I_h as ice. Polycrystalline ice deforms by inter- and intra-crystalline creep [*Glen*, 1955] and a strong preferred crystallographic orientation develops as c-axes (0001) rotate to become parallel with the direction of compression [*Doake and Wolff*, 1985; *Duval*, 1979; *Gow and Williamson*, 1976; *Kamb*, 1972]. At the microscopic level, individual grains of ice deform as dislocations slip and climb through the crystal lattice, in a process known as dislocation creep.

The rheological properties of ice are affected by many variables. For example, impurities in ice sheets are known to limit grain growth; polycrystalline material of smaller grain size may be dominated by different deformation mechanisms than its large-grained counterpart. Texture can also influence deformation behavior [*Alley*, 1992; *Humphreys and Hatherly*, 1995]. Ice flow has been modeled since 1958 using a form of the polycrystalline flow law (Eqn 1.1), known as Glen's law [*Glen*, 1958]. A form of the flow law of isotropic polycrystalline material is

$$\dot{\varepsilon}_{xy} = A d^{-m} \sigma_{xy}{}^{n} e^{-(E^*+PV^*)/RT},$$ (1.1)

Where $\dot{\varepsilon}_{xy}$ is the simple-shear strain rate, P is pressure or the mean stress, d is grain size, m is the grain size exponent, T is temperature, R is the gas constant, E^* is the activation energy, V^* is the activation volume, $A = A_o \ exp \ (-Q/(RT))$ and is a materials parameter, σ_{xy} is the simple-shear deviatoric stress, and n is the stress exponent.

The generalized tensor form of the isotropic Glen's flow law is

$$\dot{\varepsilon}_{ij} = A \tau^{(n-1)} \sigma_{ij}$$ (1.2)

In Glen's representation of the law (Eqn 1.2), $\dot{\varepsilon}_{ij}$ is the strain-rate tensor, τ is the second invariant of the stress-deviator tensor, and σ_{ij} is the deviatoric stress tensor. The materials parameter A may be modified by factors such as temperature,

pressure, grain size, impurities, salinity, and other factors. Experimental data have determined an average value of $n = 3$ [*Weertman*, 1973].

Models of flow in polycrystalline ice have routinely used Glen's law and have closely predicted ice behavior in the past [*Azuma*, 1994; *Dahl-Jensen*, 1989; *Reeh*, 1988]. Most models assume a stress exponent (n) value of 3 (Eqn. 1.2) [*Paterson*, 2001] with the intra-crystalline deformation mechanism of dislocation creep being favored at high stresses and low temperatures [*Duval, et al.*, 1983]. Recent research has explored some of the conventional parameter choices made in this modeling; for example, some models show alternatives to Glen's law [*Azuma*, 1994; *Castelnau, et al.*, 1998]. Using n = 3 for the stress exponent implies that dislocation creep is the dominant deformation mechanism and that the contribution to deformation from other deformation mechanisms is very small.

In fact, natural conditions for ice sheets include low deviatoric stress (10^4-10^5 Pa) and temperatures that vary with depth [*Paterson*, 2001]. These conditions should activate other deformation mechanisms available to polycrystalline ice, including grain boundary diffusion, lattice diffusion and grain boundary sliding (GBS) [*Paterson*, 2001]. In the first process, material diffuses along grain boundaries, in the second it diffuses through the bulk of the material, while the third comprises slip of rigid grains along grain boundaries. During GBS, stress accumulates at triple junctions and other places along the grain boundary. This stress is possibly relieved by grain boundary migration, diffusion, and/or slip [*Sherby and Wadsworth*, 1989], with accommodation by slip seeming to fit the data best [*Nieh, et al.*, 1997].

Of particular interest to this study are grain-size-sensitive (GSS) creep mechanisms ($m \neq 0$ in equation 1.1), which depend on the presence of grain boundaries in materials. For GSS creep, the stress exponent, n, in equation 1.1 and 1.2 usually has a value of approximately 2 [*Goldsby and Kohlstedt*, 1997, 2001; *Goodman, et al.*, 1981; *Weertman*, 1973]. GSS creep is deformation that is typified by GBS and grain-boundary diffusion acting in concert. Recent work suggests that fine-grained ice may deform by GSS creep under conditions of low applied stress (<0.1 MPa) [*De Bresser, et al.*, 1998; *De Bresser, et al.*, 2001; *Durham and Stern*, 2001; *Durham, et al.*, 2001; *Goldsby and Kohlstedt*, 1997; *Pappalardo, et al.*, 1998] and that GSS creep (and other processes) may be significantly contributing to ice sheet deformation. All of these deformation mechanisms, and perhaps others, normally operate simultaneously under applied stress during deformation of ice. In order to accurately represent the deformation mechanisms that may be active in ice flow, models of ice flow may need to include a different value of the stress exponent, varying between 1 (diffusion) and 3 (dislocation creep) [*Duval*, 1973], with GSS creep ($n = 2$) laying in between these endmembers.

Moreover, few models include grain size or account for impurities [*Pettit and Waddington*, 2003]. Impurities have been shown to cause grain growth impingement (where grains cease to grow because their boundaries encounter an obstacle) in certain types of ice, such as ice deposited during the last ice age (which ended approximately 10,000 years ago) [*Alley, et al.*, 1986a]. Impurities such as H_2SO_4 [*Mulvaney, et al.*, 1988] and others [*Baker, et al.*, 2003; *Souchez and Lorrain*, 1991; *Wyttenbach, et al.*, 1977] have been detected at three-grain junctions in Antarctic ice. Increased impurity concentrations may cause grain-size sensitive deformation mechanisms in these ices [*Cuffey, et al.*, 2000b]. Also, small grain sizes resulting

from chemical impingement may also be the source of strong texture development [*Paterson*, 1991], and modify Glen's law through the '*A*' material parameter. If small grains deform differently than large grain sizes in ice sheets, different deformation mechanisms (n = 1 - 3) may need to be considered when modeling ice sheet flow.

1.2   Motivation and Goals

Grain size typically increases with depth in an ice sheet [*Gow*, 1969], and typical ice grains are on the order of 1 mm or larger [*Paterson*, 2001]. However, as noted above, grain size can be constrained by impurities, which prevent grains from growing. Recrystallization can make grain size smaller.

Extrapolation from laboratory experiments to models of ice deformation has increased in the last decade with the advent of new laboratory techniques to create a small initial grain size (2-10 μm) and with advanced computer-processing capabilities. Historically, glaciologists performed deformation tests on ice samples from ice cores collected from ice sheets. These natural grains have a narrow distribution of grain size and are on the order of 1 mm in average size. As a result, models of ice sheets do not incorporate grain size.

I used fine-grained (2-10 μm) ice in these laboratory experiments for several reasons: 1) smaller grain sizes make experiments possible in a laboratory time-scale (several days) since a grain-size dependent strain rate is faster at smaller grain size (Eqn. 1.1), 2) investigation of the grain growth law of ice over several orders of magnitude, 3) grain-size-sensitive (GSS) deformation regimes can be explored, and

4) investigation of the theory that under certain conditions the grain size of an ice sheet may exist in a balance controlled by deformation processes.

If fine-grained ice is to serve as an analog for the larger-grained ice that is common in the natural environment, the two must exhibit similar rheological behavior. In this study, I investigated the growth law of ice to ascertain whether or not it can be extrapolated over several orders of magnitude. To date, it remains uncertain whether large-grained natural ice I_h and fine-grained laboratory ice I_h obey the same growth law.

In addition to grain size, texture is also an important property that affects rheological behavior. Texture is a quantity that may describe the degree (rotation and direction) of intracrystalline slip of lattice planes within a polycrystalline sample. Such a property may affect Glen's law. In the case of intracrystalline slip, the material may be anisotropic (or behave differently in different lattice ($hkil$) directions), and show different modeling values, depending on the crystallographic orientation distributions.

Ice cores show that ice sheets are textured at depth, with c-axes often becoming oriented perpendicular to the surface [*Alley*, 1992; *Budd and Jacka*, 1989; *Duval, et al.*, 1983; *Glen*, 1955; *Kamb*, 1959]. Additionally, grain growth may be strongly affected by texture. Highly textured materials have many low-angle boundaries, and therefore a reduced driving force for grain growth [*Humphreys and Hatherly*, 1995].

The goal of this dissertation is to study the contributions of GSS creep to the deformation of ice I_h by investigating the microstructural properties of fine-grained ice. I do this by 1) the study of grain growth and 2) the examination of texture development in fine-grained ice during ice deformation experiments. In this work I address the following questions: Do the laws of grain growth for ice extrapolate over several orders of magnitude of grain size? Is texture development different under conditions of GSS creep or dislocation creep? If so, does texture need to be incorporated as a separate set of parameters in models of ice flow? Do the results of experiments on fine-grained ice in the laboratory apply to ice in the natural environment?

In this dissertation I use three techniques to investigate the rheological behavior of fine-grained ice: LTSEM, the technique of neutron diffraction texture analysis, and *in situ* deformation with neutron diffraction for texture analysis. LTSEM and texture measurements, when used in conjunction with deformation mechanism flow models of ice (not presented here), can be used to distinguish between GSS and dislocation creep.

1.3   Low-Temperature Scanning Electron Microscopy

LTSEM is used to make grain-morphology measurements in 2-dimensions. Samples can be characterized for grain size and grain shape. Features such as triple- and four-grain junctions can also be identified. Grain size measurements are used to calculate growth rates of the fine-grained ice. Measurements are also made to document change in grain-axes lengths and to calculate grain-aspect ratios. These

measurements are used in this dissertation to quantify the amount of change in grain-axes lengths as a result of total strain of the sample.

1.4   Neutron Diffraction

Neutrons are well suited to investigate texture in materials because, unlike X rays, they have low absorption and can investigate bulk (on the order of centimeters) samples nondestructively. Neutrons easily penetrate many materials used in environmental cells. Because neutrons scatter from hydrogen incoherently, replacing deuterium for hydrogen decreases the absorption cross-section by a factor of 1000, making deuterated ice almost as transparent as aluminum, which is one of the most transparent materials to neutrons.

This dissertation uses a type of scattering called diffraction, in which coherently scattered waves interfere. During diffraction, a beam of neutrons is aimed at a given sample (ice). Polycrystalline materials, like ice, are composed of many grains and each grain has its own crystal lattice orientation. The neutron beam penetrates the sample and interacts with each atomic site on a lattice, or with each nucleus in the regular structure of a lattice. Detectors placed around the sample identify the neutrons that are scattered from the nucleus sites. The physics of diffraction is described by Bragg's Law which is written:

$$n\,\lambda = 2\,d\,\sin\theta \qquad\qquad (1.3)$$

where n is an integer, λ is the wavelength of the incident beam, d is the distance between lattice planes, and θ is the angle between the incident neutron beam and the

lattice planes. The waves reflected from nucleus sites will reinforce each other only in particular directions that are determined by the symmetry and spacing (known as the d-spacing) of the lattice. Bragg's law is used to determine the relation between atomic planes in grains and the angles of incidence at which these planes produce the most intense reflection of neutron particle waves. Deuterated ice samples provide strong coherent backgrounds for diffraction patterns where details such as particle size, strain broadening and texture can be extracted from multiple diffraction patterns.

1.4.1   Texture

Historically, the study of crystallographic texture, i.e., crystallographic or lattice-preferred orientation (LPO), in minerals and rocks dates back to the work of D'Halloy [*D'Halloy*, 1833] who concluded that the alignment of grains was an indicator of the formation process of rocks. Naumann [1850] first used the term "texture" to describe this alignment. While the field of texture analysis has long thrived in the Earth and material sciences, in the last 20 years texture measurement using neutron scattering has gained attention in the Earth sciences [*Wenk*, 2002].

Texture is a characteristic that is imparted to a material, through deformation, during recrystallization or from phase transformations [*Wenk and Van Houtte*, 2004]. The physical influences of texture are apparent in physical properties such as strength, electrical conductivity, wave propagation, deformation and anisotropy, among others [*Kocks, et al.*, 1998].

Geologists showed the importance of texture in flow models as early as 1964. The relationship between texture and flow was studied in olivine single crystals to

understand observed seismic anisotropies in the upper mantle [*Francis*, 1969; *Hess*, 1964].

Recently, several models have been advanced to characterize texture development in ice and to demonstrate anisotropic flow behavior [*Castelnau, et al.*, 1997; *Montagnat and Duval*, 2004; *Thorsteinsson*, 2002]. Experimental investigations to accompany and constrain these models have been difficult to perform in the past. Traditionally, glaciologists (both in the field and the laboratory) have made thin sections of samples and then counted grain orientations using an optical stage with cross-polarizers. This method is time-consuming and yields a low count of total grains, several hundred on average. Recently, an automatic ice fabric analyzer has improved this procedure [*Wilen*, 2000].

In the last decade, geoscientists have started to take advantage of the availability of neutrons for bulk material analysis. With the recent availability of cutting-edge neutron spectrometers and environmental cells for low-temperature measurements, a new tool is accessible for experimental work with ice. The great advantage of neutron texture measurement is fast data collection (a few hours) and bulk analysis that can measure the orientation of approximately 100,000 to 500,00 grains depending on sample size and experimental setups.

A standard quantitative method of representing texture is attained through stereographic or equal area projection. A vector perpendicular to the plane, referred to as a pole, can identify a crystallographic plane. A pole figure may be represented in a stereographic projection as a density distribution of a given pole to a chosen sample reference frame. For monochromatic neutrons, such as those from a reactor

source, a goniometer is often used to rotate a sample in the neutron beam to collect data on multiple scattering angles (or multiple d-spacings/lattice planes, i.e. See Braggs law Eqn 1.3), and a pole figure is collected based on the sample reference frame. With time-of-flight (TOF) neutron sources and a radial array of detectors (provides a detailed pole figure coverage), texture can be measured without sample rotation. In both cases, one measures intensities of neutrons diffracting from lattice planes. Intensities are then interpreted as pole densities on a pole figure. From these pole figures, the orientation distribution function (ODF) is calculated. The ODF is an orientation probability distribution that gives the probability that a specific lattice orientation is present in a sample. Once the ODF is calculated, any set of discrete crystallographic planes can be examined as a pole figure.

1.5   *In Situ* Deformation and Texture Measurement

Typically, samples are measured for texture and strain characterization after they have been deformed in a separate deformation apparatus. This type of data analysis is hindered by experimental error and is limited in direct observation of the deformation mechanism and texture development. I built an *in situ* low-temperature, deformation apparatus for neutron spectroscopy to investigate deformation and strain simultaneously and to quantitatively document deformation behavior (i.e. Strain steps, regime changes, texture) directly, and at the crystallographic level. I used the unique TOF neutron diffractometer HIPPO (High-Pressure Preferred Orientation) at the Los Alamos Neutron Science Center (LANSCE) offers an efficient way to perform texture analysis without rotating a deformation rig. This apparatus is unique in that the ability to uniaxially deform ice *in situ* during neutron diffraction does not exist anywhere in the world.

1.6 Synopsis

This study uses three different experimental methods in applications that are new to glaciology. I show that these experimental techniques each present a great advance for the fields of glaciology and ice mechanics. This dissertation also demonstrates that these innovative techniques expand the possibility of furthering the current understanding of ice rheology. My dissertation is divided into 3 sections.

Chapter 2 documents the growth rate of fine-grained ice. Six samples are statically annealed under temperature conditions of 226 – 240 K. I used low-temperature scanning electron microscopy (LTSEM) to image the ice samples. I measured grain growth rates from the grain size distributions and calculated an activation energy for fine-grained ice growth. I compared this value to that established by [*Gow*, 1969] for field data. I also extrapolated Gow's law to my fine-grained ice samples and compared the resulting growth rates to those derived from my experiments. Finally, I assessed whether fine-grained ice is a suitable analog for natural ice.

In Chapter 3, I discussed the possible contributions of GSS creep to ice sheet flow and the impact of the results on the deformation mechanism map for ice. I deformed 3 samples of fine-grained ice at temperatures of 222 – 226 K under conditions of low stress to investigate dominant deformation mechanisms. I examined the microstructure of the fine-grained ice samples with LTSEM. I used neutron diffraction on the deformed samples to measure the first quantitative texture data on fine-grained ice. I addressed a controversy in glaciology and rock mechanics

over texture development during grain-size-sensitive (GSS) creep. I also discussed the implications of these deformation test results for the deformation mechanism map of ice I_h.

In Chapter 4, I presented a deformation apparatus that I designed to perform *in situ* texture measurements using neutron diffraction to measure texture development in ice as a dynamic process. Advances in neutron science now make it possible to explore *in situ* texture development at low-temperature. This deformation apparatus is for use in the neutron diffraction instrument HIPPO (High Pressure Preferred Orientation) at the Los Alamos National Laboratory. Information on bulk texture can provide insight on how texture develops as ice undergoes deformation. I experimentally quantified the texture development in one laboratory polycrystalline ice sample. I showed that deforming unconfined ice *in situ* is a fast and accurate way to experimentally measure developing textures in ice.
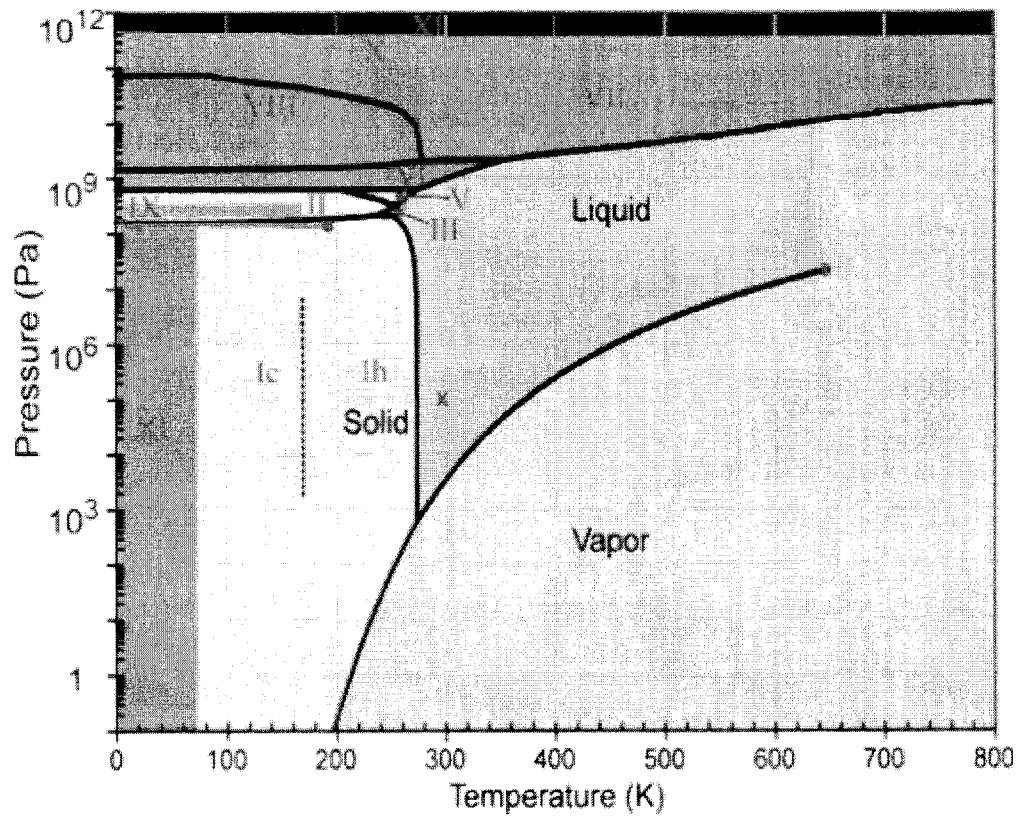
Figure 1.1. The phase diagram of ice showing phases I – XI. Amorphous phases and Ice XII are not shown. http://www.lsbu.ac.uk/water/phase.html.

Chapter 2

Grain Growth in Polycrystalline Fine-grained Ice I_h

2.1   Summary

Deformation and flow of polycrystalline ice crystals in ice sheets and glaciers may depend strongly on crystal size and temperature. We performed static annealing experiments on laboratory-grown, fine-grained polycrystalline ice I_h to investigate the rate of grain growth. Fine-grained (2-10 μm) disks of ice (25 mm diameter x 5 mm thick) were encapsulated and then annealed in a low-temperature bath. Temperature was varied from 226-240 K and annealing durations from 1 – 91 hours. Low-temperature scanning electron microscopy (LTSEM) was used to measure grain size. Grain growth rates are an order of magnitude larger than predicted by Gow [1969]. Differences in the measured and expected growth rates can be attributed to differences in the pre-exponential factor (K_o).

2.2 Introduction

Understanding of ice sheet and glacier flow has evolved in complexity over recent years. Over the last decade, specific attention through experimental work and modeling in ice has focused on the effect of grain size on ice rheology [*Budd and Jacka*, 1989; *Cole*, 2001; *Cuffey, et al.*, 2000a; *Cuffey, et al.*, 2000b; *Durham and Stern*, 2001; *Durham, et al.*, 2001; *Duval and Montagnat*, 2002; *Goldsby and Kohlstedt*, 1997, 2001; *Peltier, et al.*, 2000; *Stern, et al.*, 1997]. In this paper, we use the term "grain" to refer to a single crystal of ice in a polycrystal. This study investigates the growth rate of fine-grained ice (2-10 μm). We evaluate the extrapolation of the current growth law, which is derived from natural ice samples, to smaller grain sizes, such as those used in laboratory research.

Many researchers have proposed theories for grain growth, yet grain growth is complex and no one theory is widely accepted. Atkinson [1988] reviewed the various approaches. During normal grain growth, the form of the grain size distribution is time invariant and the overall mean grain size increases [*Atkinson*, 1988]. In polycrystalline materials under static conditions, crystal growth can be driven by surface energy [*Humphreys and Hatherly*, 1995; *Jessell, et al.*, 2003]. In a three-dimensional (3-D) array of grains, no regular grain structure with plane sides and appropriate angles between grains exists in nature [*Humphreys and Hatherly*, 1995]. Thus, grain boundaries must curve to meet equilibrium requirements at grain junctions, resulting in non-equilibrium angles. Grains will grow to minimize their total surface energy or to reduce the total interfacial area of the aggregate (Evans et al., 2001).

Grain boundaries are defined as planar defects, regions that separate 2 grains having different lattice orientations [*Novikov*, 1997]. Grain size can increase in two different ways: (1) Normal (or continuous) grain growth, during which all the crystals grow in a uniform way; (2) abnormal (or discontinuous) grain growth, consisting in an exaggerated growth of only a few larger grains at the expense of the many smaller ones [*Gottstein and Shvindlerman*, 1999; *Humphreys and Hatherly*, 1995].

For normal grain boundaries, the driving force (P) is determined by

$$P = \gamma \, C_{gb}, \qquad\qquad\qquad (2.1)$$

where γ is the surface energy density of a grain boundary (units of $J \cdot m^{-2}$) and C_{gb} (units of m^{-1}) is the grain boundary curvature (Novikov 1997), with the driving force equal to the energy per unit volume of aggregate ($J \cdot m^{-3}$). The driving force has units of stress ($N \cdot m^{-2}$), but is conventionally referred to as a force [*Alley, et al.*, 1986a]. As grain size increases, the ratio of surface area to volume decreases and the curvature decreases. The grain boundary curvature produces a surface tension that causes a chemical potential across the boundary. Surface tension is higher on smaller grains because curvature tends to be higher. This results in a migration of atoms from smaller to larger grains. Small grains will shrink because they have a high surface energy per unit volume. Thus, grain growth is driven by a combination of curvature and surface energy.

Grain size in ice sheets and glaciers has historically been neglected in ice-flow modeling [*Cuffey, et al.*, 2000b]. However regions of smaller grain size may help to

explain flow rheology in ice-age ice [*Paterson*, 1991]. Some ice-flow models use a scalar "enhancement" factor, E, to account for poorly known variables, such as texture and grain size [*Paterson*, 1991]. When it is included in flow models, grain size in ice sheets and glaciers is usually represented by an average size, which is on the order of 1 mm and larger [*Paterson*, 2001]. In their paper on Meserve Glacier, Cuffey et al., (2000a) demonstrate that in fact those models may be too simplistic when addressing some ice-flow questions, and grain size should be employed as an independent variable in modeling on some spatial and temporal scales.

It is widely accepted that ice grains grow by grain-boundary migration [*Alley*, 1992; *Alley, et al.*, 1986b; *De La Chapelle, et al.*, 1998]. Following the precedent set by the metals and ceramics community [*Burke and Turnbull*, 1955] with his research on polar firn, Gow [1969] established in the ice literature the currently accepted form of the grain-growth equation

$$D^2 = D_o^2 + Kt \tag{2.2}$$

where D is the measured mean cross-sectional area, D_o is the mean cross-sectional area at time zero, K is the growth rate of the grains, and t is time. K follows an Arrhenius type equation

$$K = K_o \exp(-E_a/RT) \tag{2.3}$$

where K_o is a constant, E_a is the activation energy of grain growth, R is the gas constant and T is temperature.

Gow's research was conducted on samples from snow mines and ice cores from several locations in Antarctica and Greenland. In order for laboratory research to occur on a short time scale (on the order of days), we conduct many experiments on ice with a much finer grain size. Equation 1.1 shows that a grain-size dependent strain rate is faster for smaller grain sizes (d in eqn 1.1). If fine-grained ice is to serve as an analog for the larger-grained ice that is more typically found in the natural environment, it must exhibit rheological properties similar to those of larger-grained natural ice. To date, no documentation exists confirming that the same processes operate for both large-grained natural ice I_h and fine-grained laboratory ice I_h.

An experimental approach to systematically study grain growth is needed to test the extrapolation of Gow's growth equation to other grain sizes. In this paper we document the growth rates of fine-grained (2-10 μm) laboratory-synthesized polycrystalline ice I_h samples through a series of static annealing experiments. We compare our grain-growth rates with those predicted using Gow's [1969] coefficients in Equations (2.2) and (2.3) to evaluate the extrapolation of Gow's results over several orders of magnitude.

2.3   Methods

Six static-anneal experiments were performed at atmospheric pressure, at temperatures of 226 to 240 K and annealing times up to 91 hours (Table 2.1). Initial grain size was reduced to 2-10 μm by a procedure established by Stern et al (1997), where an ice sample is converted to ice II by pressurizing to 300 MPa. The sample is held for 15 minutes and converted quickly back to ice I by a fast venting of gas (< 3 s to 50 MPa). Low-Temperature Scanning Electron Microscopy (LTSEM)

substantiated the yield of dense ice with porosity < 1 %. LTSEM verified that the ice had equant grain shapes and a uniform grain size of approximately 2-10 µm, with a homogenous and isotropic size (Figure 2.1) [*McDaniel, et al.*, 2002; *Stern, et al.*, 1997].

Samples were sectioned into disks that were 5 mm thick. Aluminum cans were constructed with lids bearing low-temperature o-rings. Samples were placed inside the aluminum cans and sealed tightly to prevent leakage from the low-temperature bath. The low-temperature fluid bath from Hart Scientific has a 44-liter capacity and a programmable temperature regulation from 188 to 300 K to a rms deviation of less than 0.1 K. When monitored for temperature deviation, we found no horizontal or vertical gradient in the bath. The cans were suspended in the low-temperature bath at the same height across the bath to ensure a uniform temperature for all samples.

Upon removal from the bath, samples were stored in an ultra-low temperature freezer at approximately 188 K. In preparation for LTSEM, a small section of each sample (0.75 x 0.75 x 0.5 cm) was mounted with clamps in a brass sample holder. The sample holder has a thin floor to maintain close thermal contact with the stage on which it is mounted. Samples were quickly transferred in liquid nitrogen (LN_2) to the Gatan Alto 2100 low-temperature preparation chamber (evacuated and pre-chilled below 100 K), which was in turn attached to a LEO 982 field emission SEM. A scalpel was used to fracture the sample and remove a piece of surface ice, exposing fresh ice for scanning. This step is necessary to remove any deposits of condensation, as well as any material that may have reacted with the atmosphere during transfer to

the preparation chamber of the LTSEM. This step also allows us to avoid grains whose growth rates may have been altered by proximity to the sample surface.

After we fractured the ice, we transferred samples under vacuum directly into the SEM scanning chamber. The sample temperature was continuously monitored by thermocouples placed in the sample stages of both the preparation chamber and the SEM chamber. Imaging was conducted at temperatures below 105 K and vacuum below 10^{-5} mbar, using low voltage (≤ 3 kV) to minimize sample alteration or beam damage to the sample surface [*Stern, et al.*, 2004].

Grain size distributions were measured from the LTSEM photomicrographs using the Scion Image-processing package (Scion Corporation). Grains were manually outlined and approximated as ellipses. A best-fit ellipsoid major and minor axis was identified for each grain and used to estimate grain cross-sectional area. The mean and median grain sizes were calculated for each sample (Table 2.1).

2.4   Results

Figure 2.3 shows a SEM photomicrograph of ice annealed at 226 K for 1 hour and Figure 2.4 shows ice annealed at 226 K for 91 hours. An example of an outline of these images, as done in the image analysis program SCION Image, is shown in Figure 2.5. We calculated growth rates (K) from equation (2.2) based on the mean grain areas in Table 2.1. Figure 2.2 shows mean grain-growth rates as a function of inverse temperature.

Grain-size distributions of the raw data are shown in Figure 2.6 (a-g). All samples show increasing average grain size. Figure 2.7 shows the distributions

normalized by the mean grain area and the total grain count of each sample. Normal grain growth is indicated by the log-normal distribution and the increased mean grain area of each sample [*Granqvist and Buhrman*, 1976]. The log-normal distribution is defined as a random variable whose logarithm has a normal distribution [*Moran*, 1968]. Figure 2.8 shows the fit of our grain-size data to a log-normal distribution.

In order to test the accuracy at fine grain size of the proposed growth law for ice [*Gow*, 1969], we compare our measured growth rates to growth rates predicted by Gow's work, using his activation energy of 48.57 kJ mol^{-1} and his counting methods. Gow measured the area of the largest 25% grains of each section, based on his decision that the smaller grains visible in a 2-dimensional (2-D) section are not representative of the overall grain size of the ice cores. For comparison purposes, we calculated the growth rates for each sample using only the 25% largest grains. The results are shown in Table 2.2. Grain-size distributions for the largest 25% grains in our samples are shown in Figure 2.9. All samples show growth rates faster than those predicted by Gow (Figure 2.10).

2.5 Discussion

After annealing for many hours, the grain-size distributions are consistent with normal grain growth [*Humphreys and Hatherly*, 1995]. Because the grains in the initial material fall in a narrow size-distribution range, some time must pass during which some grains get smaller and approach their vanishing point, while other grains grow before the average grain size can change appreciably. Inevitably, some grains shrink quickly because they are small.

The distributions of grain sizes in samples annealed for short time periods (1 and 6 hours) do not show significant grain growth. These samples have little to no change in mean grain area (Table 2.1). The median values of these samples are less than that of the initial material. The low median values of these distributions indicate that the relative fraction of grains with smaller cross-sections remains high.

These samples are affected by an initial period of transient grain-size adjustment. During transient grain-size adjustment, the grain-size distribution shows an initial increase in the fraction amount of both smaller and larger grain sizes. Overall, the mean grain size may not increase as expected with normal grain growth; in fact, the mean grain size may change very little or not at all. This is because many grains are shrinking, but have not yet vanished. The transient grain-size adjustment period may occur in some settings in the natural environment, such as in newly fallen snow or in ice grains undergoing rapid recrystallization as they move into warmer regions deep in an ice sheet. Usually this initial transient period can be neglected for the purposes of understanding grain growth in ice in an icesheet.

However, there are some experimental factors that may affect our samples and contribute to the transient grain-size adjustment period. First, several microstructural properties of our initial material remain uncharacterized. The pressure-release technique used to create the samples may impart a non-random starting crystallographic preferred orientation, or texture, to our samples. This technique may also create a variable distribution of dislocation densities in the samples. These factors may influence the driving force for grain growth [*Humphreys and Hatherly*, 1995]. Second, there may be a period of time required for the samples to reach the set annealing temperature in the low-temperature bath. The samples are stored at a

temperature of 190 K and placed directly into the bath. The samples must increase approximately 30 – 50 degrees K to reach the set annealing temperature. The temperatures of the samples could not be directly measured in these experiments. Short annealing durations may not have allowed enough time for the samples to equilibrate with the temperature of the bath and as a result grain growth may be slower than expected in these samples.

Conversely, samples annealed for longer durations (23 hours +) have at least roughly doubled in mean grain area (Table 2.1), and also display the log-normal size distribution characteristic of normal grain growth (Figure 2.8). We might expect that the size distribution cannot migrate from the narrow distribution characteristic of the initial material, to the log-normal shape characteristic of normal grain growth until at least half of the molecules in a sample have crossed grain boundaries. This could correspond to at most a doubling of mean grain size. It is expected that the transient period is shorter at warmer temperatures, where grain growth is faster, than at cooler temperatures. More experiments are needed to verify that the transient grain-size adjustment period has run its course when mean grain size has doubled under a range of initial conditions. This corresponds to between 6 hours and 23 hours of annealing at the initial grain size and temperature in our experiments.

To get a lower-bound estimate of the normal growth rate, we neglect the impact of the initial transient period during which growth rates are slow. Our measured growth rates are still more than an order of magnitude faster than those predicted by using Gow's equation with his experimentally determined parameters, when we compare them using his methods (using only the largest 25% grains from each sample) (Figure 2.9). In order to represent the entire sample, we examine the

growth rates as predicted by all of the grain areas in each sample, not just the 25% largest grains. Using our measured grain area data for samples that have achieved steady growth (those that have more than doubled in mean grain area), we compared the mean grain area from all of the grain areas in each sample with the mean grain area of the subset of the largest 25% grains. On average, the ratio between these values is approximately 0.39 (with a standard deviation of ± 0.06). We multiplied Gow's mean grain area by this ratio and extracted a new value for D and D_0 from equation 2.2, and the activation energy and K_0 from equation 2.3. We used these values to predict the expected growth rates for our samples based on the coefficients derived from Gow's data (Table 2.3).

Figure 2.11 shows the growth rates from Table 2.3 and our measured growth rates for our samples. Our measured growth rates for all of the grains in each sample are approximately an order of magnitude faster than those predicted by Gow. The measured growth rate data show that Gow's equation does not extrapolate well to fine-grained size. Since the growth rates are faster than predicted by Gow's grain-growth equation, and since different growth mechanisms may be occurring in fine-grained ice, it would not be surprising if the activation energy might have a different value. However, using regression analysis on our measured steady growth rates, we calculate the activation energy of grain boundary self-diffusion to be 51 kJ mol^{-1} ± 15 kJ mol^{-1}, which matches Gow's calculation of 48.5 kJ mol^{-1}, and other published values of activation energy [*Paterson*, 2001].

In its simplest form, Gow's grain-growth equation does not extrapolate well to fine-grained size. However, we have found that while the measured growth rates are faster than those predicted by Gow's equation, the activation energies are

comparable. This indicates that for both natural ice and our fine-grained ice, grain growth is a function of thermal activation. We suggest that the differences in the measured and expected growth rates can be attributed to differences in the pre-exponential factor (K_o) of equation 2.3.

The pre-exponential factor K_0 could be affected by several factors, such as impurities, bubbles, texture of grains, and grain shape. Gow's study used samples from polar firn. Impurities such as H_2SO_4 [*Mulvaney, et al.*, 1988] and others [*Baker, et al.*, 2003; *Souchez and Lorrain*, 1991; *Wyttenbach, et al.*, 1977] have been detected at three-grain junctions in Antarctic ice. It is known that impurities can limit grain growth [*Humphreys and Hatherly*, 1995]. Conversely, our fine-grained ice has very little to no impurity content. As mentioned earlier, the initial texture of the fine-grained ice is not characterized, and texture can influence grain growth [*Humphreys and Hatherly*, 1995]. A strong texture is sometimes correlated with the presence of many low-angle grain boundaries, which have a reduced driving force for grain growth. Another influence on grain growth is grain shape. Our samples have only been characterized only in two dimensions. Three–dimensional analysis would reveal whether the grains in our samples have any axes of non-equant length, which would make the grain shapes non-equant and possibly affect grain growth. Finally, the ice in Gow's study was from a dynamic setting (interior of an ice sheet), while our samples are annealed under static conditions.

Further analyses to explore these possible effects on grain growth are beyond the scope of this study. Primarily, it is important to characterize the properties mentioned above in the initial ice samples before annealing, in order to correctly interpret the growth rates of annealed samples. It is likely that some or all of these

factors may influence the pre-exponential factor in equation 2.3. In order to accurately extrapolate Gow's growth equation to grain sizes outside of his study, we must further explore the microphysics contained in the pre-exponential factor.

Our experiments provide the first published data that are suitable for the calculation of the growth rates of fine-grained (2-10 micron) hexagonal ice. More measurements of growth rates between 220 K and 240 K would improve our understanding of grain-growth processes. In order to better understand the transient grain-size adjustment period, future work should include experiments to investigate growth rates and size distributions at intermediate times before the mean grain size doubles.

This investigation has implications for understanding the deformation of glacial ice. While this study has focused on grain growth under static conditions, we also need to understand the growth of fine-grained ice under the dynamic conditions of deformation. For example, the dominant mechanism of deformation in ice may vary as a function of grain size [*Budd and Jacka*, 1989; *De Bresser, et al.*, 1998; *De Bresser, et al.*, 2001; *Durham and Stern*, 2001; *Duval, et al.*, 2000; *Goldsby and Kohlstedt*, 1997, 2001; *Montagnat and Duval*, 2000].

In order to test the effect of grain size on deformation rates, *in situ* testing of ice samples using neutron scattering could provide valuable, non-destructive measurements. Grain size and other parameters can be monitored as the ice deforms, with instantaneous data. This capability would provide data that have not previously been attainable, improving our understanding of ice deformation and rheological

properties of ice sheets. This *in situ* deformation apparatus is now available *[McDaniel, et al., 2005]*.

2.6   Conclusions

Our results are significant in establishing grain growth rates for fine-grained ice under conditions of atmospheric pressure and temperatures as applicable to natural ice settings, such as in glaciers and ice sheets. Further analyses should be performed for longer annealing times and more temperatures to refine the activation energy value. Differences in the measured and expected growth rates can be attributed to differences in the pre-exponential factor (K_o). More experiments are needed under a range of initial conditions to verify that the transient grain-size adjustment period has run its course when mean grain size has doubled. These results should be considered when employing fine-grained laboratory ice as an analog for ice in the natural environment. Further work is needed to extend our understanding of grain growth to dynamic growth conditions.

Table 2.1. Statistics of cross-sectional areas of grains in 6 annealed ice experiments. T is temperature in Kelvin and Duration is annealing time in the low temperature bath. Samples are listed in order of increasing temperature, beginning with the initial material for reference.

Sample	T (K)	Duration (Hr)	Mean Grain Area (μm^2)	Standard Deviation (μm^2)	Median (μm^2)
Initial Material	200	0	**19.74**	± 13.82	**17.84**
SAI1	226	1	16.92	± 19.88	9.91
SAI3	226	91	48.51	± 57.43	32.26
SAB4	230	6	22.54	± 28.25	13.46
SAD1	234	1	21.02	± 21.47	14.37
SAD3	234	54	92.77	± 127.56	51.00
SAC4	240	23	52.31	± 52.84	36.52

Table 2.2. Measured and predicted growth rates using 25% largest crystals. Predictions used Equation 2.3 with Gow's (1969) parameter values for activation energy (48.6 kJ/mol^{-1}) and pre-factor K_0 (5.3 x 10^6), for grain sizes and temperatures in this study. Because Gow used only the 25% largest grains in each of his samples, here we also calculate our growth rates from the largest 25% grains in each sample.

Sample	T	Gow's K (10^{-4} μm^2/s)	K (10^{-4} μm^2/s) (Calculated elliptical area)
SA	200	0.000	N/A
SAI1	226	0. 311	10.6
SAI3	226	0. 311	2.4
SAB4	230	0. 487	7.9
SAD1	234	0. 753	33.5
SAD3	234	0. 753	10.0
SAC4	240	1.405	10.3

Table 2.3. Measured and predicted growth rates using all crystals. Growth rate is predicted by using Equation 2.3 with Gow's [1969] parameter values for activation energy (48.6 kJ/mol^{-1}) and pre-factor K_0 (5.3 x 10^6), for grain sizes and temperatures in this study. Because Gow used only the 25% largest grains in each of his samples, we applied a correction to Equation 2.3 to get the predicted mean. For SAI1, the mean cross-sectional area was less than that of the initial material. See Discussion section for an explanation.

Sample	T (K)	Gow's K (10^{-4} μm^2/s)	K (10^{-4} μm^{2}s^{-1})
SA	200	N/A	N/A
SAI1	226	0. 099	-7.8
SAI3	226	0. 099	0.9
SAB4	230	0. 16	1.3
SAD1	234	0. 24	3.6
SAD3	234	0. 24	3.8
SAC4	240	0. 45	3.9
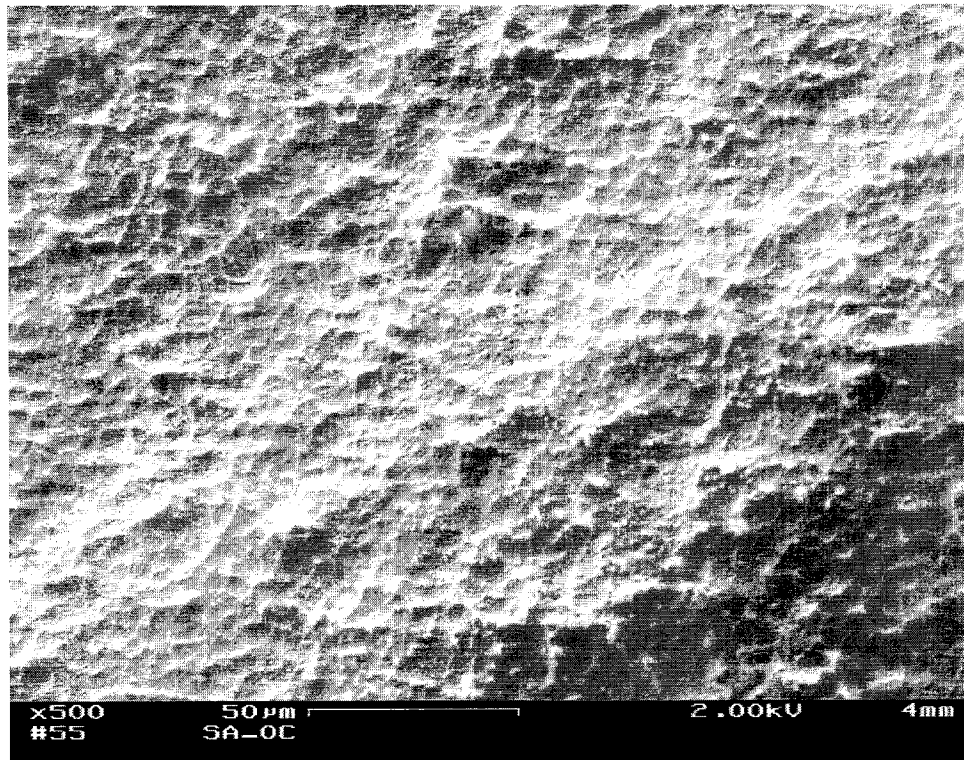
Figure 2.1. LTSEM Photomicrograph of the initial material for all the annealing experiments. Scale is given on the image. Grain boundaries appear as raised ridges.
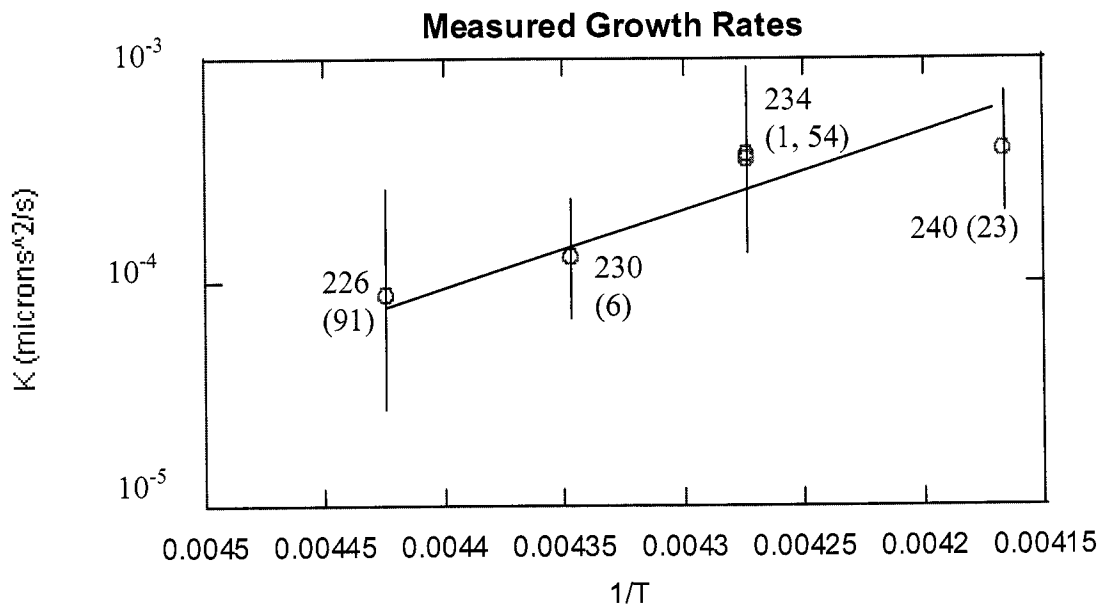
Figure 2.2. Measured growth rates of 5 samples that annealed for times ranging from 1 to 91 hours. Each data point is labeled with the temperature (degrees K) at which the sample was annealed and the annealing time (hours) in parenthesis. Error bars are shown for each point. The sample that annealed for 1 hour at 226 K is not shown.
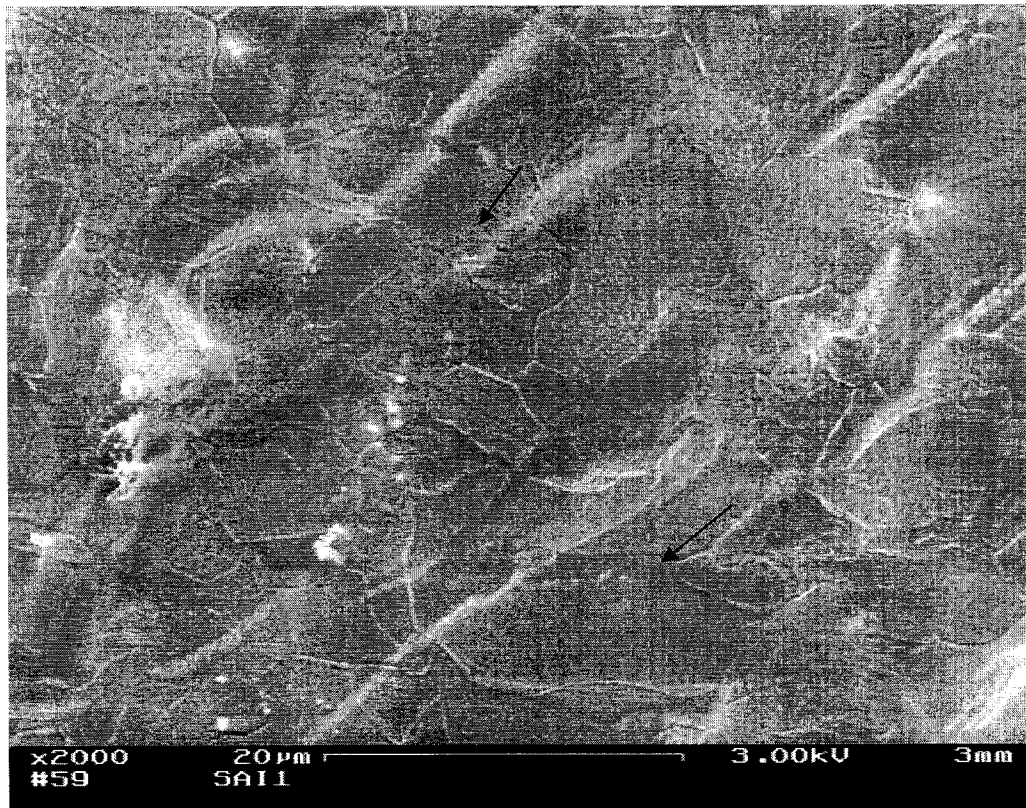
Figure 2.3 Sample SAI1, ice annealed at 226 K for 1 hour. Scale is shown on the image. Grain boundaries are visible as lines or thin channels. Lower black arrow points to a larger grain with a long major axis, and upper black arrow points to a cluster of smaller, more equant grains.
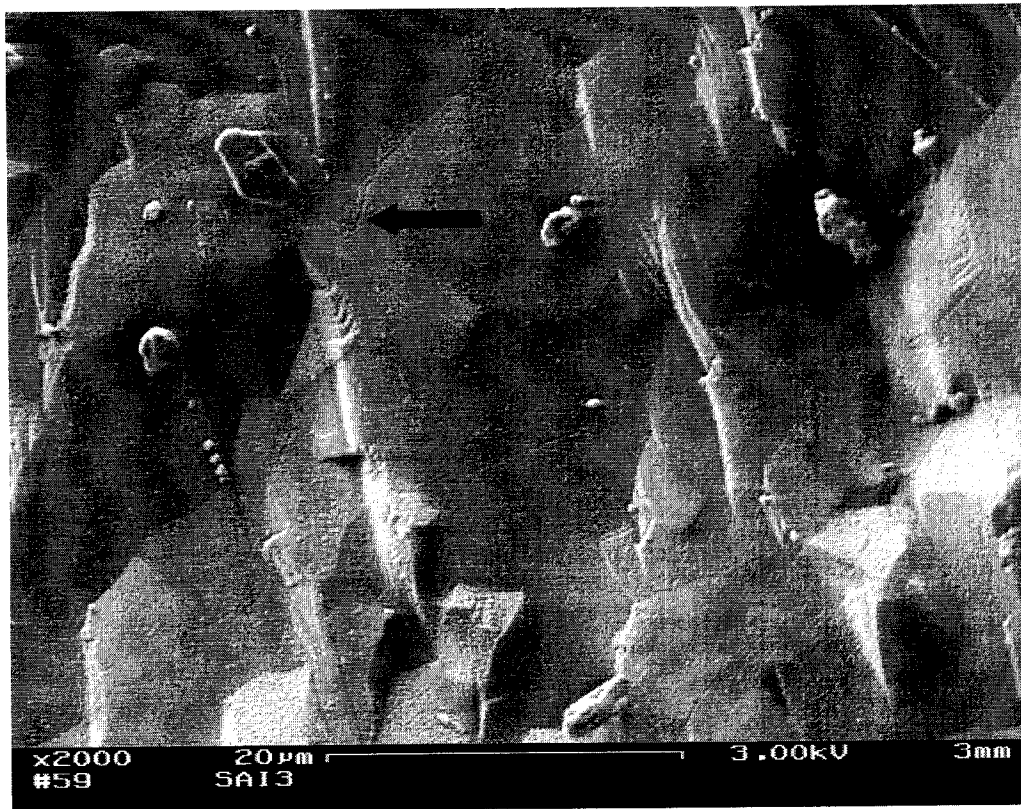
Figure 2.4. Sample annealed for 91 hours at 226 K. The scale is shown on the image and grain boundaries (black arrow) are visible as lines outlining grains.
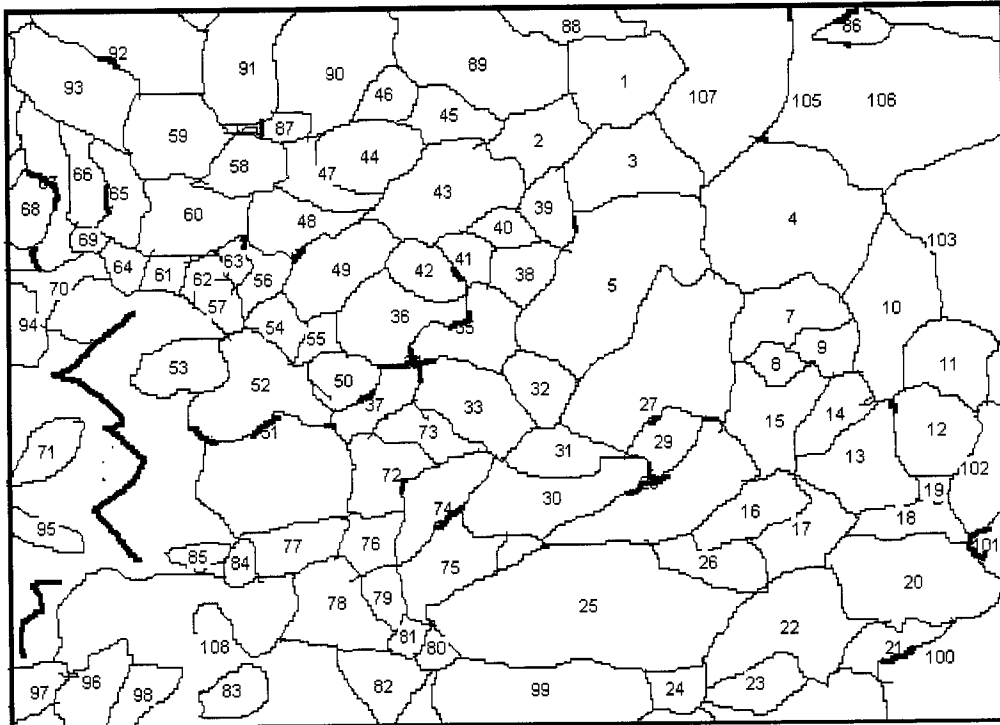
Figure 2.5. A manual outline of grains of figure 2.3 performed in Scion Image Analysis program. Numbers identify individual grains.

Figure 2.6. Distribution of grain areas in each sample, estimated from LTSEM measurements. The cross-sectional area of the grain is used to represent the grain sizes of the ice samples. Vertical axis is number of grains in area bin.

Initial Material

226 K for 1 hour

226 K for 91 Hours

234 K for 54 Hours

240 K for 23 Hours

234 K for 1 Hour

234 K for 54 Hours
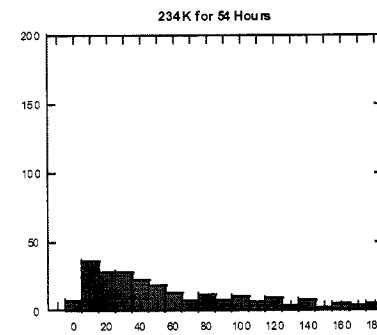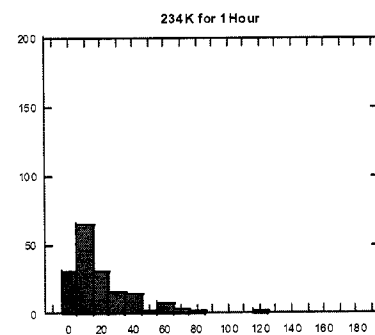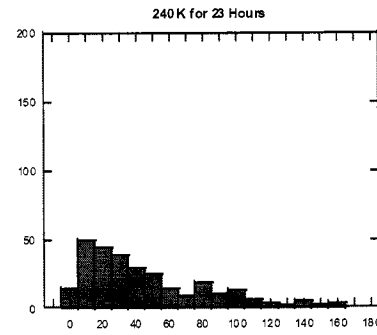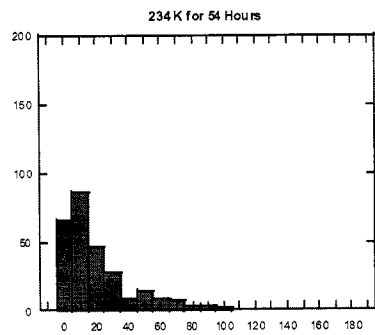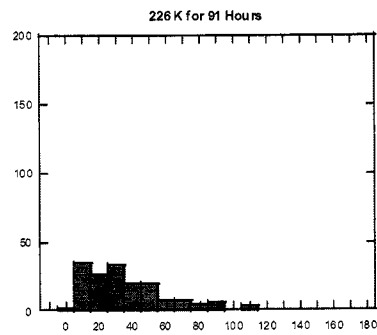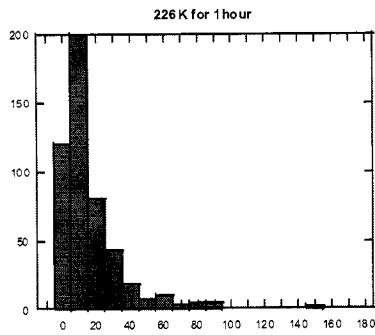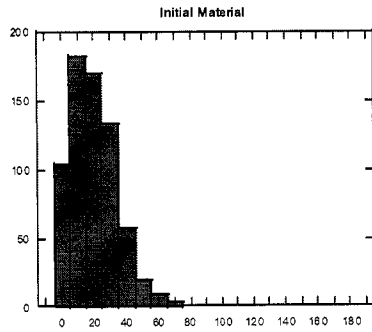
Grain area (μm²)   Grain area (μm²)

Figure 2.7. Area distribution of all grains in sample, estimated from LTSEM measurements. The cross-sectional area of the grain is used to represent the grain sizes of the ice samples. Grain areas are normalized by the mean grain area M of each sample. Grain counts are normalized by the total number N of grains per sample. Vertical axis shows crystal-area probability density.
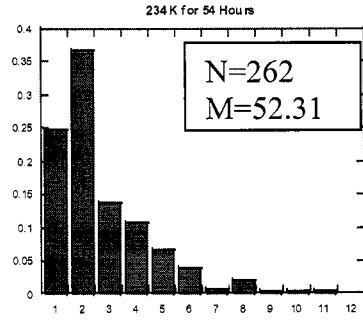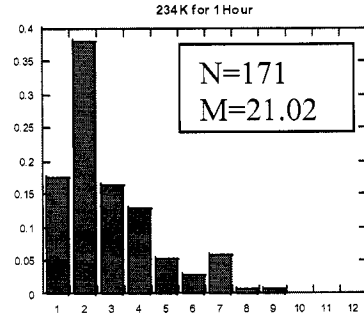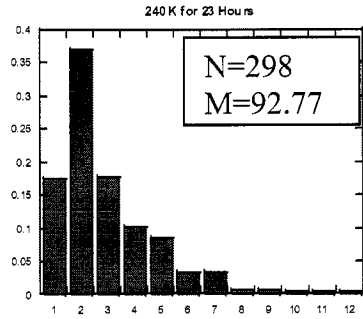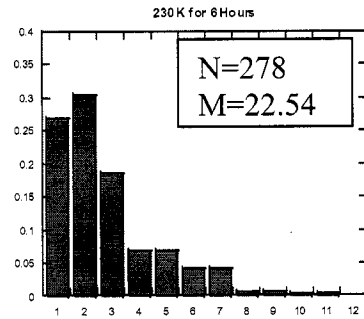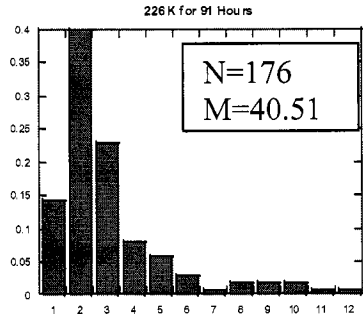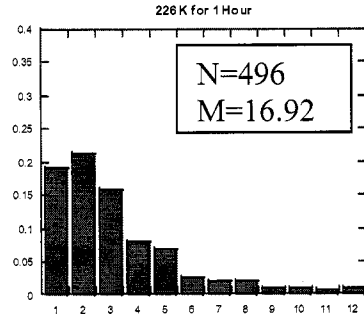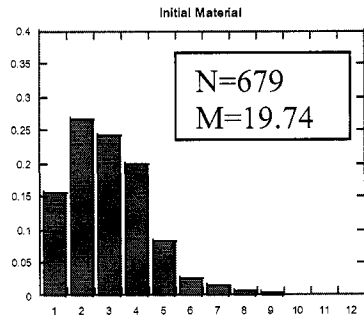
Normalized Grain
Normalized Grain
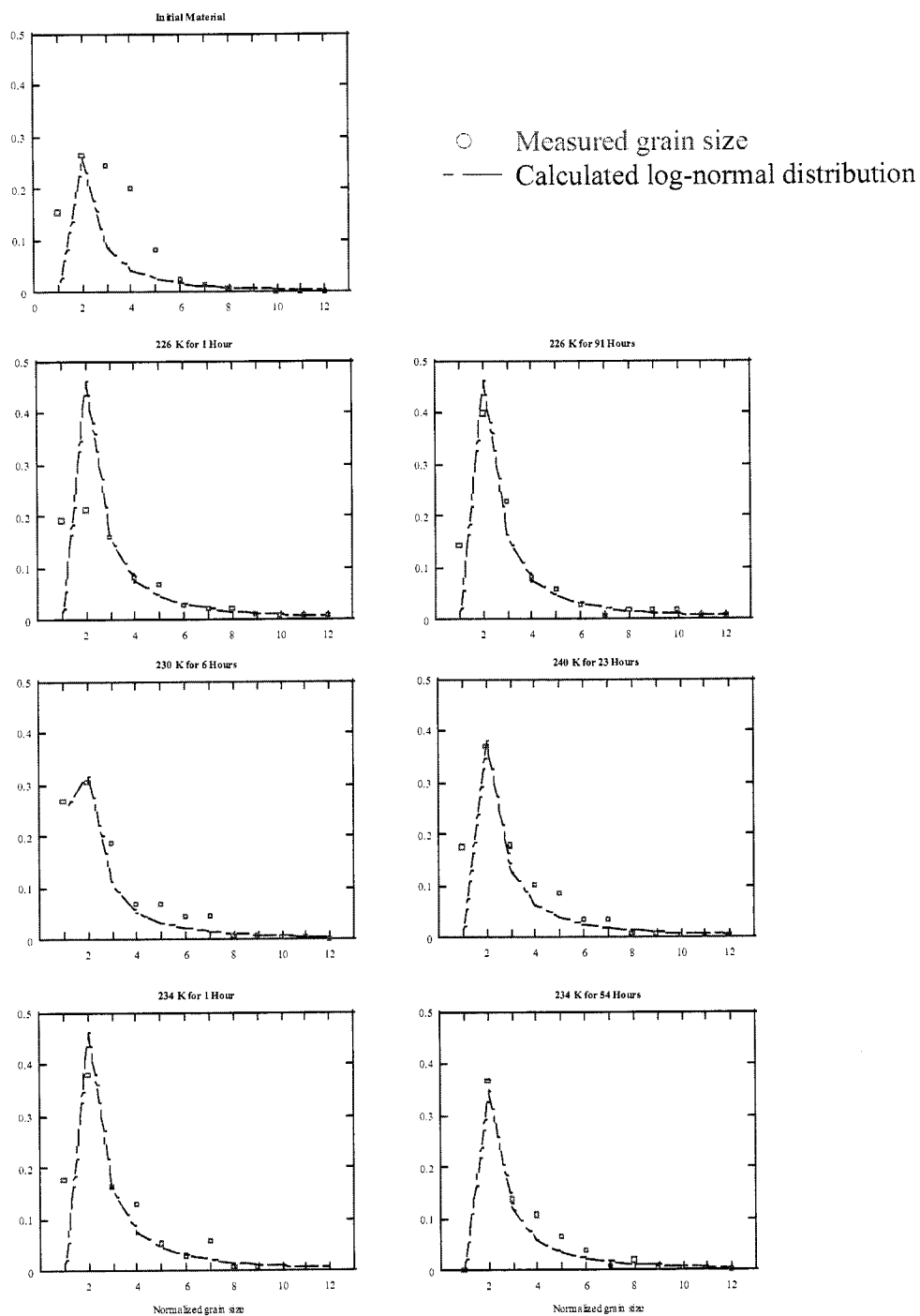
Figure 2.8 Log-normal distribution curve fits (blue) and normalized grain areas from measured samples (red circles). Vertical axis shows crystal-area probability density. Grain areas are normalized by the mean grain area of each sample.
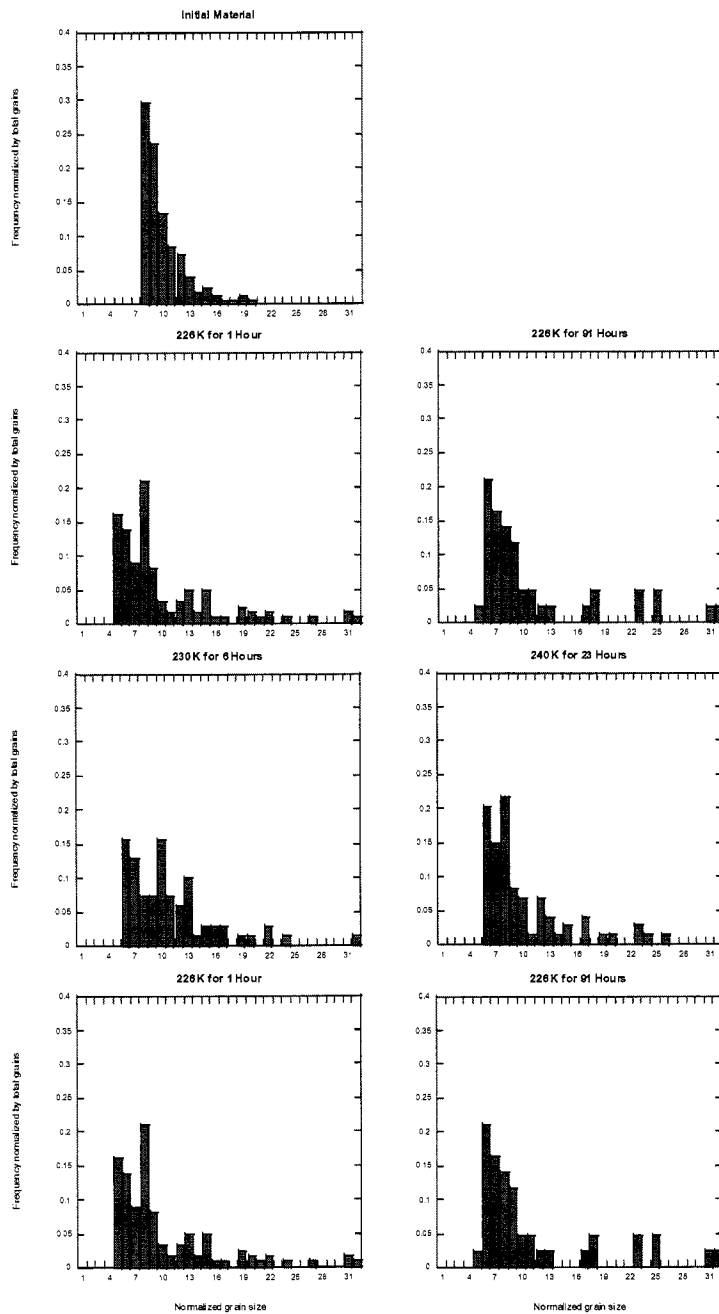
Figure 2.9 Grain-size distributions of the largest 25% grains of each of our samples. Grain areas are normalized by the mean grain size of the samples.
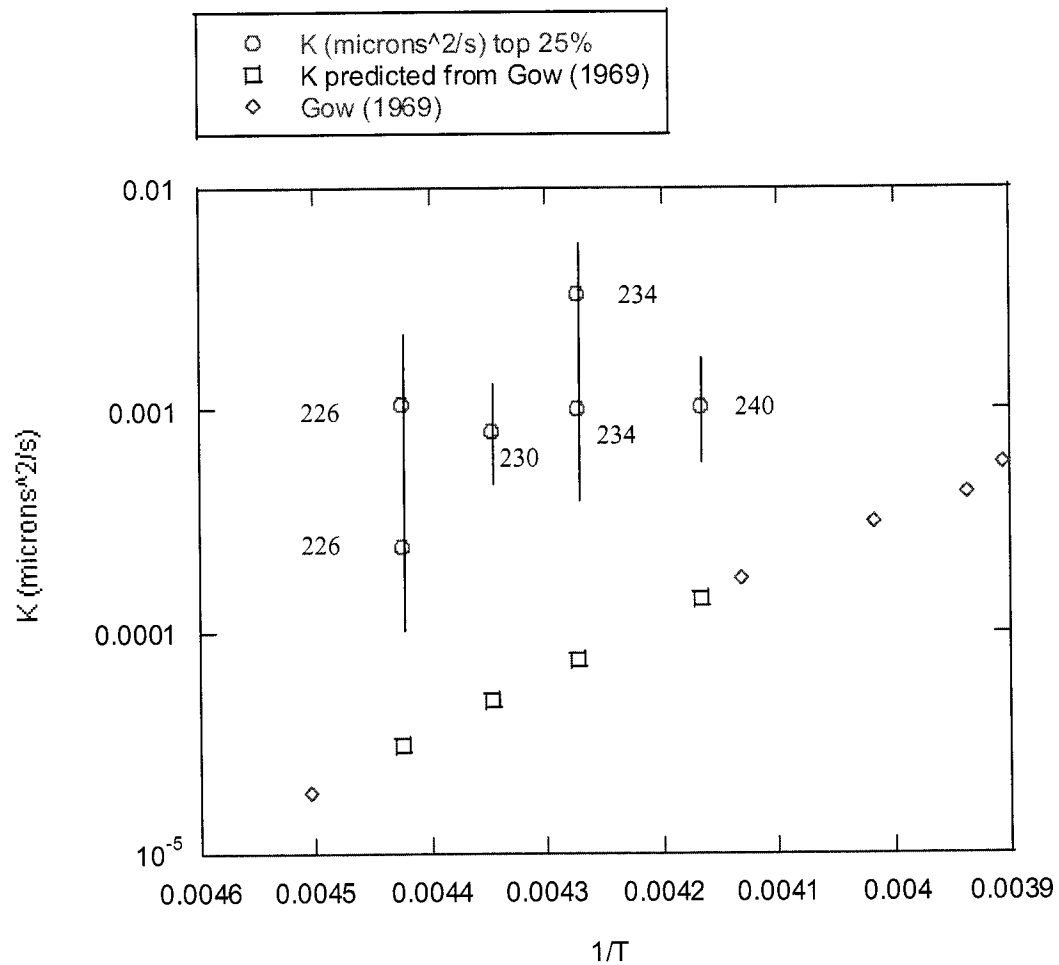
Figure 2.10 Growth rates of the largest 25% grains from the annealed samples of this study (red circles) plotted with error bars. Each point is listed with temperature and duration of annealing in parentheses. Green diamonds are data points from Gow [1969]. Blue squares are expected growth rates calculated from Gow's growth law [1969].
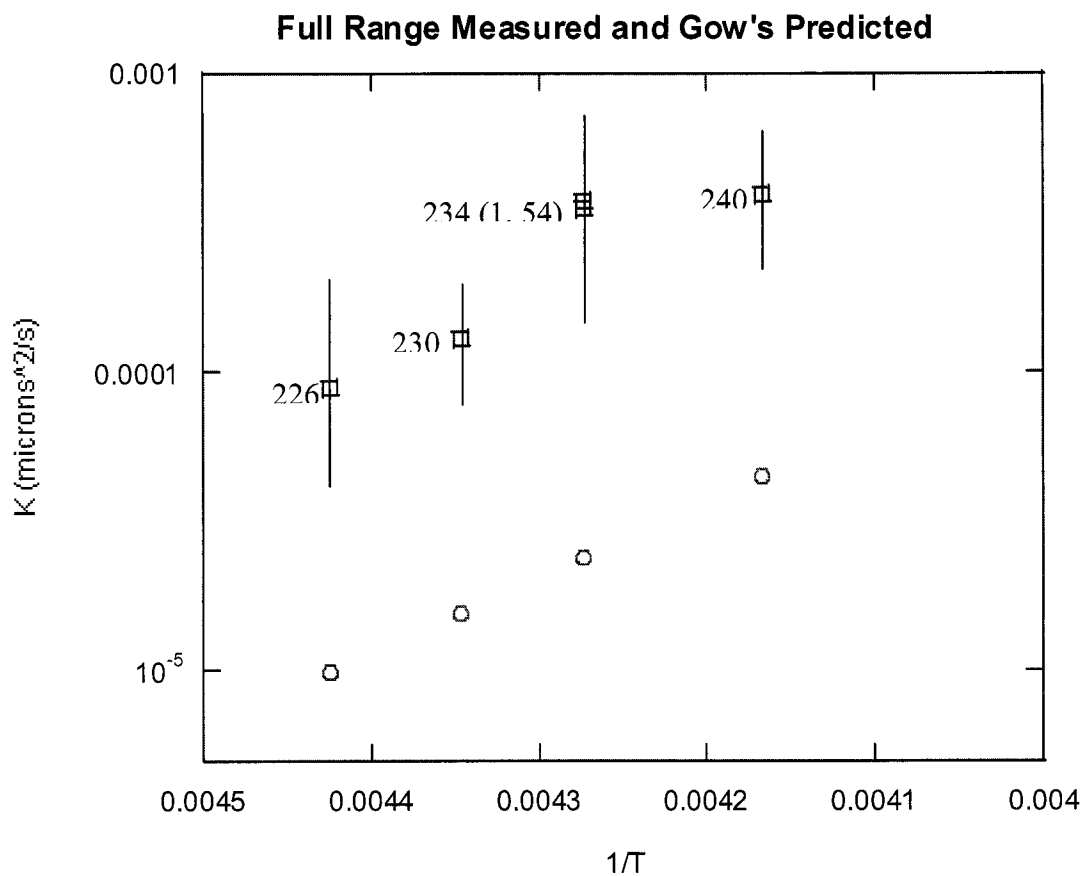
Figure 2.11 Squares show measured mean growth rate as function of temperature T, using all grains in each image. Circles show corresponding mean growth rates predicted with Equation 2.3 and parameter values from Gow [1969], with a correction factor to account for use of full size distribution rather than 25% largest crystals (see text) Error bars shown are estimated from the standard deviation of mean grain size for each sample (Table 2.3).

Chapter 3

An Investigation of Deformation Mechanisms through Quantitative Texture Analysis by Neutron Diffraction of Experimentally Deformed Fine-Grained D_2O Ice I_h

3.1   Summary

Quantitative textures in fabricated fine-grained (2-10 μm) polycrystalline D_2O ice cylinders were deformed and then measured by monochromatic neutron diffraction to investigate deformation mechanisms in fine-grained ice I_h. Three fine-grained ice cylinders were deformed at constant-strain rate in a 350-MPa gas deformation apparatus at T=222 K, 224 K, and 226 K, and to 20%, 28% and 17% total strain, respectively. All samples developed a uniaxial texture during deformation with (0001) poles parallel to the axis of compression. Low-temperature scanning electron microscopy of two samples after deformation showed increased grain-aspect ratios and four-grain junctions. The results suggest that the deformation in these experiments may be a combination of deformation mechanisms.

3.2   Introduction

A key to investigating the rheological behavior of ice, at both planetary and terrestrial conditions, is understanding its micro-physical flow mechanisms. Deformation of ice can give rise to dynamic recrystallization and grain boundary migration. Such processes may lead to changing grain sizes, which are predicted to reach steady state in laboratory experiments over time [*Poirier*, 1985]. However, models do not typically include grain size as a free variable in governing flow laws for polar ice sheets. In this study, we investigate the contribution of grain-size sensitive (GSS) creep to texture development, or lattice-preferred orientation (LPO), and examine the flow mechanisms that may give rise to this texture. In this paper, we use the term "ice" to refer to ice I_h, or the hexagonal form of ice.

Ice in a glacier may deform by inter- and intra-crystalline creep [*Glen*, 1955]. At the microscopic level, individual grains of ice deform as dislocations slip and climb through the crystal lattice, in a process known as dislocation creep. Other deformation mechanisms available to polycrystalline ice include grain-boundary diffusion, lattice diffusion and grain-boundary sliding (GBS) [*Paterson*, 2001]. In the first process, material diffuses along grain boundaries, in the second it diffuses through the bulk of the material. The third mechanism comprises slip of rigid grains along grain boundaries. Of particular interest to this study are grain-size sensitive (GSS) creep mechanisms that depend on the presence of grain boundaries in materials. GSS creep is typified by GBS and grain-boundary diffusion. During GBS, stress accumulates at grain junctions and other places along the grain boundary. This stress is possibly reduced by grain-boundary migration, diffusion, and/or slip [*Sherby and Wadsworth*, 1989], with accommodation by slip seeming to fit the data best

[*Nieh, et al.*, 1997]. Recent work suggests that fine-grained ice may deform by GSS creep under conditions of low applied stress (<0.1 MPa) [*De Bresser, et al.*, 1998; *De Bresser, et al.*, 2001; *Durham and Stern*, 2001; *Durham, et al.*, 2001; *Goldsby and Kohlstedt*, 1997, 2001]. All of these deformation mechanisms, and perhaps others, may operate simultaneously under applied stress during deformation of ice.

One property that has been minimally investigated for polycrystalline ice is grain size. Grain size in an ice sheet varies depending on depth and strain path history, with typical values of initial surface grains from 0.25 – 1 mm and sizes of 1 – 4 mm at the firn-ice transition (region where porous snow is converted to ice with air bubbles) [*Paterson*, 2001; *Thorsteinsson, et al.*, 1997]. Below this transition, grain size can increase to several centimeters. Formerly, most models of ice sheet flow have treated grain size as an insignificant parameter and independent of strain rate. However, recent work on basal ice (ice at the bottom of a glacier or ice sheet) of Meserve Glacier and the Dye 3 borehole in Greenland, suggests that grain size may affect ice flow in some locations [*Cuffey, et al.*, 2000a; *Cuffey, et al.*, 2000b]. In this study, fine-grained ice refers to ice grains with an initial diameter of 2-10 μm.

A scalar form for the flow law of isotropic polycrystalline material, including fine-grained ice is

$$\dot{\varepsilon} = Ad^{-m}\sigma^{n}e^{-(E^{*}+PV^{*})/RT} \tag{3.1}$$

Where $\dot{\varepsilon}$ is the strain rate, P is pressure, d is grain size, m is the grain-size exponent, T is temperature, R is the gas constant, E* is the activation energy, V* is the

activation volume for creep, n is the stress exponent and A is a material constant. Values for the variables in the flow law may be different for the various deformation mechanisms that are active in a given deforming material [*Poirier*, 1985].

Previous laboratory investigations of flow in fine-grained ice by Stern et al., [1997], Durham et al., [2001] and Goldsby and Kohlstedt [1997, 2001] have shown that flow in laboratory-synthesized polycrystalline ice samples can depend on grain size, a parameter that may change due to persistent grain growth or recrystallization. If flow mechanisms depend on grain size, then grain size may play an integral part in ice-flow dynamics, and therefore texture development.

Grain size may be a variable during deformation. Gow [1969] and Duval [1983] showed that ice grains grow faster at higher temperatures. In the dislocation-creep regime, the density of dislocations and other defects increases with deviatoric stress, raising the internal energy of the grains, giving rise to bulge nucleation and/or progressive subgrain rotation, and thus creating smaller grains. As grain sizes decrease and the density of grain boundaries increases, grain-boundary sliding and diffusion, which are dominant during GSS creep, will contribute more to the overall deformation. Under conditions favoring grain-boundary migration and other mechanisms of grain growth, dislocation creep may become important again. It has been postulated [*De Bresser, et al.*, 1998; *De Bresser, et al.*, 2001; *Steinemann*, 1955] that when both GSS and dislocation creep are actively contributing to deformation, grain size will reach a balance in size.

Most calculations of flow in ice use a creep exponent of n=3, a value associated with dislocation creep in the isotropic polycrystalline flow law (3.1)

[*Paterson*, 2001]. However, Weertman [1970] modeled the recrystallization of ice (using 1 mm to 1 cm grain size) and determined that around 0.1 MPa, or conditions of low deviatoric stress, GSS mechanisms may begin to dominate over dislocation creep mechanisms. Goodman et al. [1981] also predicted a change in deformation mechanism dominance in ice of 1 mm grain size. From those studies, a predicted value of n = 2 is expected when GSS is the dominant deformation mechanism.

Several laboratory studies on ice rheology at low stress (<1 MPa) independently conclude that the stress exponent of the ice flow law (3.1) is approximately n = 1.8 during GSS creep [Durham, et al., 2001; Goldsby and Kohlstedt, 1997, 2001], confirming Goodman and Weertman's predictions. These groups independently determined that GSS flow occurs in deformation experiments of fine-grained laboratory ice and could have implications for terrestrial and planetary ice flow laws since conditions of low deviatoric stress dominate in these environments. Goldsby and Kohlstedt (2002) argued that GSS creep occurs as GBS accommodated by basal slip, and a texture will develop from this slip. In a review of GBS experimental data and modeling, Nieh et al., (1997) showed that modeling of GBS using accommodation by basal slip best fit the laboratory data.

Others have argued that GSS deformation may be occurring in ice sheets, but may not be the dominant deformation mechanism [*Duval, et al.,* 2000; *Duval and Montagnat,* 2002; *Pimienta and Duval,* 1987]. Duval and Montagnat calculated theoretical texture development in ice at 1549 m depth for the Greenland Ice Core Project (GRIP) [*Duval and Montagnat,* 2002] ice core using the Visco-Plastic Self-Consistent (VPSC) models by Tome [1999]. They showed that when GBS was assumed to accommodate 70% of the total strain, the resulting texture was random.

When they assumed that intra-crystalline slip was unaffected by GBS, the result was a non-random texture that was comparable to field observations of texture at the depth of 1549 m. Duval and Montagnat [2002] also asserted that grain-boundary migration could efficiently reduce the rate of accumulation of dislocations at grain boundaries. This can be an effective recovery process, in the form of normal grain growth or recrystallization. Grains that have undergone grain growth or recrystallization would be relatively strain-free, and both processes are known to occur throughout the thickness of an ice sheet [Alley, 1992; Budd and Jacka, 1989]. Duval and Montagnat concluded that GBS could not produce a texture in the ice if it was the dominant deformation mechanism, and they favored grain-boundary migration as the mechanism for relieving internal stress resulting from dislocation creep.

This paper addresses the question of whether texture arises solely from dislocation creep in fine-grained ice, or whether it is also attributable to GSS creep, or from a combination of the two. Texture, or preferred crystallographic orientation, is imparted to a material through deformation, during recrystallization or by phase transformations [Wenk and Van Houtte, 2004]. Texture that arises as a result of deformation has far-reaching implications for virtually all material properties that are directionally dependent, such as control heat flow, diffusion, plastic behavior, and elastic and electromagnetic wave propagation [Kocks, et al., 1998]. Ice cores show that ice sheets have texture strength that varies with depth, with the common occurrence of increasing vertical concentrations of c-axes toward the base of an ice sheet [Alley, 1992; Budd and Jacka, 1989; Duval, et al., 1983; Glen, 1955; Kamb, 1959]. For ice sheet models, it is important to understand texture in order to

quantitatively evaluate the anisotropy and flow behavior of ice sheets [*Thorsteinsson*, 2000].

Texture is commonly plotted as a pole figure. A pole figure may be represented as a 2-dimensional equal area or stereographic projection as a density distribution of a given pole to a chosen sample reference frame. The distribution of poles, usually described in multiples of random distribution (m.r.d.), represents the volume fraction, or density, of all grains with a given orientation in the sample with respect to the chosen crystallographic plane. A sample with randomly oriented grains has a pole figure of uniform density (isotropic or m.r.d. = 1). Values greater than one m.r.d. indicate a texture has developed.

Typically, orientations of the c-axis of grains in ice cores have been directly measured with a universal stage [*Duval*, 1973; *Kamb*, 1959], with several hundred grains visible in the field of view. With neutrons, we measure the orientations of approximately 100,000 grains in a bulk sample (i.e. 1 cm^3) to produce a pole figure. Table 3.1 lists neutron diffraction intensities for important ice I_h (*hkil*) reflections, where (*hkil*) are Miller indices. We used these reflections to measure the pole figures for texture analyses.

Experimental pole figures are used to construct the orientation distribution function (ODF) of a sample. The ODF gives the volume fraction of material as a function of orientation [*Heidelbach and Riekel*, 1997]. It provides a comprehensive description of the texture of the material. Using the ODF, any pole figure can be extracted from a limited amount of collected data.

While texture is often attributed to dislocation creep in ice, it is likely that various deformation mechanisms are acting in concert, not isolation [*Goodman, et al.*, 1981]. Reports of GBS accommodated by basal slip have been noted to give rise to texture in metals [*Perez-Prado, et al.*, 1998; *Perez-Prado, et al.*, 1996; *PerezPrado, et al.*, 1996]. Texture development in plastically deformed ice has been documented in various experiments [*Bennett, et al.*, 1997; *Chastel and Dawson*, 1991; *Duval*, 1981] as attributed to grain rotation following deformation through basal glide.

To investigate texture development in ice, neutron diffraction can be very useful and comprehensive. Unlike X-rays, neutrons have low absorption in most materials and therefore penetrate the bulk sample. Bulk samples of several centimeters in size can be investigated non-destructively. Likewise, environmental devices (such as cryostats) can be used since some materials used to build environmental cells (i.e. aluminum) are weak scatterers of neutrons and *in situ* experiments can be developed.

In order to scrutinize the effect of grain size on rheological behavior in ice, we used two techniques in this work to determine which deformation mechanisms were operating under a series of temperature and stress conditions in experimental fine-grained ice. We used the technique of low-temperature neutron diffraction to measure the quantitative texture in the bulk-deformed samples, and we used low-temperature scanning electron microscopy (LTSEM) to quantify the size and shape of grains in each sample. LTSEM yields information about freshly fractured ice surfaces and grain morphology [*Durham and Stern*, 2001; *Stern, et al.*, 1997].

In this study we investigated texture development in polycrystalline ice samples with different deformation histories, using neutron diffraction to document the texture after deformation in fine-grained ice. In this study, we addressed whether we can use texture, along with LTSEM analysis, to distinguish between GSS and dislocation creep during flow. We deformed three laboratory ice samples at constant-strain rates to characterize the rheology of the fine-grained ice at different temperatures (222 K, 224 K, and 226 K) and stresses (8-61 MPa) to different strains (~20%, 27% and 17%) (Table 3.2). In two of the samples we used LTSEM to quantify the grain morphology and microstructure in each sample.

3.3   Experimental Procedures

3.3.1   Initial Material

The initial material was isotropic, bubble-free polycrystalline cylinders of D_2O ice 2.54 cm in diameter. Ice was made from pure deuterated water [*Bennett, et al.*, 1997]. In neutron diffraction studies, it is common to substitute deuterium (D) for hydrogen (H) [*Wollan, et al.*, 1949]. Because neutrons scatter hydrogen incoherently, replacing H with D decreases the absorption cross-section by a factor of approximately 1000. The result is that D is a stronger scatterer of neutrons and contributes less noise to the neutron signal than H. Single-crystal studies of ice I_h [*Peterson and Levy*, 1957] show that there is no significant structural difference between D_2O and H_2O.

Initial grain size was reduced from 180-250 μm to 2-10 μm by a pressure-release procedure established by Stern et al. [1997], where an ice sample is converted to ice II by hydrostatically pressurizing to 300 MPa. The sample is held at 300 MPa

for 15 minutes then converted quickly back to ice I_h by a fast venting of gas (< 3 s to 50 MPa). Using LTSEM, we documented the yield of dense ice with equiaxial grain shapes and a grain size of approximately 2-10 μm (Figure 3.1a) [*McDaniel, et al.*, 2002; *Stern, et al.*, 1997]. The grain-size distribution of the initial material is shown in Figure 3.1b. The starting texture of the samples following the established procedure was assumed to be random [*Stern, et al.*, 1997].

After fabrication, D_2O ice cylinders were inserted into indium jackets that conform to the ice surface and protect the sample from the confining pressure gas used during the deformation experiments. Ice cylinder ends were shaved perpendicular to the cylinder axis, resulting in an initial sample length of approximately 5.3 cm for the constant-strain rate experiments. A zirconia spacer was placed parallel to the cylindrical axis of the sample and an internal force gauge was soldered onto the jacket.

3.3.2 Deformation Experiments

Three ice samples were deformed at a constant strain rate (3.9 x 10^{-7} s^{-1}, 1 x 10^{-6} s^{-1}, and 1.4 x 10^{-6} s^{-1}) in a 350-MPa gas deformation apparatus at Lawrence Livermore National Laboratory (LLNL). The deformation apparatus was immersed in a cryogenic tank for low-temperature testing [*Heard, et al.*, 1990]. A liquid nitrogen (LN_2) – cooled ethanol bath was used as a cooling medium inside the cooling tank. A hydrostatic confining pressure, provided by nitrogen gas, was maintained at approximately 50 MPa during the tests. An internal force gauge measured the stress on the sample, and displacement transducers determined the amount of incremental axial shortening of each sample. Samples were deformed to

various percent strains (20%, 27%, 17%) using a moving axial piston at a temperature range of 222 – 226 K (Table 3.2).

After each deformation experiment, the system was slowly depressurized, the deformation vessel was cooled to 190 K, and the sample was extracted from the test apparatus and stored in LN_2 for the neutron diffraction experiments. This procedure preserved ice grain structure (shape and texture). A slice of material was removed from the deformed ice cylinder for LTSEM analysis from two samples (497 and 498). Before texture analysis was performed, the indium jackets were removed from the samples. Both ends of the samples were then shortened with a band saw to create a cylinder approximately 2.5 cm long by 2.5 cm in diameter from the center of the sample for the texture experiment.

3.3.3   Texture Experiments

Quantitative bulk texture measurements were performed on the three deformed samples of deuterated hexagonal ice using monochromatic neutron radiation on the BT-8 residual stress diffractometer at NIST (National Institute of Standard and Technology, at the Center for Neutron Research (NCNR) in Gaithersburg, MD). BT-8 is well-suited for measuring texture in polycrystalline materials. It is equipped with a silicon crystal focusing monochromator, which can be optimized in its parameters for a specific experiment. The conventional nuclear reactor at NIST provided a continuous neutron beam flux on the sample of 2×10^8 neutrons cm^{-2} s^{-1}. A Si (311) reflection was used at $2\theta_M=70°$, where θ_M is the take-off angle of the crystal monochromator [$Santoro$, 2001], to provide a neutron wavelength $\lambda = 1.878$ Å, which was used throughout this series of measurements. For these

texture experiments, the monochromator was optimized to gain maximum flux on a sample with moderate resolution in diffraction. The BT-8 instrument has a position-sensitive detector with an angular opening of approximately 8 degrees in the scattering plane, providing fast data collection of multi-peak patterns. The structure of ice I as determined for D_2O by neutron powder diffraction at 121 K and atmospheric pressure is hexagonal (with crystallographic space group = P63/mmc; unit cell parameters a=4.504 Å, c=7.337 Å at 121 K [*Leadbetter, et al.*, 1985]).

To perform the texture measurements under cryogenic conditions, each of the three ice samples was mounted in an aluminum can that was attached to the end of a cold finger on the Helium-3 gas conventional closed-loop cryostat. The sample cylinder axis was mounted parallel to the cold finger. The cryostat was mounted on a four-circle Eulerian cradle goniometer for the texture measurements (Figure 3.2). Temperature at the end of the cold finger was maintained at 35K (±15K). An inset picture in Figure 3.2 shows one ice sample mounted on the BT-8 goniometer at NIST. All samples were mounted on the sample assembly and were centered and aligned with respect to the neutron beam, so that during sample rotation, scattering (and absorption) conditions remained nearly constant. The incident neutron beam was collimated using a circular aperture with a 5-mm diameter and a detector aperture of 5-mm, so that the beam's intersection (gauge volume) was aligned with the goniometer/sample axes. In this way, absorption of neutrons by the ice was minimized and transmission of the neutron beam optimized. The cold-finger chamber and sample assembly were rotated under vacuum for the texture experiments.

Neutron pole figures were collected for four ice Bragg reflections, (10-10), (0002), (10-11) and (10-12) [*Leadbetter, et al.*, 1985] (Table 3.1). Texture in samples 497 and 498 was measured by rotating the ice specimen through a range of angles ϕ around its axis of compression (cylinder axis), and through angles χ perpendicular to its axis. Data for all three ice specimens were collected in 5 degree steps (ϕ,χ), where $\phi = 0 - 360°$ and $\chi = 0 - 90°$. 723 different coordinates (ϕ,χ) of the sample were measured in a grid (Figure 3.3) [*Matthies and Wenk*, 1992]. Sample 499, was a smaller sample (9 mm diamter) and was measured with a finer grid of 1263 nodes (ϕ,χ). With this instrumental setup and data collection method, one pole figure for a sample could be collected on BT-8 in approximately 12 hours.

The four experimentally measured pole figures, with assumed axial sample symmetry, were used to recalculate pole figures from the ODF to corroborate experimental accuracy. We used the Williams-Imhof-Matthies-Vinel (WIMV) algorithm direct method in the Preferred-Orientation Package – Los Alamos (POPLA) to calculate the full ODF for each sample [*Kallend, et al.*, 1991].

3.3.4 Grain-Microstructure Measurements

Grain shape, size and microstructure were measured in samples 497 and 498 using LTSEM at the USGS Menlo Park, CA. LTSEM measurements were not made on sample 499. A portion of the samples were transferred to the Gatan Alto 2100 low-temperature preparation chamber (evacuated and pre-chilled below 100 K), which was in turn attached to a LEO 982 field-emission SEM. The cold stage was kept at its minimum temperature of 93 K. A scalpel was used to fracture the samples and remove a piece (1 mm^2) of surface ice, exposing fresh ice for scanning. After we

fractured the ice, we transferred samples under vacuum directly into the SEM scanning chamber. Figure 3.1 shows a photomicrograph of the initial material before deformation. The LTSEM photomicrographs were taken in transects across the sample surface.

To assess any microstructural change (elongation, growth) of the grains in these samples, we used the imaging program Scion Image to outline each grain visible in a photomicrograph and calculate the major and minor elliptical axes of each grain. For an example of this procedure, see Figure 3.4. Others have also used the major axis diameter to study grain growth in ice [*McCappin and Macklin*, 1984a; 1984b; *Nasello, et al.*, 1992].

3.4   Experimental Results

3.4.1   Deformation Experiments

The results of our experiments are listed in Table 3.2 and the stress-strain curves are plotted in Figure 3.5. We chose temperatures based on previous deformation experiments that indicated strain hardening at temperatures higher than approximately 220 K, which we associated with grain growth [*Durham, et al.*, 2001]. Static annealing experiments on fine-grained ice indicate detectable grain growth beginning around 226 K (McDaniel et al., in preparation). In order to minimize grain growth and explore GSS creep, we chose a temperature range of 222 – 226 K.

3.4.2 Texture Experiments

Figure 3.6 shows a measured diffraction pattern with (hk$i$l) reflections indicated. A calculated diffraction pattern for a randomly oriented powder of D_2O is shown for comparison. Deviation from a peak-height pattern for a random powder is an indication of texture. This variation of peak height points to a difference in the number of crystallographic planes oriented for particular (hk$i$l) reflections.

Figures 3.7 a, b and c show the (10-10), (0002), (10-11) and (10-12) pole figures for samples 497, 498 and 499, respectively. The top sets of figures are the experimental pole figures and the bottom sets are the recalculated pole figures for comparison. Pole figures were plotted using POPLA [*Kallend, et al.*, 1991], a standard texture-analysis program, and a 5-degree Gaussian smoothing function. Pole-density distributions for all three samples confirm the expected cylindrical texture, with (0002) poles displaying a maximum in the compression direction, as indicated by the concentration of poles around the edge of the pole figure (where χ = 0 degrees). Maxima for (10-10) for samples 497, 498 and 499 are 1.52, 1.65, and 1.41 m.r.d., respectively. The maxima are nearly twice as high for (0002) with 2.61, 2.59, and 2.24 m.r.d., respectively. Statistical analysis of experimental versus recalculated pole figures shows an approximate deviation of 5%, and good experimental accuracy.

3.4.3 Grain-Microstructure Measurements

Figure 3.a shows a photomicrograph of the initial material. The grain-size distributions were plotted using the major-axis lengths of the grains in a sample. Figure 3.1b shows a grain-size distribution of the initial material, with a distribution of 2-10 μm and a grain-size population peak at 7-8 μm. Figures 3.8a and 3.9a show photomicrographs of samples 497 and 498 post deformation and Figures 3.8b and 3.9b show the corresponding grain-size distributions from one photomicrograph of each of these samples. The range of grain size for sample 497 is 1-15 μm with a grain-size population peak at 3-5 μm. Sample 498 shows a grain-size range of 2-19 μm with a peak at 3-5 μm. These histograms of the deformed ice (497 and 498) show a change in grain-size distribution, with larger (19 μm) and smaller (2 μm) grains than the initial material (Figure 3.1a). Sample 499 was not measured.

Visual examination of the LTSEM photomicrographs of the deformed ice samples showed that grains have straight boundaries and equiaxial shape. Ratios of major to minor axes increased during deformation, indicating that grain shape was changing. The initial material had an average aspect ratio of 1.56 ± 0.56, indicating a slight initial starting texture. An exactly equiaxial grain would resemble a circle with an aspect ratio of 1. After deformation to 0.196 strain, sample 497 had a ratio of 1.83 ± 0.86. After deformation to 0.274 strain, sample 498 had a ratio of 2.07 ± 1.05.

3.5   Discussion

We performed these experiments in order to estimate the relative contributions of dislocation and GSS creep in fine-grained (2 – 10 μm) ice during deformation. While grain microstructures were similar for all 3 samples, our data show unexpected stress-strain curves. The texture experiments represent the first measurements of texture using neutron diffraction in fine-grained ice I_h. Our data also show similar texture results for each sample, although deformation conditions were significantly different.

Figure 3.10 shows a deformation mechanism map relating the fields of dominance of dislocation and GSS creep. Despite the similarities mentioned above, the conditions under which sample 498 deformed fall in the GSS creep field, whereas the conditions under which samples 497 and 499 deformed lie in the dislocation creep field.

Our values for differential stress and strain rate for sample 498 compare well with previous work on fine-grained ice under conditions of low stress [*Durham, et al.*, 2001; *Goldsby and Kohlstedt*, 1997, 2001; *Stern, et al.*, 1997]. The stress-strain curve for sample 498 (Figure 3.5) shows typical behavior for fine-grained ice at low stress, or constant work hardening up to a steady level of stress [*Stern, et al.*, 1997]. This suggests that sample 498 deformed like samples from previous experiments on fine-grained ice, showing a higher strain rate than expected from a sample deforming in dislocation creep. This type of deformation regime has been identified as GSS creep [*Durham, et al.*, 2001; *Goldsby and Kohlstedt*, 1997, 2001].

In contrast, samples 497 and 499 deformed under conditions of much higher differential stress (Table 3.2). Ice deforming by dislocation creep shows an initial elastic response that reaches a yield point and then reaches a steady-state stress [*Stern, et al.*, 1997]. Traditionally, beyond the yield point deformation becomes plastic. This yield point is associated with the onset of recrystallization [*Poirier*, 1985]. The stress-strain curves of samples 497 and 499 (Figure 3.5) are inconsistent with the curves expected for dislocation creep. Instead, like sample 498, they also show constant work hardening up to a steady level.

Grain-microstructural measurements of samples 497 and 498, with differential stresses of 42 MPa and 8 MPa, respectively (Table 3.2), show similar aspect ratios, similar grain shapes and similar grain-size distributions. If samples had deformed predominantly in the GSS creep regime, we would expect them to have aspect ratios close to that of the initial material, because equiaxial grain shape would be preserved under GSS creep.

However, our results show increasing aspect ratios in samples 497 and 498, which may be evidence of grain growth and/or grain-shape flattening. Grain flattening typically indicates dislocation glide, which suggests that dislocation creep was the dominant deformation mechanism or dislocation at least operated significantly [*Gueguen and Nicolas*, 1980]. The argument can be made that our deformation apparatus is limited to achieving approximately 30 percent total strain and the flattening we see in our samples (samples 497 and 498) may be the most we can expect. Also, some grains appear to have undergone growth, evidenced by grains that are both smaller and larger than the initial grain size. An increase in the number

fraction of smaller grains that are shrinking is expected as grains undergo growth [*McDaniel, et al.*, in preparation].

To quantify the amount of independent grain-axis change, we use the total strain of the samples. If we assume that deformation was in the dislocation creep regime for our samples, we can expect that the change in average value of grain major and minor axes would independently scale with the total strain [*Li, et al.*, 1997]. We used $d_m = d_o \exp(\varepsilon)$ to calculate the expected average grain axes changes, where d_m is the expected grain axis, d_o is the average grain axis of the initial material measured from the LTSEM images, and ε is the total strain of the sample [*Li, et al.*, 1997].

Table 3.3 lists the values of expected average grain-diameter for samples 497 and 498 (based on total strain) and our measured grain axes after deformation in both the major and minor grain axis directions. Our measured grain axes lengths are significantly less than the values expected from the total strain of our samples. This suggests that some of the deformation occurs in the GSS creep regime and that recrystallization is active in these samples.

We expect that samples deforming purely in the dislocation creep regime would develop a stronger texture than samples deforming by GSS creep. All three samples developed a similar texture in the (0002) plane of approximately 2 times m.r.d. However, sample 497 has an unexpectedly slow strain rate. We cannot find a set of parameters for equation 3.1 that can represent the strain rates of all 3 samples simultaneously. The microstructural measurements indicate that there may have been a very small initial starting texture. Ideally, this should be measured, since the pressure-release technique used to make this ice may cause variations from one

sample to the next [*Cole*, 2001]. However, these data are the first quantitative texture measurements on fine-grained ice.

There are three possible explanations for our results: pure dislocation creep, pure GSS creep, or a combination of dislocation and GSS creep.

Suppose only dislocation creep was active. In ice, when dislocation creep is the dominant deformation mechanism, the *c*-axes rotate towards the direction of compression, giving rise to highly flattened grains, creating subgrains through rotation, and producing a texture [*Duval, et al.*, 1983]. The c-axes of the ice grains thus become preferentially aligned with the cylindrical axis of the samples, which is also the axis of compression [*Paterson*, 2001].

Alternatively, suppose only GSS creep is active. A full understanding of the exact mechanisms behind GSS creep does not yet exist [*Wakai*, 2004], but it is generally agreed that equiaxial grain shape and grain-switching leading to four-grain junctions characterize GSS creep [*Humphreys and Hatherly*, 1995; *Padmanabhan and Davies.*, 1980]. Equiaxial grain shape is preserved during deformation through the relief of internal dislocation stress in the grains and at grain boundary junctions [*Nieh, et al.*, 1997]. Grain switching is the movement of four neighboring grains in two-dimensional space so that their nearest neighbors, or grains with which they share a boundary, change [*Ashby and Verrall*, 1973].

Goldsby and Kohlstedt (1997) established the presence of four-grain junctions and the occurrence of grain switching (and also straight-grain boundaries and equiaxial grain shape) as microstructural indicators of GBS and indicative of GSS

creep as the dominant deformation mechanism in their experiments on ice. Several four-grain junctions are shown (marked by black arrows) in our photomicrographs of samples 497 and 498 (Figures 3.8a and 3.9a).

However, studies have found that four-grain junctions also occur under other conditions, such as static grain growth (McDaniel et al., in preparation) and deformation by shearing and recrystallization [*Ree and Park*, 1997]; thus, they are not unique identifiers of GSS creep. Without conducting studies on marked grains during deformation, it would be difficult to know if grain switching is occurring in any deformation experiment. This is challenging in ice deformation because distinct grains need to be tagged and deformation must occur in the bulk volume of the sample (ie. not exposed to any surface except other ice grains).

The third option is that both GSS and dislocation creep mechanisms are active. Our data suggest that neither dislocation nor GSS creep operates alone in our experiments. It is more likely that GSS and dislocation creep are both operating. Our data show stress-strain curves (Figure 3.5) that are characteristic of GSS creep and an increase in average grain-axis length that is smaller than expected from the overall strain of the samples if only dislocation creep were active. Our data also show increased aspect ratios from those of the initial material. While these observations would seem to support the presence of GSS creep, in samples 497 and 499 the values of stress and the strain rates are much higher than those established in the literature for GSS creep. For this reason, we expected to find dislocation creep dominant in samples 497 and 499. These findings indicate that it remains unclear how much GSS creep contributes to deformation in fine-grained ice. Since grains do not grow at the same rate, and in fact some recrystallize to a smaller size, the deformation of different

grains may be more influenced by one deformation regime than the other. In fact, GSS and dislocation creep may be in a balance in these samples, as postulated by de Bresser (1998, 2001).

It remains uncertain whether GSS creep can produce a texture in ice. More experiments are needed to quantify the contribution of GSS and dislocation creep to texture development during deformation of fine-grained ice. In order to define the contribution of processes that affect texture during deformation, such as recrystallization and grain growth, more grain-microstructure measurements are also needed.

We suggest that for ice under low-deviatoric stress, as in an ice sheet, GBS occurs and that accommodation by basal slip is likely. Also, dislocation creep and grain-boundary migration occur simultaneously. All of these mechanisms together can give rise to texture in ice. Each deformation mechanism has a given set of material constants that defines the mechanism, and it may be important to identify and include all of these values in both experiments and models. We do not think that it is possible to distinguish between these mechanisms with our experiments. We suggest that a balance of mechanisms occurs, and therefore we see texture development in ice samples. This implies that ice sheet flow models should incorporate texture information and allow for variability of the stress exponent, n, and grain size, d, to fully represent deformation in the flow equation of ice.

In order to further investigate texture development and the effect on ice sheets as a result of GSS creep, future experiments on fine-grained ice are needed with samples deformed at both low ($0.1 \leq \sigma \leq 10$) and high ($\sigma > 10$ MPa) deviatoric stress.

Optimal experiments would have *in situ* neutron diffraction and deformation of ice, which is now available (McDaniel et al., *in press).*

A quantitative texture model could further assess the contributions of GSS and dislocation creep in these samples. Model simulations using GSS creep accommodated by dislocation creep or dislocation creep alone could be compared. For example, if results from GSS creep underestimate the texture, than that is an indication that dislocation creep is likely contributing a significant amount to deformation.

3.6   Conclusions

We present the first quantitative texture measurements on fine-grained ice. All three of our samples show stress-strain curves typical of GSS creep, even for samples deformed under conditions of high stress. Grain-morphology results show that dislocation creep, GSS creep and/or recrystallization are active in the deformation of these samples. This suggests that both dislocation creep and GSS creep were active during deformation. We suggest that four-grain junctions are not unique identifiers of GBS and their presence cannot be used as evidence of GSS creep. More experiments are needed to characterize the contributions of GSS creep to the deformation of fine-grained ice.

Table 3.1. Neutron-diffracton intensities at 121 K (Leadbetter et al., 1985) for ice I with a random orientation distribution for important reflections in this study. Indexing is based on a hexagonal cell. The incoming neutrons strike the scattering center of a set of planes (hk$i$l) and the spacing between these planes is d, or d-spacing. Calculated intensities are measured values from a random powder sample of ice predicted for the (hk$i$l). Calculated intensities have units of relative intensity or arbitrary units [*Brentano*, 1935].

hk$i$l	d(A)	Calculated Intensities
10-10	3.900	999
0002	3.6668	526
10-11	3.4437	588
10-12	2.6716	233

Table 3.2. Deformation data for polycrystalline samples. Confining pressure for all samples was 50 MPa. ε is the axial shortening strain ($\Delta l / l_o$, where l_o is the initial length).

Sample ID	Temperature (K)	ε	Duration (Hours)	Strain Rate (s^{-1})	σ (MPa)
497	222	0.196	143.7	3.9×10^{-7}	42
498	224	0.274	74.3	1.0×10^{-6}	8
499	226	0.168	34.2	1.4×10^{-6}	61

Table 3.3 Expected and measured values of grain axis length in the major and minor axis. Expected values are calculated from major and minor average grain-axis length measurements from LTSEM photomicrographs and the total strain of the sample.

Sample	ε	Major axis of initial material (μm)	Major axis length expected from ε (μm)	Major axis length measured from SEM (μm)	Difference in expected and measured Major axis length (μm)	Minor axis length of initial material (μm)	Minor axis length expected from ε (μm)	Minor axis length measured from SEM (μm)	Difference in expected and measured Minor axis length (μm)
497	0.196	6.81	8.28	6.06	2.22	4.36	5.31	3.32	1.99
498	0.274	6.81	8.95	7.63	1.32	4.36	5.76	3.69	2.07
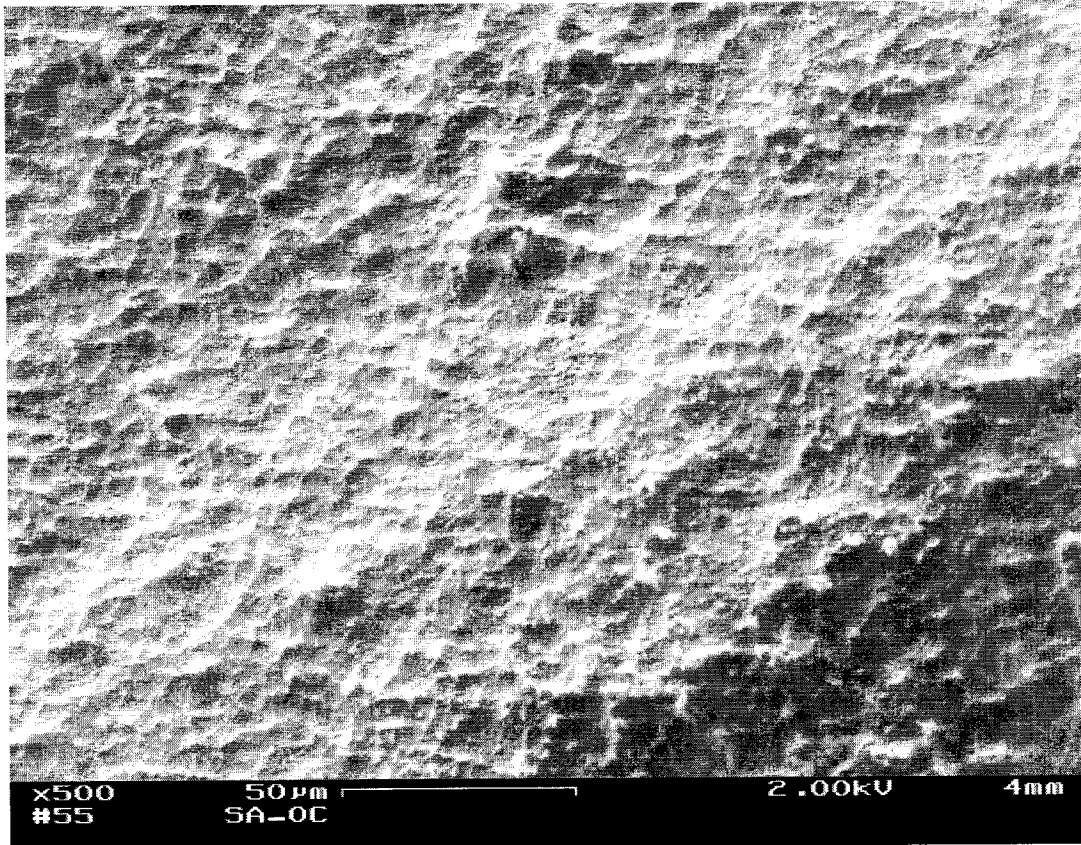
Figure 3.1a. A photomicrograph of the initial material. The scale is 50 μm. The equiaxial shapes outlined by the ridges are the grains. Unlike the deformed ice, the initial material never has grain boundaries that show up as clean lines.

Initial Material Grain Size by Major Axis Diameter

Figure 3.1b. Grain-size distribution of the initial ice material, after the pressure-release technique was performed. The distribution has a bell shape. Only a few large and small grains are present.
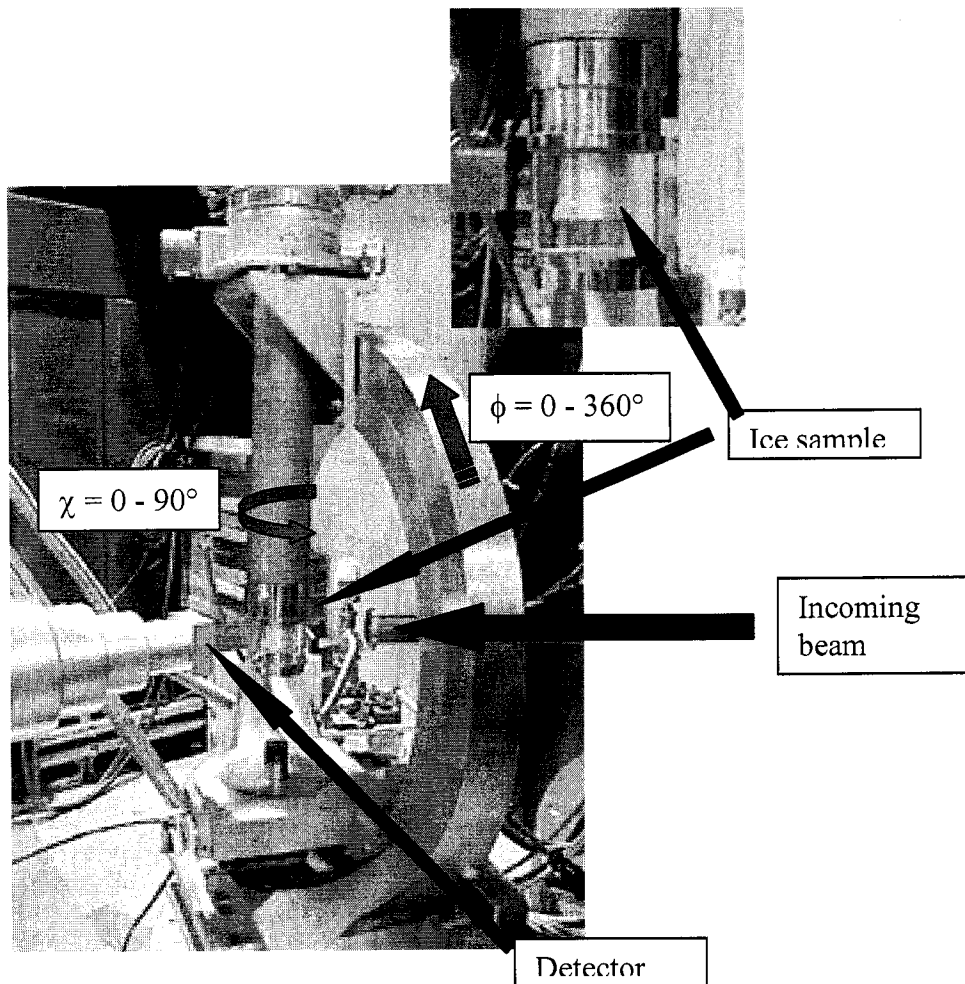
Figure 3.2. Setup of goniometer and cold-finger displex on BT-8. Neutron beam emitted from the tube on the right, detector collimation visible on the left. The Eulerian cradle is the circular devic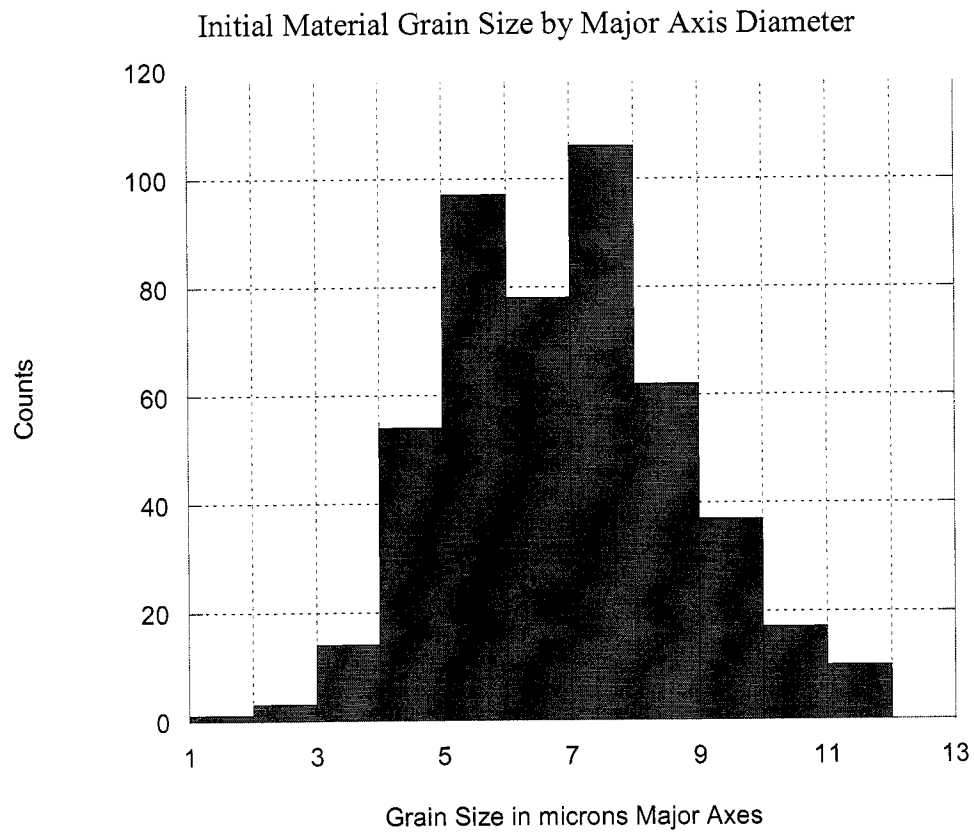e and the displex is the tube hanging down, in between the beam and the detector. The ice sample is in the aluminum can visible in the quartz windows at the end of the cold finger (displex). Inset shows close up of ice sample visible inside aluminum can, contained in cold-finger displex. Neutron beam emitted from the tube on the right, detector collimation visible on the left. Data for all three ice specimens were collected in 5 degree steps (ϕ,χ), where $\phi = 0 - 360°$ and $\chi = 0 - 90°$.
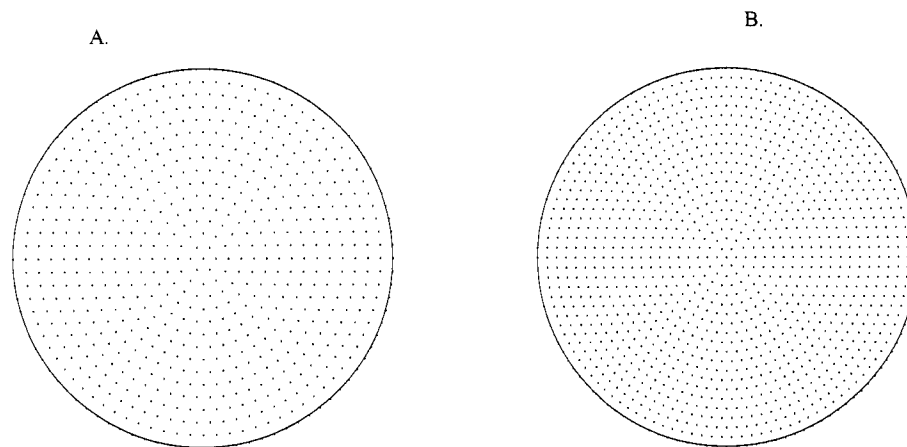
Figure 3.3. Pole figure grids used for measurement (in equal area projection). Figure A was used for samples 497 and 498. Figure B is the finer grid used for sample 499.
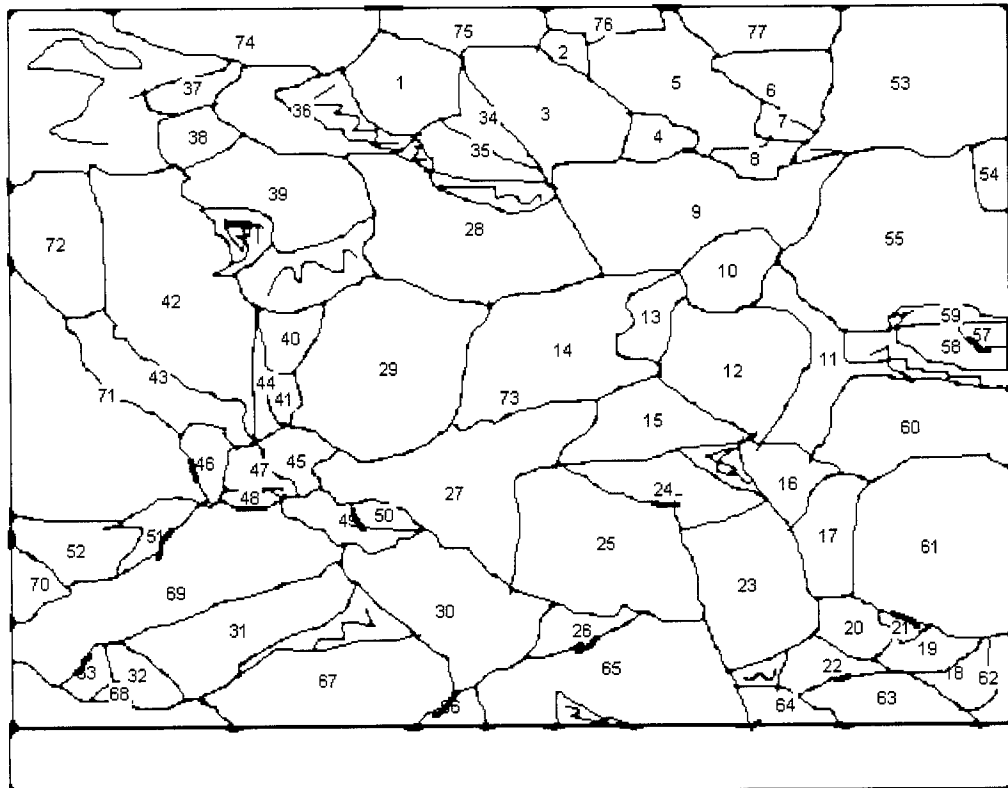
Figure 3.4. The image outline of grain boundaries. Numbers represent grain counts from the imaging program. Not all numbers are visible. Thick lines are regions where grain boundaries had to be enhanced in width for the program to recognize the grains. Areas with black wavy lines through them are regions that were too unclear to define. Most of the unclear regions are oriented so they reflect too much light from the electron beam and are white as a result, or are shadowed by a ridge in the ice and are too dark to see the grain boundaries.
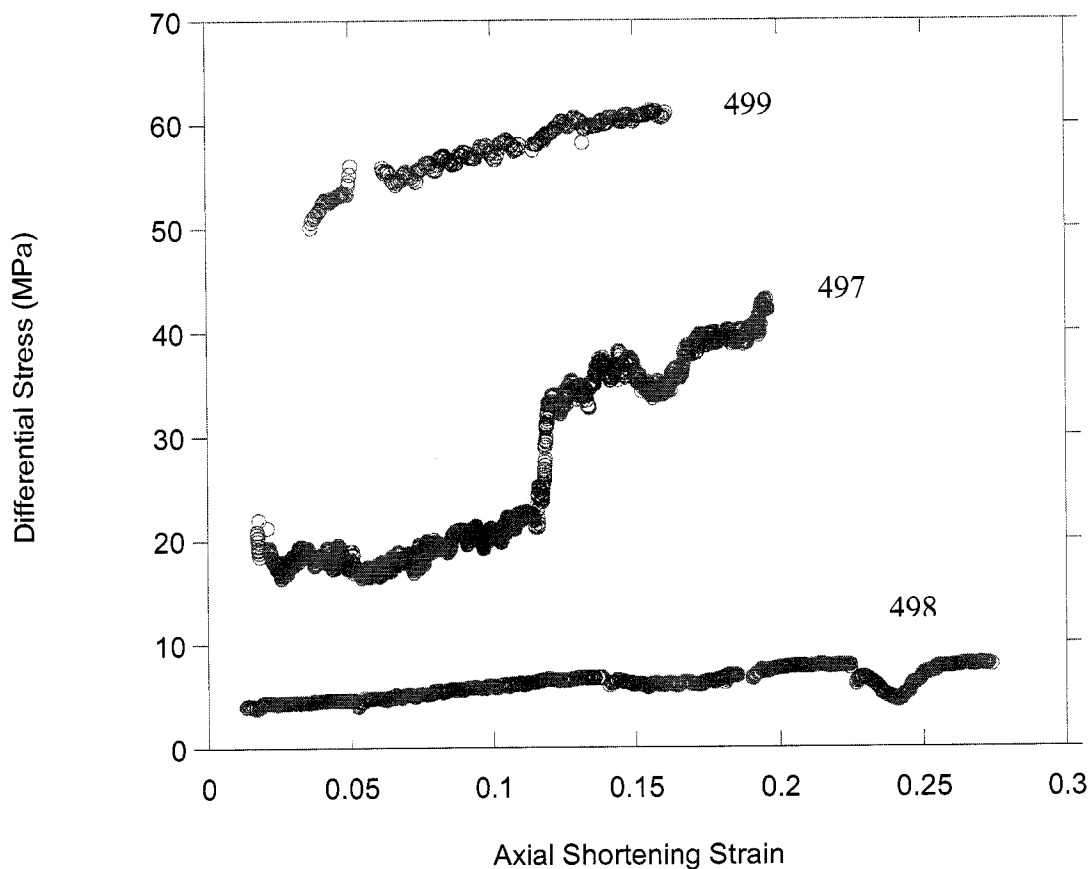
Figure 3.5. Stress-strain curves for deformed ice I_h fine-grained samples 497 (222 K), 498 (224 K) and 499 (226 K). Sample 497 showed a sudden jump in differential stress due to experimental disruption; the piston jumped forward at this point in the experiment. Although the stress suddenly increases, the final texture of the sample is a result of the total strain on the sample [*Wenk*, 1985]. Stress on sample 498 dipped at 0.224 strain, a time when the piston was withdrawn from the sample in order to reset the internal stress gage. When replaced on the sample it was not set properly to its previous position, hence the stress on the sample dropped and then resumed its level over time. Sample 499 shows a typical deformation curve for fine-grain ice I_h.

Measured and Calculated Peaks in D_2O Ice Ih Diffraction
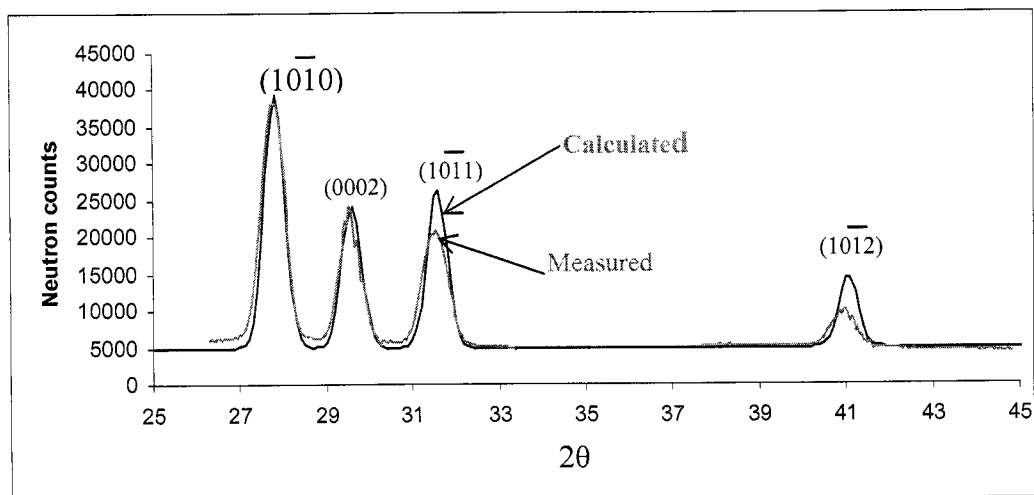
Figure 3.6. Calculated (blue) and measured (red) diffraction profile for D_2O ice. The first 3 peaks on the left were collected together and the 10-12 peak was collected alone. Neutron counts are the number of events, or neutrons that diffract with ice atomic scattering centers and are then detected. The diffractometer measures 2θ, where θ is the angle of diffraction. These are the main diffraction peaks in ice. The blue curve represents the expected location and height of the peaks for a sample with randomly oriented grains.

Figure 3.7 a, b, c. Equal-area projections of measured (top) and recalculated (bottom) pole figures for sample 497. The recalculated pole figures are calculated from the ODF that is computed from the measured pole figures. The direction of compression is in the center of the pole figures. White or blank regions are a result of scaling (recalculated pole figure shows areas that are interpolated from the ODF that are not measured in the measured pole figures). Densities are expressed as m.r.d. on a logarithmic scale. (a) Sample 497, shortened ~0.20 at 222 K. (b) Sample 498 shortened ~0.28 at 224 K. (c) Sample 499 shortened ~0.17 at 226 K. All samples show a similar texture distribution: 10-10 poles have the highest pole density on the outer circumference, because c-axes align with the direction of compression in ice, so the poles to the c-axes plot on the outer edge of the pole figure. The 0002 pole figures in ice show the poles to the basal plane. They are concentrated in the center of the pole figure because the basal planes align perpendicular to the axis of compression.

(equal-area proj.)

Measured

Recalculated

max.= 1.46

1.97
1.66
1.40
1.18
1.00
.84
.71
.60

log. scale
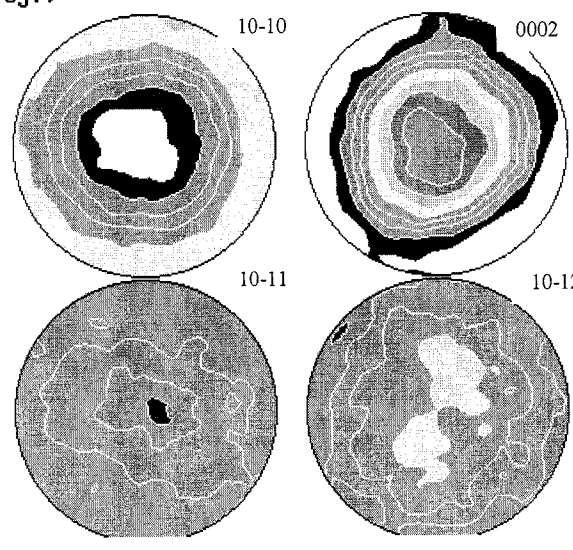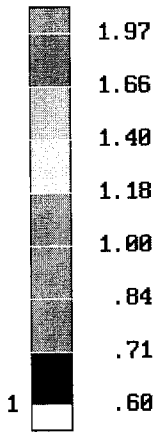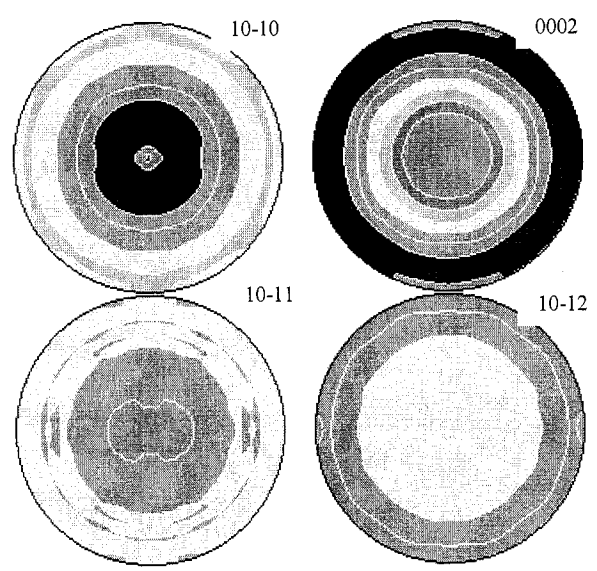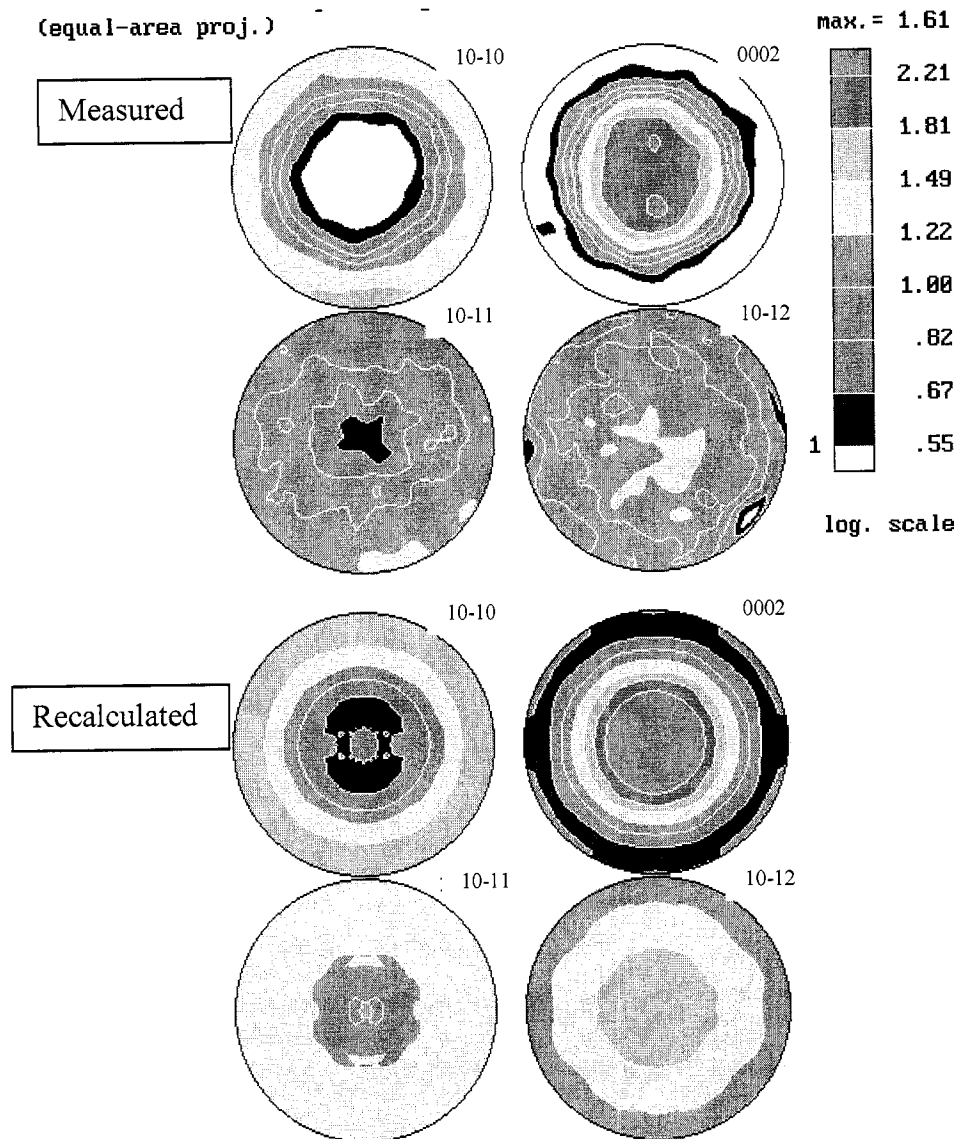
Figure 3.7b. Experimental pole figures of ice 498.
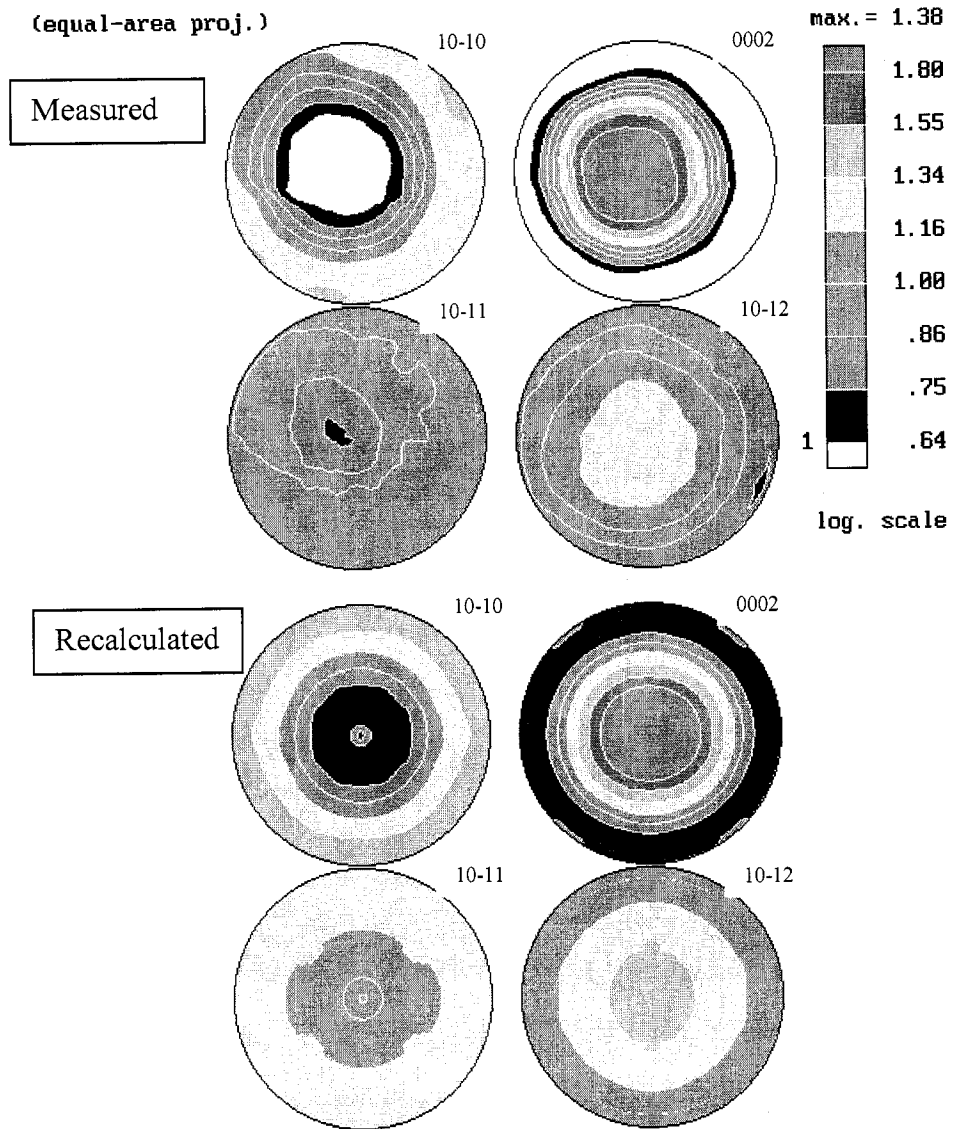
Figure 3.7c. Experimental pole figures of ice 499.
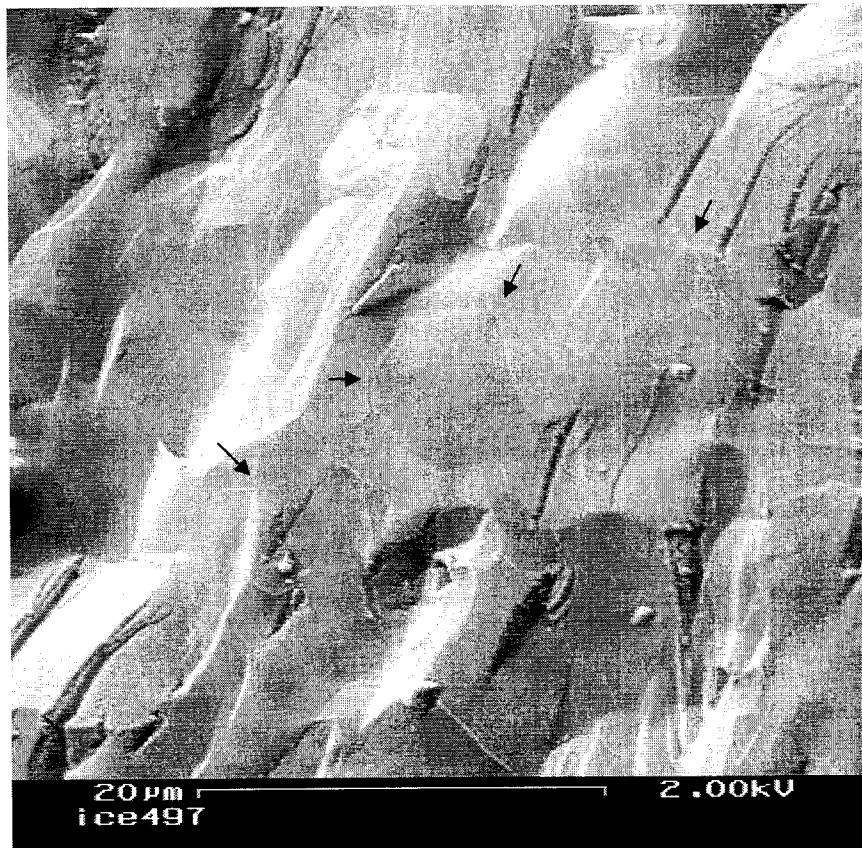
Figure 3.8a. LTSEM of ice 497 with a scale of 20μm. This sample was axially shortened by 20 %. Grains are typically larger than in the initial material, with some very large grains surrounded by much smaller grains. Grain growth is inferred. Arrows point to several four-grain junctions. Orientation of sample with respect to the axis of compression was lost during sample preparation for LTSEM.

Ice 497 Grain Size by Major Diameter
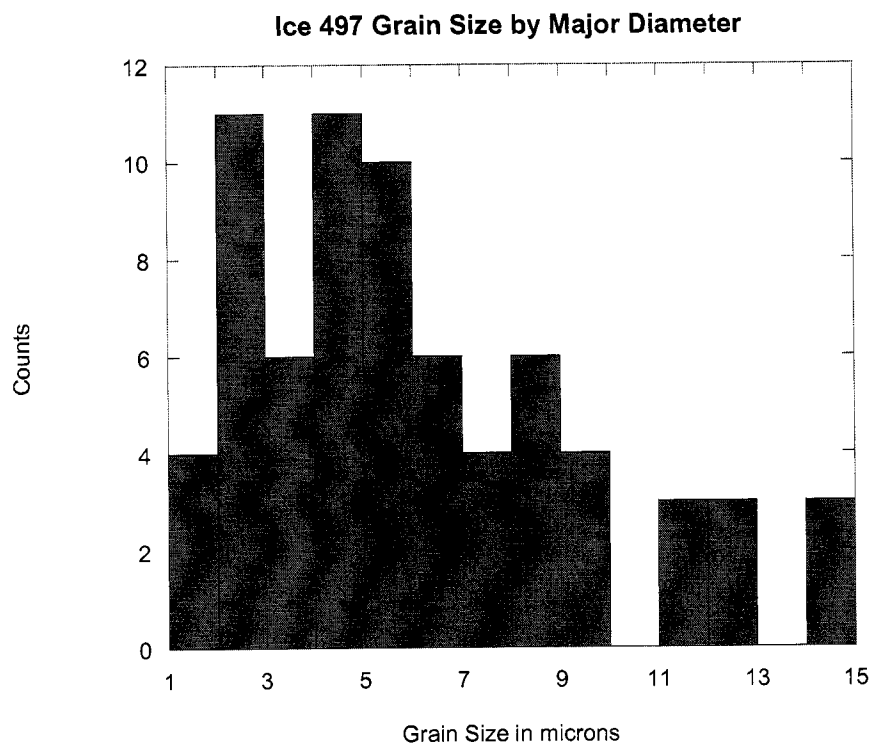
Figure 3.8b. Grain-size distribution of sample 497 after deformation. Grain size is defined by the major-axis diameter of each grain. See text for more detail on measuring grains.
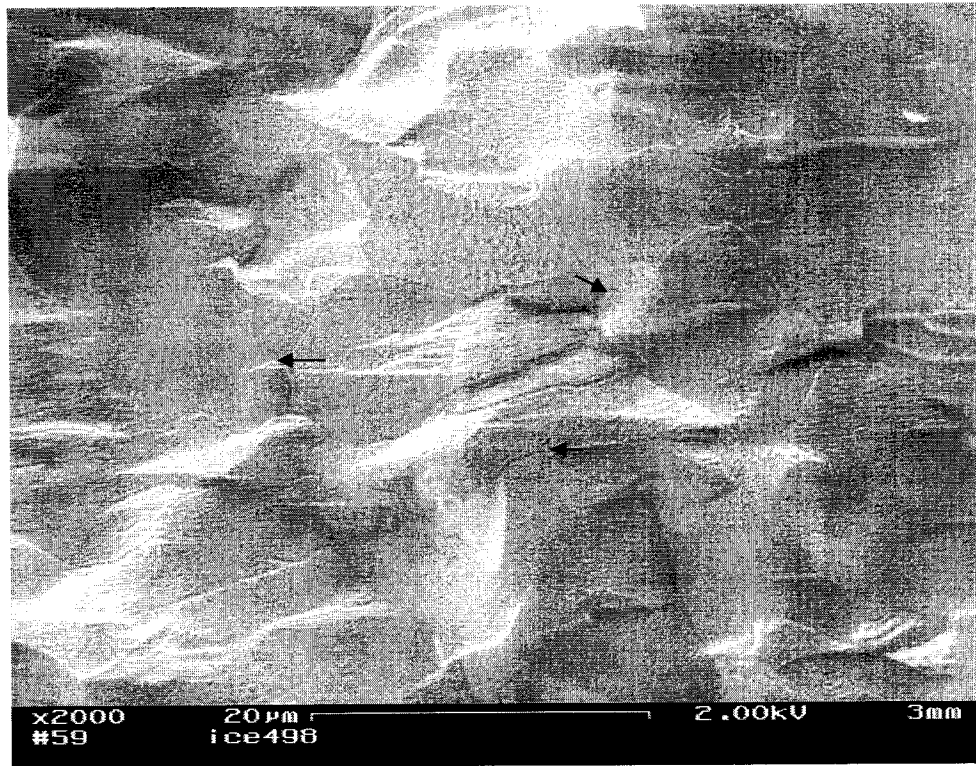
Figure 3.9a. LT SEM of sample 498 at 20µm resolution after deformation. Arrows show four-grain junctions. Sample orientation with respect to axis of deformation was lost during sample preparation for LTSEM.

Ice 498 Grain Size by Major Diameter

Grain size in microns
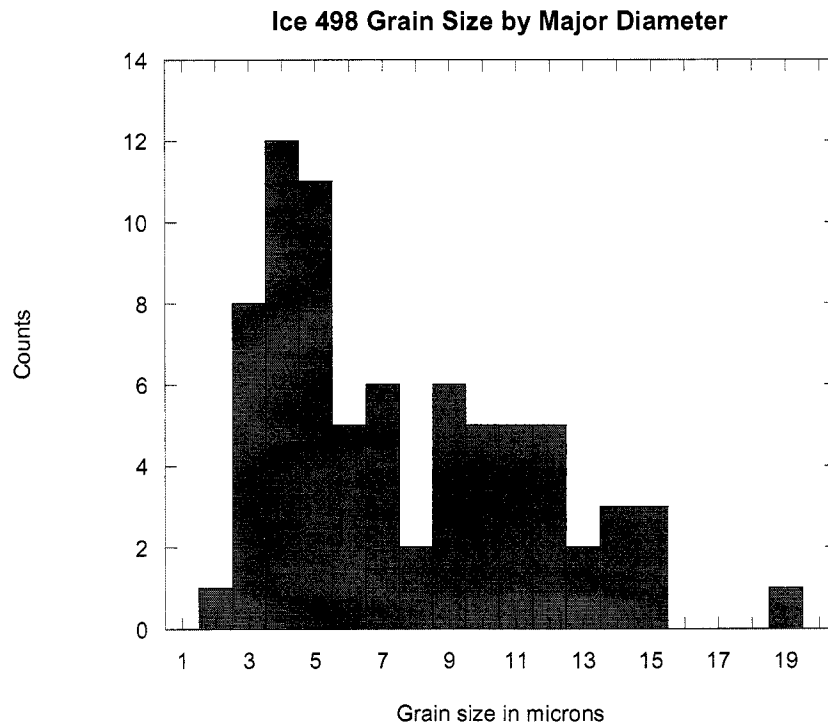
Figure 3.9b. Grain-size distribution of sample 498. Grain sizes are measured by the major-axis diameter of each grain. See text for explanation. Sample 498 has a similar distribution to 497. Compared to the initial material, 498 has an increased range of grain size.
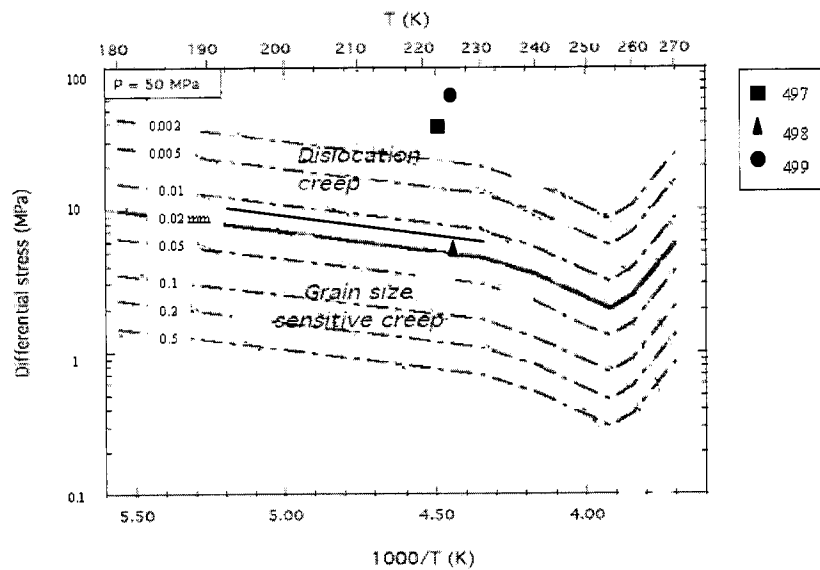
Figure 3.10. Deformation-mechanism map of ice. The dash-dot blue lines represent the boundary between GSS and dislocation creep, dependent on grain size. The solid blue line depicts the boundary when the average grain size is 20 microns in the sample. The conditions of deformation of our 3 ice samples are plotted. The samples had initial grain size of 2-10 microns, and some grains increased in size to approximately 20 microns. If we define our grain size as between 10 and 20 microns (black line), conditions for sample 498 fall in the GSS creep field while conditions for samples 497 and 499 fall in the dislocation creep field. Modified from plot by WB Durham.

Chapter 4

An *in situ* Deformation Apparatus for Time-of-Flight Neutron Diffraction: Texture Development of Polycrystalline Ice I_h

4.1 Summary

We document the first experiment and a new *in situ* deformation apparatus built for neutron diffraction investigations of polycrystalline materials in low-temperature environments. We performed texture analysis of polycrystalline ice I_h deformed uniaxially between 220 and 240 K using time-of-flight (TOF) neutron diffraction on the High Intensity Preferred Orientation (HIPPO) diffractometer at the Manuel Lujan Neutron Scattering Center at Los Alamos National Laboratory (LANL). The new deformation apparatus operates at 1 atmosphere of ambient pressure, and over temperatures in the range of 77 K $<T<$ 298 K, and accommodates up to 68 kilograms of uniaxially applied load. It is suitable for diffraction studies of any bulk polycrystalline material, ideally cylindrical in shape, and is adaptable to multiple neutron spectrometers, including those at other polychromatic and monochromatic neutron facilities. The first experiment on a hexagonal ice sample demonstrates development of fiber texture in the direction of the applied load. The equipment has many applications to Earth science, glaciology, and ice engineering.

4.2   Introduction

Because glaciers and ice sheets comprise the most-mobile solid surfaces on planet Earth, investigating deformation mechanisms in polycrystalline ice has been key to understanding the short- and long-term geophysical evolution of the earth, and has been instrumental in ice-engineering applications. There is a need in these fields to measure natural and experimental ice samples at the atomic level during deformation under *in situ* or real-time conditions.

The crystallographic structure and unique physical behavior of ice have been studied for over a century, not only to understand the evolution of the Earth and glacial flow, but also to use ice as a model material for materials and ceramics sciences. The form of ice (I_h) found on Earth has a hexagonal crystal structure that leads to a wealth of unique physical properties also found in natural rocks and some metals. Here and throughout the paper we refer to hexagonal ice I_h as ice.

To investigate the crystallographic behavior of polycrystalline fine-grained (2-10 µm) ice under real-time load conditions, we built an *in situ* low-temperature, deformation apparatus for neutron spectrometry. In the past, laboratory investigations of deformation regimes in polycrystalline ice have been restricted to investigations where the ice sample is deformed, removed from the deformation apparatus, and then measured for crystallographic information [*Bennett*, 1994; *Bennett, et al.*, 1997; *Goldsby and Kohlstedt*, 1997; *Montagnat, et al.*, 2003; *Stern, et al.*, 1997]. As a result, only the final texture of a sample can be measured; the stages of texture development during the experiment are lost.

To investigate polycrystalline ice samples crystallographically during deformation and temperature changes, we designed and built a low-temperature deformation apparatus to deform ice *in situ* using time-of-flight (TOF) neutron diffraction on the unique High-Pressure-Preferred Orientation (HIPPO) diffractometer [*Wenk, et al.*, 2003] housed at the Manuel Lujan Jr. Neutron Scattering Center (Lujan Center) at LANL in Los Alamos, New Mexico, USA. The deformation apparatus is suitable for virtually any polycrystalline sample of appropriate size with a length and width up to 2.54 cm x 2.54 cm in size. The new apparatus is suitable for most spectrometers at the Lujan Center and may be adapted for use at other neutron source facilities.

With this apparatus, we measured deformation and crystallographic strain directly and simultaneously, including deformation-regime changes and texture (preferred crystallographic orientation) development. Neutrons are ideal probes for bulk-materials analyses and are well suited to investigation with special environments. As relatively weak scatterers, they are also nearly transparent to many materials that are used to build environmental cells, and large bulk samples containing light and heavy elements and coarse grains can be analyzed quantitatively.

To achieve our scientific goal of measuring the texture evolution in a polycrystalline ice sample during deformation and at glacial temperatures, we built a deformation rig with a sliding-piston cylinder. This paper presents the first experimental results using the new deformation rig, we have measured texture evolution *in situ* of laboratory-produced, polycrystalline ice under load.

4.3   Experimental Design

Our goal was to build an apparatus to apply a constant load to a polycrystalline sample, suitable for neutron-diffraction experiments at low temperatures. Our scientific goal was to relate texture evolution to strain in ice. For this task we chose to design a rig for the new TOF neutron diffractometer HIPPO. HIPPO sits on Flight Path 4 at the Lujan Center, with a time-average flux on a sample of ~1×10^7 neutrons cm^{-2} s^{-1}. The diffractometer has approximately 1393 He^3 gas tube detectors that surround the large (30 cm diameter, 183 cm deep) sample chamber, at 5 different scattering angles in 360-degree rings. To detect the diffracted neutrons, this instrumental set-up is ideal for efficient quantitative *in situ* measurement with environmental cells; the multiple scattering angles and detectors combined with TOF diffraction analyses allow for simultaneous multiple peak analysis without rotating a sample or sample environment. On HIPPO, a full diffraction pattern (0.12 Å < d < 47.5 Å, where d is the spacing between diffraction planes) may be collected almost instantaneously. Refinements of the TOF patterns allow for not only a detailed quantitative texture analysis, but also analysis of complex crystal structures, phase proportions, grain shapes, residual stresses and crystallographic textures, simultaneously. Various Rietveld methods provide standard analyses for HIPPO [*Lutterotti, et al.*, 1997; *Rietveld*, 1967; *VonDreele*, 1997; *Wenk, et al.*, 2003; *Wenk, et al.*, 1998].

Five design objectives were identified for the apparatus to achieve *in situ* deformation and characterization of polycrystalline ice using neutron diffraction. The first requirement was to accommodate large samples for bulk measurement in the HIPPO chamber. Second, the sample chamber of the deformation apparatus needed

to be isolated from the surrounding ambient atmosphere so that a controlled environment could be maintained around the sample to protect the integrity of the sample and its crystal structure. The third requirement was to have low-temperature capability and adequate temperature control to keep the sample at a chosen temperature or to warm or cool the sample quickly. Fourth, easy access to the platform had to exist for supporting the weight of the load material (or the dead-load stage) for quick, convenient load increase or decrease. Finally, due to the cumbersome hoses normally attached to the apparatus for temperature control, we did not want to rotate the entire set-up in order to achieve adequate pole-figure coverage.

To address these design objectives, first we designed an aluminum deformation apparatus to fit into the HIPPO chamber and to accommodate a sample size of approximately 2.54 cm length by 2.54 cm width. The deformation rig holds a sample at the end of a cold finger, and perpendicular to the applied load (Figure 4.1). Figure 4.2 shows an engineering sketch of the apparatus sitting in the HIPPO chamber. A load plate sits perpendicular to the sample cold finger, and bears multiple circular weight plates to increase or decrease the load. Our sample was cylindrical in shape for texture measurement to avoid absorption corrections; however samples of different sizes and shapes could be used. A sample may be smaller in size, but cannot be larger or the apparatus would not have a tight seal, and temperature control would be compromised.

Second, to achieve temperature control in a the environment around the sample, we built a vacuum chamber around the sample using 0.0580 cm thick aluminum "windows" (Figures 4.1 and 4.2). This aluminum is thin enough to allow

easy penetration by neutrons. Aluminum is a weak coherent and incoherent scatterer of neutrons and is commonly used in sample environments [*Bailey*, 2003].

Third, we used a temperature controller to regulate the flow of liquid nitrogen to the sample chamber. To protect the sample from direct contact with the liquid-nitrogen coolant, it was wrapped in thin aluminum foil (again nearly transparent to neutrons). Thermocouples attached to the base of the sample chamber measured temperatures at the base of the sample. Low-temperature o-rings provided seals to the sample chamber for both constant temperature and vacuum maintenance.

Fourth, the rig is top-loading with a series of weighted plates to minimize time to change applied loads. We transfer ed the sample into the cooled sample chamber of the deformation apparatus outside the HIPPO chamber to minimize time between sample changes. The load plate can be accessed through the diffractometer 'top hat,' so that the rig and sample remain isolated in the chamber while load is increased or decreased.

Last, there was no need to rotate the press for texture analyses for two reasons: the advantage of a TOF analysis, and the unique design of HIPPO. Traditionally, texture was measured using monochromatic radiation (a nuclear-reactor source). Usually, diffractometers at a reactor source have detectors that move in order to collect data at different d-spacings in the sample. This results in a necessary sample rotation, which is difficult with environmental cells. The diffraction pattern for the sample is collected in parts, as the detector moves, which can require a collection time on the order of many days.

In a neutron TOF measurement, neutrons with multiple wavelengths are collected simultaneously. In other words, an entire diffraction pattern is collected at once and in a matter of hours. The design of diffractometers can also be used to exploit the multiple scattering intensities available from TOF neutrons. We chose to use HIPPO because it is comprised of 1393 detector tubes grouped into 59 detector banks and arranged in a circular array. This allows texture measurements to be done on very few sample orientations. Coverage of pole figures by HIPPO detectors (Figure 4.3a) for this study is shown in Figure 4.3b. We do not use all available detectors in our analysis because the deformation rig blocked some of the detector panels. This coverage is adequate for a calculation of the orientation distribution function (ODF) when cylindrical symmetry can be assumed based on the applied load.

The main body of the press was built almost entirely of aluminum, which is strong enough to sustain a load, is nearly invisible to neutrons, and can be fitted with various "top hats" and therefore adapted to several diffractometers in the Lujan Center. The piston and the ball bearings in the shaft of the cylinder that make the piston slide unhindered were built of steel. In a collected diffraction pattern, the aluminum peak from the deformation apparatus is small and does not affect peak fitting during Rietveld refinement.

4.4   Experiment and Results

Figure 4.4 shows the deformation apparatus with the ice sample mounted on the displex just before loading the rig into the HIPPO sample chamber. The main cylindrical shaft of the press sits perpendicular to the top hat. The sliding steel piston

is attached perpendicular to a flat plate that fits inside the top hat and holds the loading plates. The piston is positioned inside the shaft of the deformation apparatus and rests against the top of the sample. The sample is inserted through the bottom of the rig and a stationary holder is screwed in flush against the bottom of the sample to hold it in place.

For the first experiment we loaded a fine-grained (2-10 μm) polycrystalline laboratory-fabricated [*Stern, et al.*, 1997] ice sample (2.23 cm length by 2.54 cm diameter) into the deformation apparatus. The piston was flush against the upper surface of the sample, which was shaved flat during sample preparation and loaded into the sample chamber. The deformation rig was placed into the HIPPO chamber and a load of 20 kg was placed on the ice sample parallel to the sample axis. Using a constant load, the sample was shortened a total of 0.2667 cm in length for a total strain of 0.210. Temperature was varied between 230 K and 266 K over a period of 7.5 hours (Figure 4.5).

Diffraction patterns were collected in five-minute intervals over 7.5 hours while maintaining the constant load. Figure 4.6 shows the ice diffraction patterns as a function of orientation after 110 minutes of deformation at a 20 kg load and the principle peaks for hexagonal ice (10-10), (0002), (10-11) and (10-12). Each color in the figure represents a different detector bank in the circular array of high angle banks for HIPPO, and therefore a separate orientation. These colors match the colors of the detector bank coverage in a pole figure as plotted in Figure 3b. If no texture were present, the individual diffraction patterns would have similar peak-height ratios throughout the patterns with respect to orientation. The difference in intensity indicates that a texture has developed in this sample.

We collected the TOF neutron data in 5-minute real-time intervals on all 1393 HIPPO detectors, and examined textures as a function of increasing temperature, using Rietveld analysis and the direct inversion method MAUD (Material Analysis Using Diffraction) texture package [*Lutterotti, et al.*, 1997]. MAUD uses a Marquardt least-squares method to fit diffraction powder peaks and to obtain the ODF for a texture analyses. We used the Extended-Williams-Imhof-Matthies-Vinel (E-WIMV) algorithm direct method to compute our spectra collected on HIPPO [*Wenk, et al.*, 1994]. We used the program to calculate the pole figures for the relevant ice diffraction peaks.

Figure 4.7 a-c shows the (10-10), (0002), (10-11) and (10-12) pole figures for the ice sample at three times during the 7.5 hour deformation. Pole figures are plotted in equal-area projection in multiples of random distribution (m.r.d.) with the direction of stress in the center of the pole figure. Figure 4.7a shows pole figures measured at T= 230 K after 148 minutes of total deformation time (out of 450 minutes). Figures 4.7 b and c show pole figures at T= 239 K after 298 minutes of total deformation and T= 240 K after 448 minutes of deformation, respectively.

Texture analyses of these three time intervals reveal a similar pole distribution for the sample as time increases, with twice as many (0002) poles parallel to the compression axis than as normal to it. The sample has 2.28 m.r.d. at 148 minutes, 2.19 m.r.d. after 298 minutes, and 2.32 m.r.d. at 448 minutes.

4.5 Discussion

This work demonstrates a first successful measurement of texture in polycrystalline ice I during *in situ* low–temperature deformation under constant load. First results compare well with previous results on texture in ice I. Natural glacial samples show this development of c-axes oriented parallel to the compression direction arising from slip on the basal plane [*Kamb*, 1972; *Kamb*, 1961]. Models also demonstrate this dominance of the basal plane [*Castelnau, et al.*, 1996]. Results show that there are approximately twice as many (0002) poles parallel to, than perpendicular to, the axis of compression. This result is expected at this temperature regime where laboratory experiments have shown that easy basal slip occurs in ice at these temperatures, allowing crystallographic c-axes to rotate and align with the compression direction [*Durham, et al.*, 1983; *Duval*, 1979].

We could improve these pole figures by 1) increasing the number of neutron counts and 2) rotating the apparatus in the HIPPO chamber. Collecting for longer count intervals would give sharper diffraction peaks, making Rietveld refinement more accurate. Also, rotating the deformation apparatus inside the HIPPO chamber would achieve better pole figure coverage. With ice, which in this case has fiber texture, rotation was not necessary for a good ODF calculation. However, with a sample of lower symmetry, rotation is necessary.

Overall, the rig performance was good and the design proved successful. Temperature control was irregular due to the length of the liquid nitrogen hoses and placement of the liquid nitrogen dewar, which was limited by size and space within

the experimental room. A solution would be a cold source such as liquid nitrogen or liquid hydrogen in a dewar located inside the HIPPO chamber or directly above the HIPPO door. This would eliminate the distance the cooling medium needs to travel, and thus less pressure would be needed in the dewar to keep a constant flow for cooling. This would also eliminate ice forming by condensation on the cables, which had to be de-iced several times throughout the experiment to achieve a constant flow of LN_2 (ensuring no blockage due to freezing). Also, placing the cooling medium in the HIPPO chamber would allow for rotation of the deformation rig; one rotation of 90° or 180° would improve the coverage of pole figures.

The texture results are not unexpected. With increasing strain and warming temperatures, we expected to see the texture increase. However, our experimental conditions varied. We present two possible explanations for our results: the texture could be inherited from the initial sample or a balance has arisen between strain-causing-fabric development and recrystallization. Since we were unable to measure the initial texture of the initial material, we do not know if the ice had a completely random initial texture or if some texture was imparted in the making the initial material. Future experiments should be performed on a material whose initial texture is known.

Future work in ice deformation and texture analyses includes *in situ* characterization of texture development at various temperatures and ambient pressure conditions as a means of exploring dominant deformation mechanisms in ice. Another important factor to investigate is changing grain size. While theoretically this should be possible with neutron diffraction, there is no accepted technique for this measurement. The use of low-temperature scanning electron microscopy would

be useful in characterizing the grain morphology of samples after they have been deformed in the *in situ* apparatus.

Geologists, materials scientists and chemists could use this rig to explore any low temperature or ambient temperature material parameters that would respond to the load applicable by this apparatus. Also, research in liquid-chemistry fields where solids may form under varying temperature conditions could also be carried out with this rig.
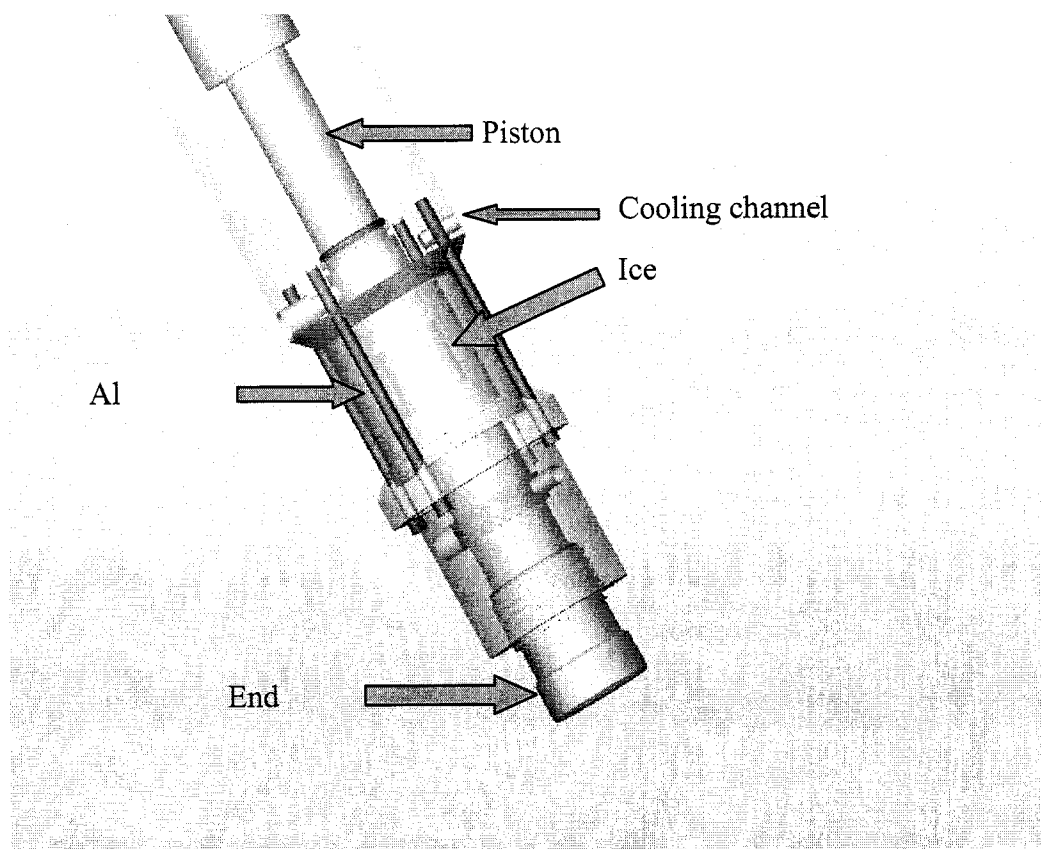
Figure 4.1. A close-up schematic diagram of the deformation apparatus. The ice sample is visible in the deformation chamber, marked by an arrow. The top of the ice sample is flush with the piston (bearing load plates) and the bottom of the sample is held in place by the end plug. 4 cooling channels sit at 90° intervals above the sample; only 2 are visible in this image; one is labeled. Image courtesy of Mark Taylor.
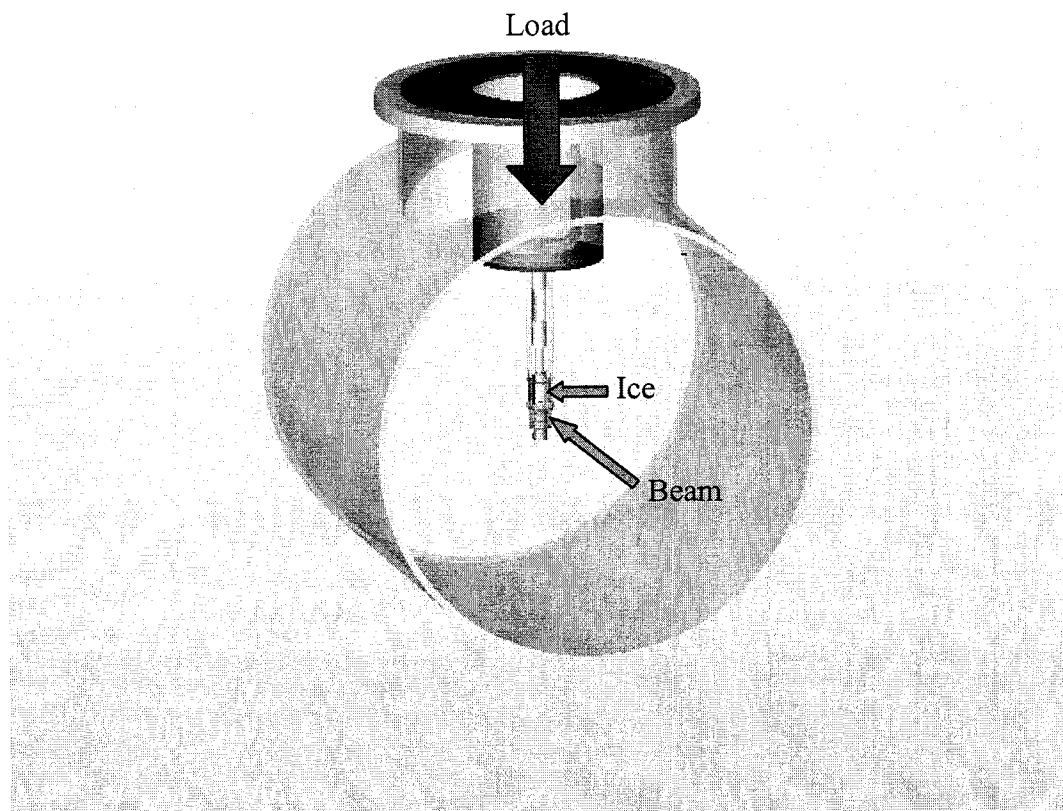
Figure 4.2. The deformation apparatus lowered into the HIPPO chamber. The weights are placed on top of the apparatus on a plate (not pictured here) directly below the red arrow marking the load direction. The direction of the neutron beam is shown. Image courtesy of Mark Taylor.
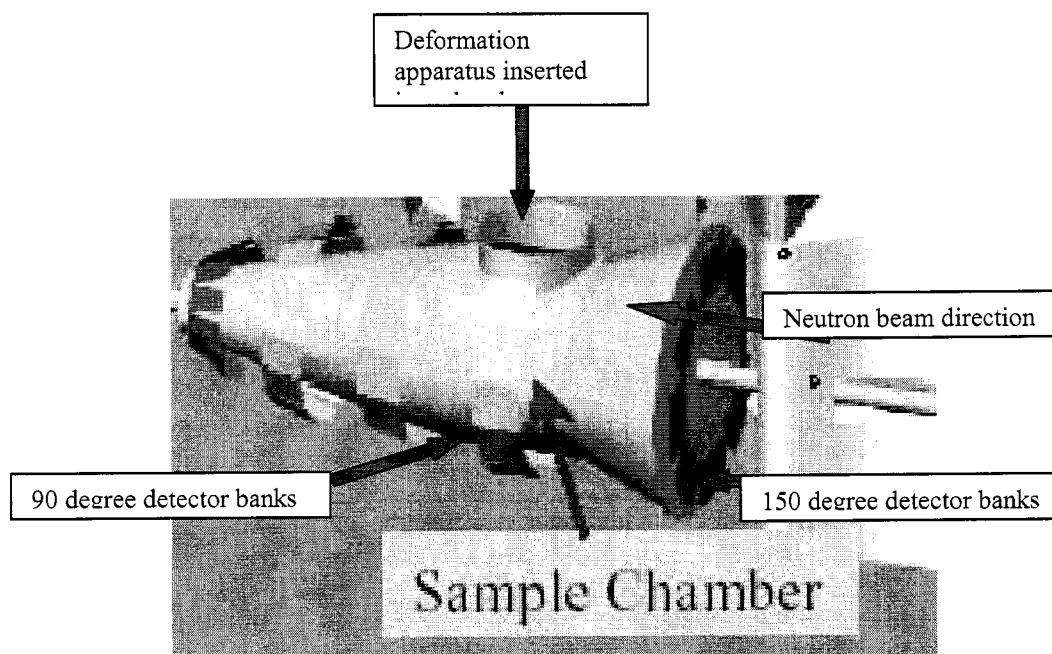
Figure 4.3a. HIPPO detector banks and sample chamber. The detector banks are marked by different colors. The circular array of these banks, which is possible with TOF neutron measurements, increases pole-figure coverage and minimizes the need for rotation of the apparatus. The neutron beam (marked with an arrow) comes into the HIPPO chamber from the right. The deformation apparatus is inserted through the top of the chamber so that the sample sits at the level of the beam.
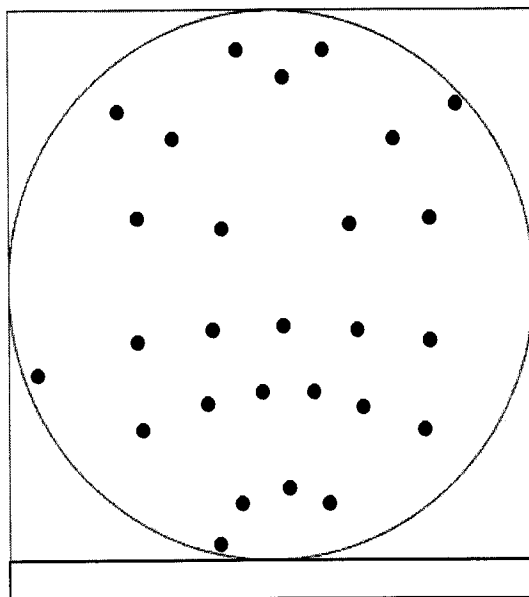
Figure 4.3b. Pole-figure coverage of HIPPO detector banks produced in MAUD. Each number represents a different set of banks. The center of the pole figure is the compression axis. The neutron beam is going into the page, perpendicular to the pole figure.
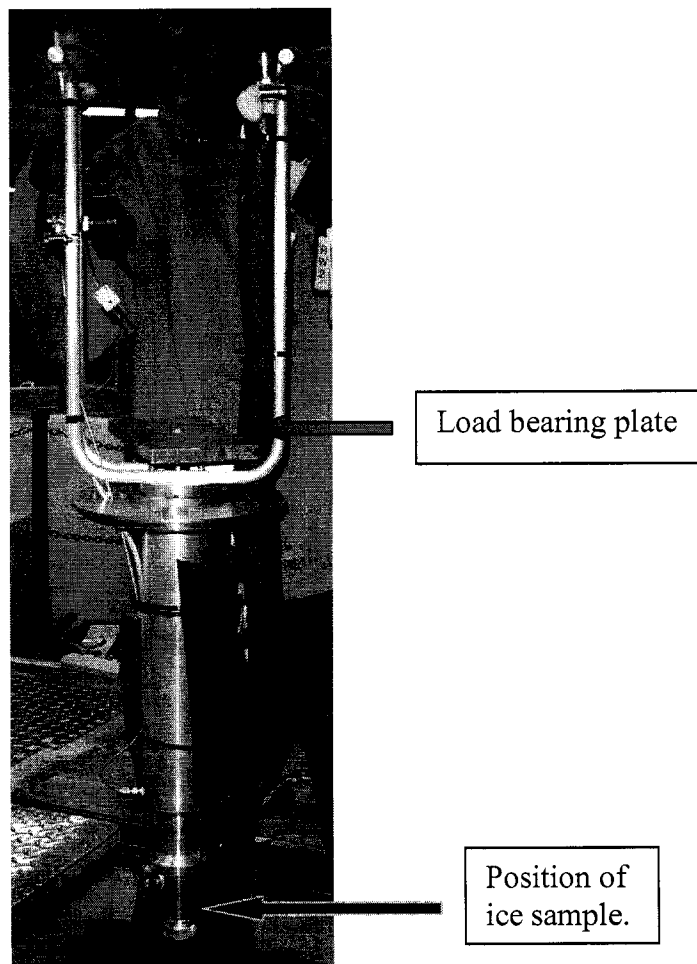
Figure 4.4. The deformation rig is positioned above the HIPPO chamber, ready for insertion into the chamber. HIPPO instrument scientist Darrick Williams is holding the rig. Arrow shows location of ice sample in the deformation chamber. The load plate is visible between the U-shaped handles. Weights are placed on the plate after the deformation rig is inside the HIPPO chamber.
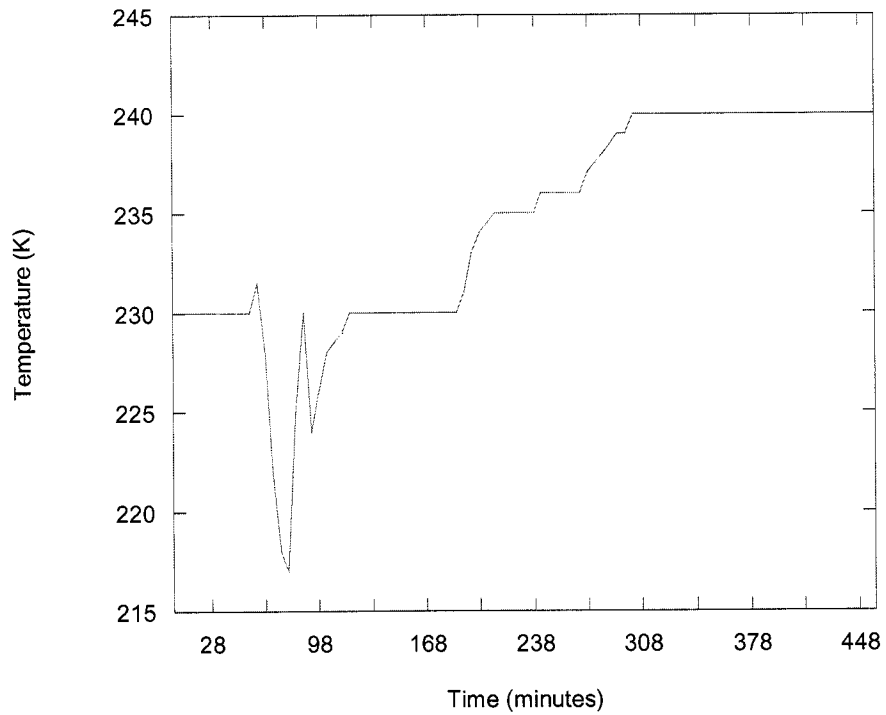
Figure 4.5. Temperatures and time spent at each temperature. Temperature
fluctuated as the level of the liquid nitrogen in the dewar decreased. The cooling
lines from the dewar to the deformation rig were long (4.6 m) which also caused a
problem for maintaining a steady temperature. Future experiments on the rig will use
a cooling medium that sits within or on top of the HIPPO chamber, creating shorter
travel routes for the cooling medium. This will help stabilize the temperature during
an experiment.
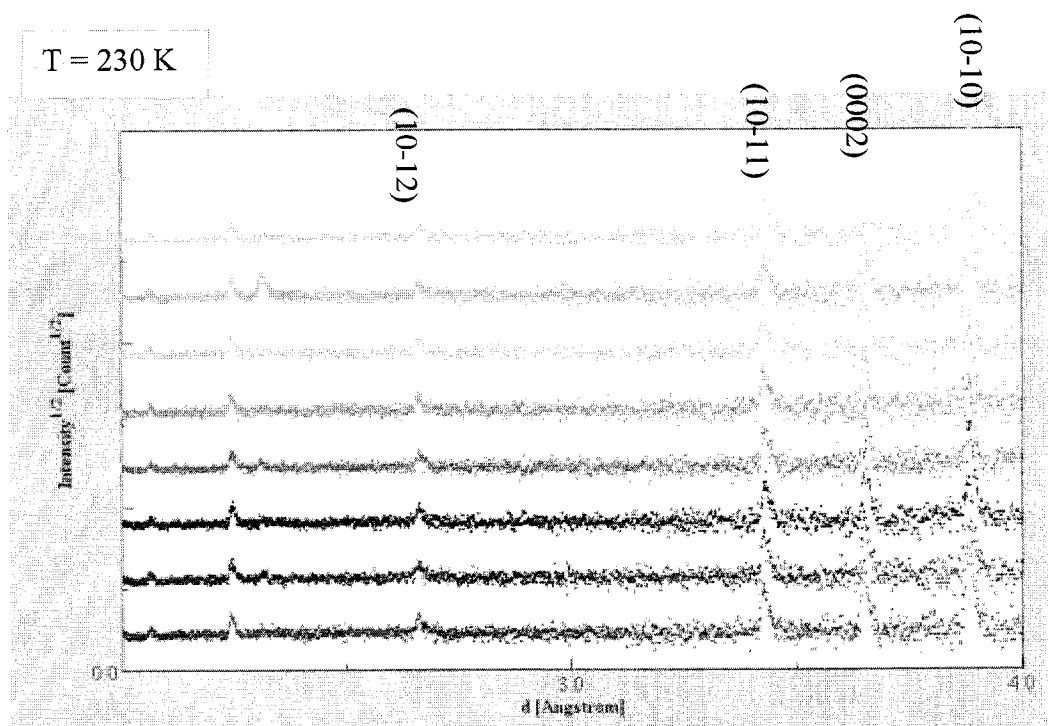
Figure 4.6. Ice diffraction pattern in HIPPO of high-angle (150 degree) detector banks after 148 minutes of deformation at a temperature of 230 K. Each color represents a different detector bank in the circular array of high angle banks for HIPPO. The vertical axis shows intensity scaled by counts, or the number of counts of neutrons reflected off different crystallographic planes. The four prominent peaks for hexagonal ice are labeled with their Miller indices (hk$i$l).
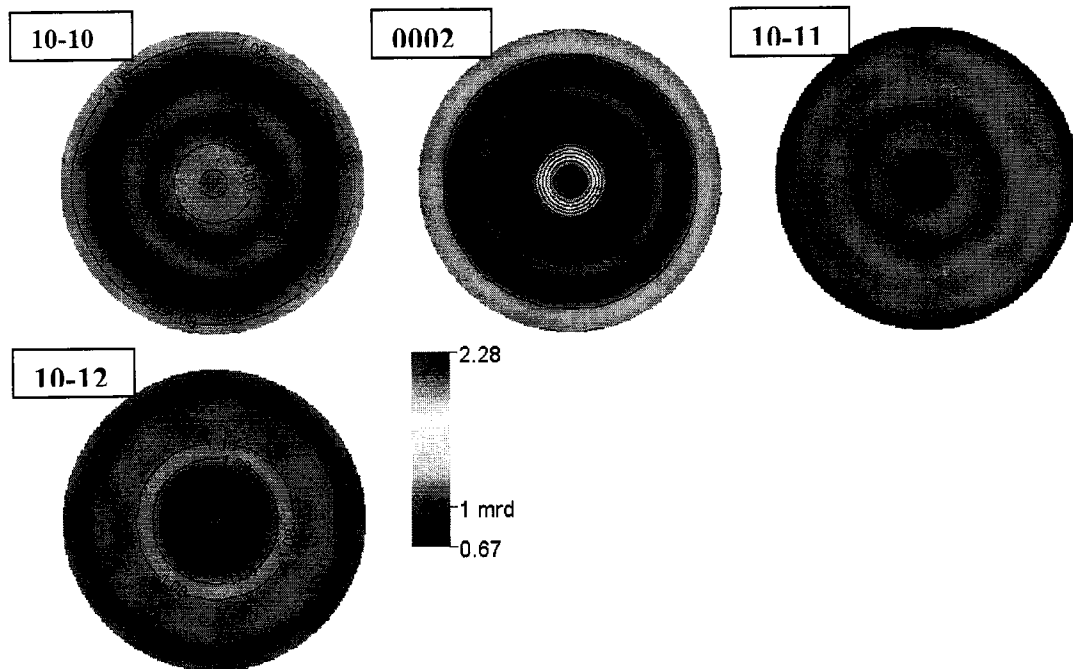
Figure 4.7a. Equal-area projection of pole-density distribution in ice after 148 minutes of deformation with temperature at 230 K.
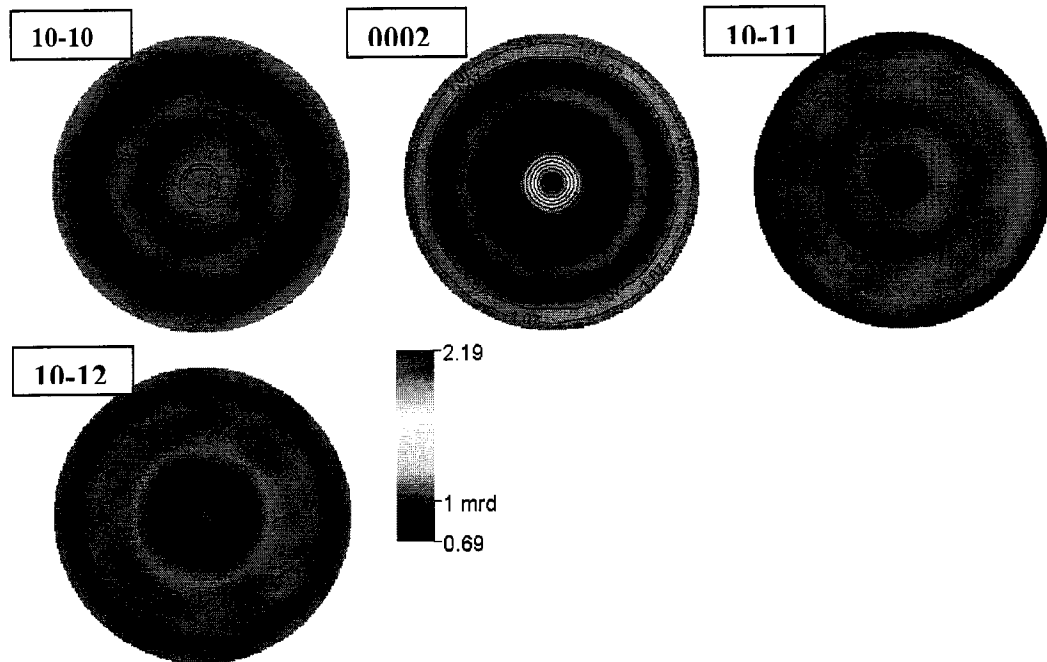
Figure 4.7b. Equal-area projection of pole-density distribution in ice after 298 minutes of deformation. Temperature was 239 K.

10-10

0002

10-11

10-12

2.32

1 mrd

0.72
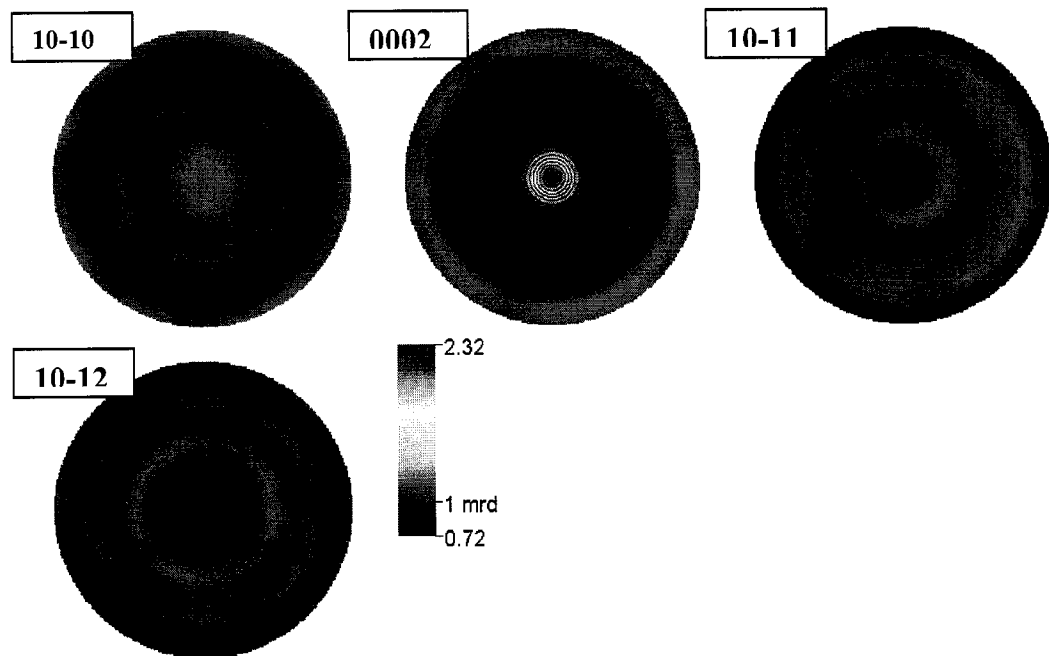
Figure 4.7c. Equal-area projection of pole-density distribution in ice after 448 minutes of deformation. Temperature was 240 K.

Chapter 5

CONCLUSIONS

In this dissertation I use three techniques to further the understanding of fine-grained ice as an experimental analog for natural ice found in ice sheets: low temperature scanning electron microscope (LTSEM), monochromatic neutron diffraction with previously deformed samples and *in situ* time-of-flight (TOF) neutron diffraction, and a new *in situ* deformation/texture apparatus. Each chapter in this work has addressed a unique approach to measurements of fine-grained ice. The highlight of this work is that these techniques open many possibilities for future research. If field measurements can be reproduced with laboratory measurements of ice, the current understanding of ice deformation and grain growth will be greatly advanced. In particular, these measurements can enhance models of ice flow.

The current knowledge of ice flow arises mostly from ice-velocity measurements collected in the field and structural measurements collected on ice cores. Advanced models reconstruct ice-sheet physics to interpret the structures found in the cores. These models grow more complex as our understanding of what makes ice flow increases. For practical reasons, we cannot collect cores with as much frequency as we desire. Also, we cannot monitor changes of the ice in an ice sheet at the grain-size scale. The controlled situation of a laboratory test can contribute to our understanding of how ice flows and how microstructures develop in response to flow.

One of the most troubling aspects of laboratory measurements is that they cannot be performed at the exact grain size and time scales of ice sheets. Ice sheets deform over hundreds of thousands of years and can have grain sizes on the order of several centimeters. It is widely debated in the field of glaciology whether or not laboratory measurements of fine-grained ice, and fine-grained ice physics, can be extrapolated up to the large scale of ice sheets. In other words, can you use small grains and faster deformation rates to simulate how ice in an ice sheet evolves?

This work indicates that these extrapolations from the laboratory scale to natural settings, such as in an ice sheet, must be made with caution. As shown in Chapter 2, for grains under static-annealing growth conditions, fine-grained ice does not follow the same growth law as ice found in ice sheets. Other factors must be considered, such as the period of transient grain-size adjustment that these samples undergo. In my samples, 3 samples annealed for short durations are still affected by the transient grain-size adjustment period. In order to know when the samples are undergoing normal grain growth, the experiments on fine-grained ice must be carried out until the grain-size distributions fit log-normal distributions. Growth experiments should begin once the transient grain-size adjustment period has passed and normal grain growth is occurring.

Nonetheless, experiments on fine-grained ice are valuable. We currently have no other way to explore the balance of deformation mechanisms in the GSS / dislocation creep regimes. Small grain sizes are needed experimentally to perform these tests on the short time scales that are part of laboratory work and to be able to explore grain-size sensitive mechanisms.

For the texture measurements made in Chapter 3, samples were deformed first and then measured for texture. My results from Chapter 3 show that arguments based on microstructure, such as the straightness of grain boundaries, the presence of four-grain junctions and the shape of grains (flattened or equiaxed), as well as the difference in independent major and minor axis lengths after deformation, are not sufficient to determine which mechanisms dominate. In fact, my texture results show that ice samples deformed under conditions of low stress, where we expect to see GSS creep dominate, develop a non-random texture. Ice that is deformed under conditions where dislocation creep should dominate develops a similar non-random texture. Under these conditions, LTSEM reveals that the samples are identical in microstructure.

In my experiments, it is likely that both GSS and dislocation creep are contributing to deformation, and that neither mechanism is dominant. These results indicate that further work is needed with both texture measurements and LTSEM to investigate the boundary between these two regimes, as it may be broader than has previously been suggested. Ice may not deform under the dominance of dislocation creep alone under conditions of low stress, and assigning the value of 3 (dislocation creep) for the stress exponent (n) in equation 3.1 may not be fully representative of this situation. The capability to do both the deformation and texture measurements at the same time was not available at the time of these measurements, and the need for a device to measure texture while deformation is occurring became clear.

In order to assess the effects of a dynamic environment on grain size, such as in an ice sheet, the deformation apparatus that I designed for use with neutron scattering presents a new possibility to the field of glaciology. This apparatus, in

conjunction with TOF neutron diffraction, allows for the fast collection of data (on the order of hours). With this new deformation instrument we can further explore the question of extrapolation from the laboratory to field data. The *in situ* deformation apparatus provides a unique opportunity for an exploration of GSS and dislocation creep. Experiments done under different conditions of stress will allow the investigation of the boundary between these two deformation mechanisms. When supported by LTSEM data (measuring grain characteristics such as grain flattening and growth), these texture measurements may allow the determination of a clearer boundary between GSS and dislocation creep.

The *in situ* deformation apparatus demonstrates the capability of collecting texture data for ice in a continuous time series. This tool offers a unique ability for ice experimentalists, and this data is potentially very powerful for understanding the complexities of ice flow at certain conditions. This apparatus can be applied to experimentally reconstructing the deformation found in ice sheets.

There are several situations where grain size could be smaller than expected in an ice sheet. Polygonization of crystals and impurity-hindered grain growth can contribute to small grain size in an ice sheet [*Thorsteinsson, et al.*, 1995; *Weiss, et al.*, 2002]. In fact, ice-age ice creates an entire layer of dusty or dirty ice from ice deposited during the last glaciation that causes a strain rate enhancement of 2.5 times that of Holocene period ice [*Paterson*, 1991]. As a result of the impurities, impingement on the grain boundaries keeps grain boundary migration hindered and grain size remains small. The implication is that these regions can produce localized effects that may or may not affect ice-sheet flow. Also, as more snow deposition occurs with time, these layers will increase in depth in an ice sheet. The interaction

of these layers with local features (bedrock, ridges, additional impurities from erosion) could alter how ice flows; potentially, under the right conditions (low stress), it could have a large impact on the flow of an ice sheet.

There are many uses of the deformation apparatus that I built with neutron scattering, for the glaciology community as well as other geoscientists, material scientists, and chemists. The power of conducting experiments *in situ* is that many factors can be controlled (stress, temperature, duration) and the result of any perturbation to these conditions is instantly available while the deformation continues. Also, many of these environmental conditions can be explored with multiple samples in a time period of days. This means that a large quantity of data can be collected in a relatively short time frame, something that has not previously been achievable without the technological advances of neutron scattering.

Specifically for glaciology, future experiments with the *in situ* deformation apparatus can be undertaken to reproduce the texture that is found in ice sheets. Important experiments further exploring the effects of low stress on dominant deformation mechanism in polycrystalline ice can be extended from the results I present in Chapter 3. The ability to monitor ice deformation (at a grain-to-grain scale) as it occurs is a window into the depth of an ice sheet without disturbing the immediate environment of the ice, something that is ideal but unachievable outside of the laboratory. This dissertation introduces these advances in instrumentation to glaciology, and they could potentially expand the understanding of ice deformation to new levels.

Most importantly, the techniques of neutron scattering present a myriad of possible routes of experimentation. My dissertation presents only a few potential aspects of ice sheet flow that can be studied with neutrons. Neutron scattering facilities at national laboratories and universities are available at no cost to investigators of any field. These data, however, should not stand alone. The ability to recreate the texture of an ice sheet, both in localized regions and for the whole ice mass, could provide compelling evidence of the microstructural details of ice flow and better our understanding of the climatic record recreated from ice cores. Laboratory and field measurements are enhanced when combined with models. Ice sheet dynamics remain complex and fascinating, and a combined effort between laboratory and modeling communities within glaciology is needed to further our understanding.

REFERENCES

Workshop on the Polar Regions of Mars: Geology, Glaciology and Climate History (LPI/TR-92-08, Part 1), paper presented at Workshop on the Polar Regions of Mars: Geology, Glaciology and Climate History (LPI/TR-92-08, Part 1). 13-15 Nov. 1992, Houston, TX, USA, Houston, TX, USA: Lunar & Planetary Inst, 1992, 1992.

Alley, R. B. (1992), Flow-law hypotheses for ice sheet modeling, *Journal of Glaciology*, *38*, 245.

Alley, R. B. (2000), *The two-mile time machine: ice cores, abrupt climate change, and our future*, vii, 229 p. pp., Princeton University Press, Princeton, N.J.

Alley, R. B., et al. (1986a), Grain-growth in polar ice.1.theory, *Journal of Glaciology*, *32*, 413.

Alley, R. B., et al. (1986b), Grain-growth in polar ice.2. Application, *Journal of Glaciology*, *32*, 425.

Ashby, M. F., and P. Duval (1985), CREEP OF POLYCRYSTALLINE ICE, *Cold Reg Sci Technol*, *11*, 285.

Ashby, M. F., and R. A. Verrall (1973), Diffusion-accommodated flow and superplasticity, *Acta Metallurgica*, *21*, 149.

Atkinson, H. V. (1988), Theories of normal grain growth in pure single phase systems, *Acta Metallurgica*, *36*, 469-491.

Azuma, N. (1994), A flow law for anisotropic ice and its application to ice sheets, *Earth and Planetary Science Letters*, *128*, 601.

Bailey, I. F. (2003), A review of sample environments in neutron scattering, *Zeitschrift fur Kristallographie, 218*, 84.

Baker, I., et al. (2003), The microstructural location of impurities in ice, *Canadian Journal of Physics, 81*, 1.

Bennett, K. (1994), Deformation of High-Pressure, Low-Temperature Polycrystalline Ice: Mechanical Properties, Texture and Microstructure, University of California, Berkeley.

Bennett, K., et al. (1997), Preferred crystallographic orientation in the ice I to II transformation and the flow of ice II, *Philosophical Magazine A (Physics of Condensed Matter: Structure, Defects and Mechanical Properties), 76*, 413.

Brentano, J. C. M. (1935), The quantitative measurement of the intensity of x-ray reflections from crystalline powders.

Budd, W. F., and T. H. Jacka (1989), Review of ice rheology for ice sheet modelling, *Cold Reg Sci Technol, 16*, 107.

Burke, J. E., and D. Turnbull (1955), Recrystallization and grain growth, *Progress in Metal Physics, 3*, 220.

Castelnau, O., et al. (1997), Modelling viscoplastic behavior of anisotropic polycrystalline ice with a self-consistent approach, *Acta Materialia, 45*, 4823.

Castelnau, O., et al. (1996), Viscoplastic modeling of texture development in polycrystalline ice with a self-consistent approach: comparison with bound estimates, *Journal of Geophysical Research, 101*, 13851.

Castelnau, O., et al. (1998), Anisotropic behavior of GRIP ices and flow in central Greenland, *Earth and Planetary Science Letters, 154*, 307.

Chastel, Y. B., and P. R. Dawson (1991), Comparison of polycrystalline rolling simulations with experiments, paper presented at Modeling the Deformation of Crystalline Solids presented at the Annual Meeting of the Minerals, Metals, and Materials Society; Feb 17-21 1991; New Orleans, LA, USA, Warrendale, PA, USA: Publ by Minerals, Metals & Materials Soc (TMS), 1991, 1991.

Cole, D. M. (2001), The microstructure of ice and its influence on mechanical properties, *Engineering Fracture Mechanics*, *68*, 1797.

Cuffey, K. M., et al. (2000a), Deformation properties of subfreezing glacier ice: role of crystal size, chemical impurities, and rock particles inferred from in situ measurements, *Journal of Geophysical Research*, *105*, 27895.

Cuffey, K. M., et al. (2000b), A renewed argument for crystal size control of ice sheet strain rates, *Journal of Geophysical Research*, *105*, 27889.

D'Halloy, O. (1833), Introduction à la Géologie.

Dahl-Jensen, D. (1989), Steady thermomechanical flow along two-dimensional flow lines in large grounded ice sheets, *Journal of Geophysical Research*, *94*, 10355.

De Bresser, J. H. P., et al. (1998), On dynamic recrystallization during solid state flow: effects of stress and temperature, *Geophysical Research Letters*, *25*, 3457.

De Bresser, J. H. P., et al. (2001), Grain size reduction by dynamic recrystallization: can it result in major theological weakening? *International Journal of Earth Sciences*, *90*, 28.

De La Chapelle, S., et al. (1998), Dynamic recrystallization and texture development in ice as revealed by the study of deep ice cores in Antarctica and Greenland, *Journal of Geophysical Research*, *103*, 5091.

Doake, C. S. M., and E. W. Wolff (1985), Flow laws for ice in polar ice sheets, *Nature, 314,* 255-257.

Durham, W. B., et al. (1983), Experimental deformation of polycrystalline H{sub 2}O ice at high pressure and low temperature: preliminary results, *Journal of Geophysical Research, 88,* 377.

Durham, W. B., and L. A. Stern (2001), Rheological properties of water ice - Applications to satellites of the outer planets, *Annual Review of Earth and Planetary Sciences, 29,* 295.

Durham, W. B., et al. (2001), Rheology of ice I at low stress and elevated confining pressure, *Journal of Geophysical Research, 106,* 11031.

Duval, P. (1973), Flow of polycrystalline ice under low stresses, *Comptes Rendus Hebdomadaires des Seances de l'Academie des Sciences, Serie A (Science Mathematiques), 277,* 703.

Duval, P. (1979), Creep and recrystallization of polycrystalline ice, *Bulletin de Mineralogie, 102,* 80.

Duval, P. (1981), Creep and fabric of polycrystalline ice under shear and compressive stress, *Journal of Glaciology, 27,* 129.

Duval, P., et al. (2000), Deformation and recrystallization processes of ice from polar ice sheets, *Annals of Glaciology, 30,* 83.

Duval, P., et al. (1983), Rate-controlling processes in the creep of polycrystalline ice, *Journal of Physical Chemistry, 87,* 4066.

Duval, P., and M. Montagnat (2002), Comment on "Superplastic deformation of ice: experimental observations" by D. L. Goldsby and D. L. Kohlstedt - art. no. 2082, *Journal of Geophysical Research-Solid Earth, 107,* 2082.

Ferrigno, J. G., et al. (2002), Coastal-change and glaciological maps of the Antarctic peninsula, *U.S. Geological Survey Fact Sheet, FS-017-02*.

Francis, T. J. G. (1969), Generation of seismic anisotropy in the upper mantle along the mid-oceanic ridges, *Nature, 221*, 162.

Glen, J. W. (1955), The creep of polycrystalline ice, *Proceedings of the Royal Society of London Series A-Mathematical and Physical Sciences, 228*, 519.

Glen, J. W. (1958), Physics of ice movement, *Nature, 182*, 1560.

Goldsby, D. L., and D. L. Kohlstedt (1997), Grain boundary sliding in fine-grained ice I, *Scripta Materialia, 37*, 1399.

Goldsby, D. L., and D. L. Kohlstedt (2001), Superplastic deformation of ice: experimental observations, *Journal of Geophysical Research, 106*, 11017.

Goodman, D. J., et al. (1981), The plasticity of polycrystalline ice, *Philosophical Magazine A (Physics of Condensed Matter, Defects and Mechanical Properties), 43*, 665.

Gottstein, G., and S. Shvindlerman (1999), *Grain boundary migration in metals: Thermodynamics, kinetics, and applications*, 384 pp., CRC Press, New York.

Gow, A. J. (1969), On the Rates of Growth of Grains and Crystals in South Polar Firn, *Journal of Glaciology, 8*, 241-252.

Gow, A. J., and T. Williamson (1976), RHEOLOGICAL IMPLICATIONS OF THE INTERNAL STRUCTURE AND CRYSTAL FABRICS OF THE WEST ANTARCTIC ICE SHEET AS REVEALED BY DEEP CORE DRILLING AT BYRD STATION, *CRREL Rep.*

Granqvist, C. G., and R. A. Buhrman (1976), Ultrafine metal particles, *Journal of Applied Physics*, *47*, 2200-2219.

Gueguen, Y., and A. Nicolas (1980), Deformation of Mantle Rocks, *Annual Review of Earth and Planetary Sciences*, *8*, 119-144.

Heard, H. C., et al. (1990), A triaxial deformation apparatus for service at 77<T<273 K, *The brittle ductile transition in rocks, Geophys. Monogr. Ser., 56, edited by A.G.Duba, W.B. Durham, J.W. Handin, and H.F. Wang.*, 225-228, AGU, Washington, D.C.

Heidelbach, F., and C. Riekel (1997), Quantitative texture analysis with a small beam, *ESRF Experiment Reports January Newsletter*.

Hess, H. H. (1964), Seismic anisotropy of the upper most mantle under oceans, *Nature*, *203*, 629.

Hubbard, A. (1999), High resolution modelling of the advance of the Younger Dryas Ice Sheet and its climate in Scotland., *Quaternary Research*, *52*, 27-43.

Humphreys, F. J., and M. Hatherly (1995), *Recrystallization and Related Annealing Phenomena.*, First ed., 497 pp., Pergamon Press, Tarrytown, N.Y., U.S.A.

Jessell, M. W., et al. (2003), The preservation potential of microstructures during static grain growth, *Journal of Metamorphic Geology*, *21*, 481.

Kallend, J. S., et al. (1991), POPLA - An integrated software system for texture analysis, *Textures and Microstructures*, *14*, 1203.

Kamb, B. (1972), Experimental recrystallization of ice under stress, in *Flow and Fracture of Rocks - The Griggs Volume, Geophys. Monograph 16*, edited, pp. 211-241, Washington, D.C.

Kamb, W. B. (1959), Ice petrofabric observations from Blue Glacier, Washington, in relation to theory and experiment, *Journal of Geophysical Research*, *64*, 1891.

Kamb, W. B. (1961), Thermodynamic theory of nonhydrostatically stressed solids, *Journal of Geophysical Research*, *66*, 259.

Kocks, U. F., et al. (1998), *Texture and anisotropy: preferred orientations in polycrystals and* their effect on materials properties, 676 pp., Cambridge University Press, New York.

Leadbetter, A. J., et al. (1985), The equilibrium low-temperature structure of ice, *Journal of Chemical Physics*, *82*, 424.

Li, F., et al. (1997), Grain elongation and anisotropic grain growth during superplastic deformation in an Al-Mg-Mn-Cu alloy, *Acta Materialia*, *45*, 3887.

Lutterotti, L., et al. (1997), Combined texture and structure analysis of deformed limestone from time-of-flight neutron diffraction spectra, *Journal of Applied Physics*, *81*, 594.

Matthies, S., and H. R. Wenk (1992), Optimization of texture measurements by pole figure coverage with hexagonal grids, *Physica Status Solidi A*, *133*, 253.

McCappin, C. J., and W. C. Macklin (1984a), Crystalline structure of ice formed by droplet accretion II: annealed samples and application, *J Atmos Sci*, *41*, 2447.

McCappin, C. J., and W. C. Macklin (1984b), Crystalline structure of ice formed by droplet accretion. I: fresh samples, *J Atmos Sci*, *41*, 2437.

McDaniel, S. M., et al. (2005), in preparation.

McDaniel, S. M., et al. (2002), Grain Growth in Polycrystalline Fine-grained Ice I_h, paper presented at EOS Transactions. AGU abstracts.

Montagnat, M., and P. Duval (2000), Rate controlling processes in the creep of polar ice, influence of grain boundary migration associated with recrystallization, *Earth and Planetary Science Letters*, *183*, 179.

Montagnat, M., and P. Duval (2004), The viscoplastic behaviour of ice in polar ice sheets: experimental results and modelling, *Academie des Sciences. Comptes Rendus, Physique*, *5*, 699.

Montagnat, M., et al. (2003), Lattice distortion in ice crystals from the Vostok core (Antarctica) revealed by hard X-ray diffraction; implication in the deformation of ice at low stresses, *Earth and Planetary Science Letters*, *214*, 369.

Moran, P. A. P. (1968), *An Introduction to Probability Theory*, 317 pp., Clarendon, Oxford.

Mulvaney, R., et al. (1988), Sulphuric acid at grain boundaries in Antarctic ice, *Nature*, *331*, 247.

Nasello, O. B., et al. (1992), Grain growth in pure ice, effects of mobile bubbles., paper presented at Physics and chemistry of ice: papers presented at the Symposium on the Physics and Chemistry of Ice, held in Ottawa, Canada, 14-18 August 1972., Royal Society of Canada, Ottawa.

Naumann, C. F. (1850), *Lehrbuch der Geognosie.*, 1000 pp., Engelmann, Leipzig.

Nieh, T. G., et al. (1997), *Superplasticity in metals and ceramics*, Cambridge University Press, Cambridge.

Novikov, V. (1997), *Grain growth and control of microstructure and texture in polycrystalline materials.*, 174 pp., CRC Press, New York.

Padmanabhan, K. A., and G. J. Davies. (1980), *Superplasticity: mechanical and structural aspects, environmental effects, fundamentals and applications.*, Springer-Verlag, New York.

Pappalardo, R. T., et al. (1998), Geological evidence for solid-state convection in Europa's ice shell, *Nature*, *391*, 365.

Paterson, W. S. B. (1991), Why ice-age ice is sometimes 'soft', *Cold Regions Science and Technology*, *20*, 75.

Paterson, W. S. B. (2001), *The Physics of Glaciers*, Third ed., 481 pp., Butterworth/Heinemann, Oxford.

Peltier, W. R., et al. (2000), Ice-age ice-sheet rheology: constraints from the Last Glacial Maximum form of the Laurentide ice sheet, *Annals of Glaciology*, *30*, 163.

Perez-Prado, M. T., et al. (1998), Grain boundary sliding and crystallographic slip during superplasticity of Al-5%Ca-5%Zn as studied by texture analysis, *Materials Science & Engineering A (Structural Materials: Properties, Microstructure and Processing)*, *A244*, 216.

Perez-Prado, M. T., et al. (1996), Texture gradient evolution in Al-5%Ca-5%Zn sheet alloy after tensile deformation at high superplastic strain rate, *Scripta Materialia*, *35*, 1455.

PerezPrado, M. T., et al. (1996), Texture gradient evolution in Al-5%Ca-5%Zn sheet alloy after tensile deformation at high superplastic strain rate, *Scripta Materialia*, *35*, 1455.

Peterson, S. W., and H. A. Levy (1957), A single-crystal neutron diffraction study of heavy ice, *Acta Crystallographica*, *10*, 70.

Petrenko, V. F., and R. W. Whitworth (1999), *The Physics of Ice*, 373 pp., Oxford University Press, Oxford.

Pettit, E. C., and E. D. Waddington (2003), Ice flow at low deviatoric stress, *Journal of Glaciology*, *49*, 359-369.

Pimienta, P., and P. Duval (1987), RATE CONTROLLING PROCESSES IN THE CREEP OF POLAR GLACIER ICE, *J Phys Paris Colloq*, *48*, 243.

Poirier, J.-P. (1985), *Creep of crystals: high-temperature deformation processes in metals, ceramics and minerals*, 260 pp., Cambridge University Press, Cambridge.

Poirier., J.-P. (1985), *Creep of crystals: high-temperature deformation processes in metals, ceramics and minerals*, 260 pp., Cambridge University Press, Cambridge.

Ree, J. H., and Y. Park (1997), Static recovery and recrystallization microstructures in sheared octachloropropane, *Journal of Structural Geology*, *19*, 1521.

Reeh, N. (1988), A flow-line model for calculating the surface profile and the velocity, strain rate, and stress fields in an ice sheet, *Journal of Glaciology*, *34*, 46.

Rietveld, H. M. (1967), Line profiles of neutron powder-diffraction peaks for structure refinement, *Acta Crystallographica*, *22*, 151.

Santoro, A. (2001), Past and present crystallographic work at the NBS/NIST reactor, *Journal of Research of the National Institute of Standards and Technology*, *106*, 921.

Sherby, O. D., and J. Wadsworth (1989), Superplasticity-recent advanced and future directions, *Progress in Materials Science*, *33*, 169.

Souchez, R. A., and R. D. Lorrain (1991), *Ice composition and glacier dynamics*, x, 207p. pp., Berlin, Germany: Springer-Verlag, 1991.

Steinemann, s. (1955), Flow and recrystallization of ice., *Association Internationale de Hydrologic Science, 4*, 449-462.

Stern, L. A., et al. (1997), Grain-size-induced weakening of $H\{sub\ 2\}O$ ices I and II and associated anisotropic recrystallization, *Journal of Geophysical Research, 102*, 5313.

Stern, L. A., et al. (2004), Scanning electron microscopy investigations of laboratory-grown gas clathrate hydrates formed from melting ice, and comparison to natural hydrates, *American Mineralogist, 89*, 1162.

Thorsteinsson, T. (2000), Anisotropy of Ice I_h: Development of Fabric and Effects of Anisotropy on Deformation, University of Washington, Seattle.

Thorsteinsson, T. (2002), Fabric development with nearest-neighbor interaction and dynamic recrystallization, *Journal of Geophysical Research, 107*, ECV3.

Thorsteinsson, T., et al. (1995), Crystal size variations in Eemian-age ice from the GRIP ice core, Central Greenland, *Earth and Planetary Science Letters, 131*, 381.

Thorsteinsson, T., et al. (1997), Textures and fabrics in the GRIP ice core, *Journal of Geophysical Research, 102*, 26583.

Tome, C. N. (1999), Self-consistent polycrystal models: a directional compliance criterion to describe grain interactions, *Modelling and Simulation in Materials Science and Engineering, 7*, 723-738.

VonDreele, R. B. (1997), Quantitative texture analysis by Rietveld refinement, *Journal of Applied Crystallography, 30*, 517.

Wakai, F. (2004), Dynamics of grain boundary network in ceramics superplasticity, *Nippon Seramikkusu Kyokai Gakujutsu Ronbunshi/Journal of the Ceramic Society of Japan*, *112*, 472.

Weertman, J. (1970), The creep strength of the earth's mantle, *Reviews of Geophysics and Space Physics*, *8*, 145.

Weertman, J. (1973), Creep of ice, paper presented at Symposium on the Physics and Chemistry of Ice, 14-18 Aug. 1972, Ottowa, Ont., Canada, Ottowa, Ont., Canada: Royal Soc. Canada, 1973, 1973.

Weiss, J., et al. (2002), Dome Concordia ice microstructure: impurities effect on grain growth, *Annals of Glaciology*, *35*, 552.

Wenk, H. R. (1985), *Preferred Orientation in Deformed Metals and Rocks: An Introduction to Modern Texture Analysis*, 610 pp., Academic Press, INC., Orlando.

Wenk, H. R. (2002), Texture and anisotropy, *Reviews in Mineralogy & Geochemistry*, *51*, 291.

Wenk, H. R., et al. (2003), Texture analysis with the new HIPPO TOF diffractometer, *Nuclear Instruments & Methods in Physics Research, Section A (Accelerators, Spectrometers, Detectors and Associated Equipment)*, *515*, 575.

Wenk, H. R., et al. (1998), BEARTEX: a Windows-based program system for quantitative texture analysis, *Journal of Applied Crystallography*, *31*, 262.

Wenk, H. R., et al. (1994), Deconvolution of superposed pole figures by discrete OD methods: comparison of ADC and WIMV for quartz and calcite with trigonal crystal and triclinic specimen symmetry., *Textures and Microstructures*, *22*, 233-260.

Wenk, H. R., and P. Van Houtte (2004), Texture and anisotropy, *Reports on Progress in Physics*, *67*, 1367.

Wilen, L. A. (2000), A new technique for ice fabric analysis, *Journal of Glaciology*, *46*, 129-139.

Wollan, E. O., et al. (1949), Neutron diffraction study of the structure of ice, *Physical Review*, *75*, 1348.

Wyttenbach, A., et al. (1977), Determination of impurities in ice-cores form the Jungfrau-joch by neutron activation analysis, *Journal of Radioanalytical Chemistry*, *38*, 405.

Vita

Shannon McDaniel was born in Washington, D.C. She currently calls Los Alamos, NM, home. At Oberlin College in 1996, she earned a Bachelor of Arts degree in Geology and Biology. In 2005 she earned a Doctor of Philosophy at the University of Washington in Earth and Space Sciences.